

CHALMERS



A Refined Vehicle Dynamic Model for Driving Simulators

Master's Thesis in Automotive Engineering

EMANUELE OBIALERO

Department of Applied Mechanics
Division of Vehicle Engineering and Autonomous Systems
Vehicle Dynamics
CHALMERS UNIVERSITY OF TECHNOLOGY
Göteborg, Sweden 2013
Master's thesis 2013:10

MASTER'S THESIS IN AUTOMOTIVE ENGINEERING

A Refined A Refined Vehicle Dynamic Model for
Driving Simulators

EMANUELE OBIALERO

Department of Applied Mechanics
Division of Vehicle Engineering and Autonomous Systems
Vehicle Dynamics
CHALMERS UNIVERSITY OF TECHNOLOGY
Göteborg, Sweden 2013

A Refined Vehicle Dynamic Model for Driving Simulators

EMANUELE OBIALERO

© EMANUELE OBIALERO 2013

Master's Thesis 2013:10

ISSN 1652-8557

Department of Applied Mechanics

Division of Vehicle Engineering and Autonomous Systems

Vehicle Dynamics

Chalmers University of Technology

SE-412 96 Göteborg

Sweden

Telephone: + 46 (0)31-772 1000

Cover:

View of *Sim IV*, the driving simulator used for this Master's thesis activity, located at VTI office in Göteborg, Sweden.

Chalmers Reproservice/ Department of Applied Mechanics
Göteborg, Sweden 2013

A Refined Vehicle Dynamic Model for Driving Simulators

Master's Thesis in Automotive Engineering

EMANUELE OBIALERO

Department of Applied Mechanics

Division of Vehicle Engineering and Autonomous Systems

Vehicle Dynamics

Chalmers University of Technology

ABSTRACT

Driving simulators play an important role in the automotive field, especially in the research about human factors and in the development of driving assistance systems. For this reason, driving experience should be as close as possible to reality. The mathematical model, describing vehicle dynamics, plays a fundamental part in providing this “reality feel”, since it is used by the simulator to compute vehicle motion.

This Master's thesis has the aim of refining an existing vehicle dynamic model for a driving simulator, developed in Modelica ® programming language, in order to make the driving experience closer to reality. In particular, this work is focused into two areas: the first concerns the development of vertical dynamics, in order to extend the degrees of freedom of the vehicle model from ten to fourteen. The second is related to the development of a more accurate steering system model, for both improving the steering feel and the steering dynamics.

The vehicle model has been validated through different steps. First of all, its response to different manoeuvres has been compared with the one provided by a real car. This comparison has been made by confronting the model data with the real vehicle ones, coming from test track measurements. Then the model has been tested in the simulator by different drivers, who had to evaluate its behaviour.

Key words:

Vehicle dynamics, vertical dynamics, non-linear suspensions, friction models, steering feel, steering system modelling, driving simulator, Modelica ®, model validation.

Contents

| | |
|--|-----|
| ABSTRACT | I |
| CONTENTS | III |
| PREFACE | VI |
| NOTATIONS | VII |
| | |
| 1 INTRODUCTION | 1 |
| 1.1 Driving simulator | 1 |
| 1.2 Project definition | 3 |
| 1.3 Model characteristics | 3 |
| 1.4 Model limitations | 4 |
| | |
| 2 BACKGROUND | 5 |
| 2.1 Motivations | 5 |
| 2.2 Programming language | 5 |
| 2.3 Description of the starting VDM | 6 |
| 2.3.1 Chassis | 6 |
| 2.3.2 Suspensions | 9 |
| 2.3.3 Steering system | 12 |
| 2.4 Summary | 14 |
| | |
| 3 MODEL FOR NON-LINEAR VERTICAL DYNAMICS | 15 |
| 3.1 Vertical dynamics: an overview | 15 |
| 3.1.1 The quarter car models | 16 |
| 3.1.2 Half car model | 19 |
| 3.1.3 Full car model | 21 |
| 3.2 Non-linear vertical dynamics model | 22 |
| 3.3 Non-linear springs | 31 |
| 3.3.1 Front springs | 33 |
| 3.3.2 Rear springs | 35 |
| 3.3.3 Spring tuning | 36 |
| 3.4 Non-linear shock absorber | 37 |
| 3.4.1 Shock absorber modeling | 39 |
| 3.5 Suspension model: summary | 41 |
| | |
| 4 STEERING SYSTEM | 44 |

| | | |
|-------|--|-----|
| 4.1 | Steering: an overview | 44 |
| 4.2 | Rack and pinion model | 47 |
| 4.3 | Mathematical modelling | 50 |
| 4.4 | Friction modelling | 53 |
| 4.5 | Power steering modelling | 57 |
| 4.6 | Steering system model: summary | 60 |
| 4.7 | Refined VDM: an overview | 62 |
| 5 | MODEL VALIDATION | 65 |
| 5.1 | Comparison with real data | 65 |
| 5.1.1 | Steady state driving | 65 |
| 5.1.2 | Transient response | 69 |
| 5.1.3 | Straight driving | 73 |
| 5.2 | Comparison between VDM-10 and VDM-14 | 75 |
| 5.2.1 | Lateral acceleration | 75 |
| 5.2.2 | Roll rate | 76 |
| 5.2.3 | Yaw rate | 77 |
| 5.2.4 | Pitch rate | 78 |
| 5.2.5 | Conclusion | 79 |
| 5.3 | Validation in <i>Sim IV</i> | 80 |
| 5.3.1 | Tests for evaluating the overall functionality | 80 |
| 5.3.2 | Tests for evaluating the steering response | 80 |
| 6 | CONCLUSIONS | 87 |
| 7 | FUTURE WORK | 88 |
| 8 | REFERENCES | 89 |
| 9 | APPENDICES | 91 |
| B.1 | Coordinate system | 93 |
| B.2 | Wheels | 94 |
| B.3 | Tires | 95 |
| B.4 | Driveline | 98 |
| B.5 | Braking system | 101 |

Preface

This Master's thesis has been performed from October 2012 to April 2013 at VTI's Göteborg office and it is done in collaboration between VTI and Chalmers University of Technology.

During this thesis an existing vehicle dynamic model, written in the Modelica® format, has been refined into two areas: suspensions and steering. The new refined model has been validated both with a comparison with real data and with simulator experiments, performed at VTI with the new *Sim IV* simulator.

This work wouldn't have been possible without the great support provided by my supervisor, Fredrik Bruzelius, who proved to be not only a great professor, but also a great friend. Special mention should be done to Bruno Augusto for his patience in teaching me how to use the simulator and for helping me to get everything working properly.

Great thanks go also to professors Bengt Jacobson (Chalmers University) and Mauro Velardocchia (Politecnico di Torino) for having made this experience possible and for having found the time to help me despite their many commitments, and to my family for having always supported me.

Working at VTI has been an incredible experience to which all my colleagues contributed with their kindness and huge empathy. Big thanks goes to all VTI employees: Anna Arvidsson, Tania Dukic, Lennart Folkesson, Anders Genell, Sara Linder, Arne Nåbo, Jesper Sandin, Peter Sandqvist, Christina Stave, Niklas Strand, Robert Thomson, Erik Yderberg, Eva Åström, Mikael Örgen, Megersa Abate and Maria Kreusslein. Thank you for having made me feel like at home every day, for your Swedish classes, for having involved me in many VTI initiatives and for having taught me the "Swedish way".

I also would like to thank all the volunteers who participated to the simulator experiments: Sebastian Brust, Maike Hildebrandt, Niklas Strand, Alexander Panagiotidis, Stylianos Mentetis, Bengt Jacobson, Farnaz Sharifi Brojerdi, Arne Nåbo, Niko, Joan Arajol, Elpidoforos Arapantonis, Iago Vázquez, Tellier Louis, Adythia Aerikere, Cyrill Chambosse, Devansh Metha and Tomek Stec.

Finally, life is not only working. So, a special thanks goes to my friends Danilo, Lorenzo, Alessandro, Ermes, Danilo for having supported me and to all my friends in Göteborg, who made these six months unique: Josip, Jan, Louise, Francois, Cyrill, Hanna, Frauke, Esther, Sharon, Claire, Caroline, Annika, Iago, Patricia, Harold, Jacob and Stelianos. Thanks for all the good moments shared together.

Göteborg, April 2013

Emanuele Obialero

Notations

Romans upper case letters

| | |
|---|---|
| A Assistance coefficient. | $D_{sr r}$ Slow rebound damping coefficient of rear shock absorbers. |
| A_{servo} Area of the piston in the servo assistance cylinder. | $D_{sr f}$ Slow rebound damping coefficient of front shock absorbers. |
| A_{pad} Brake pad area. | D_{rack} Rack damping. |
| CF Dahl model coulomb friction level. | D Steering wheel and column damping. |
| C Normalized thread stiffness. | $D_{shock f}$ Damping coefficient of shock absorber in front suspension. |
| C_x Vehicle drag coefficient. | $D_{shock r}$ Damping coefficient of shock absorber in rear suspension. |
| C_{servo} Servo assistance coefficient. | $F_{GVM i}$ Force on suspension i in full weight vehicle configuration. |
| $CompMz_r$ Self-aligning torque compliance rear wheels. | $F_{bump stop i}$ Force on suspension i due to bump stopper intervention. |
| $CompMz_f$ Self-aligning torque compliance front wheels. | $F_{curb i}$ Force on suspension i in curb weight vehicle configuration. |
| $CompFy_r$ Lateral force compliance rear wheels. | F_f Heave natural frequency of the front sprung mass. |
| $CompFy_f$ Lateral force compliance front wheels. | F_p Force acting on the pinion. |
| C_{input} Clutch position. | F_{servo} Servo assistance force. |
| $C_{f pad}$ Disk-pad friction coefficient. | FX_i Total tire force in longitudinal direction. |
| D_{pitch} Pitch axis torsion damping. | FY_i Total tire force in lateral direction. |
| $D_{roll f}$ Front axle roll damping. | $F_{antiroll i}$ Force produced by the anti-roll bar in suspension i . |
| $D_{roll r}$ Rear axle roll damping. | F_{bank} Bank resistance force. |
| D_{sw} Steering wheel damping coefficient. | F_{ci} Force transmitted by suspension I to the chassis. |
| $D_{fb f}$ Fast bump damping coefficient of front shock absorbers. | F_{di} Force produced by the damper in suspension i . |
| $D_{fb r}$ Fast bump damping coefficient of rear shock absorbers. | F_{drag} Drag resistance force. |
| $D_{fr f}$ Fast rebound damping coefficient of front shock absorbers. | $F_{ext,y}$ Lateral external forces. |
| $D_{fr r}$ Fast rebound damping coefficient of rear shock absorbers. | $F_{ext,x}$ Longitudinal external forces. |
| $D_{sb f}$ Slow bump damping coefficient of front shock absorbers. | |
| $D_{sb r}$ Slow bump damping coefficient of rear shock absorbers. | |

| | |
|--|---|
| F_r Heave natural frequency of the rear sprung mass. | $K_{antiroll\ r}$ Rear anti-roll bar torsion stiffness. |
| F_{ri} Force transmitted by the road to wheel i . | K_{sf} Stiffness of the spring in front suspension. |
| FR_i Resistant force on the rack. | K_{sr} Stiffness of the spring in rear suspension. |
| $F_{rolling\ i}$ Rolling resistance force at wheel i . | K_t Tire vertical stiffness. |
| $F_{rolling}$ Rolling resistance force. | $K_{0\ r}$ Stiffness of the spring of rear suspensions in normal operative area. |
| F_{si} Force produced by the spring in suspension i . | $K_{bump\ f}$ Stiffness of bump stopper of front suspensions. |
| F_{slope} Slope resistance force. | $K_{bump\ r}$ Stiffness of bump stopper of rear suspensions. |
| Fx_i Longitudinal force tire i . | K_s Dahl model spring constant. |
| $Fx_{i_wo_rlx}$ Tire longitudinal force without taking into account relaxation length. | L_1 Distance between CG and front axle. |
| Fy_i Lateral force tire i . | L_2 Distance between CG and rear axle. |
| $Fy_{i_wo_rlx}$ Tire lateral force without taking into account relaxation length. | $L_{lever\ f}$ Front anti-roll bar lever arm. |
| Fz_i Tire vertical force. | $L_{lever\ r}$ Rear anti-roll bar lever arm. |
| I_{wheel} wheel and tire moment of inertia. | Mr_i Resistant torque produced by the tire forces around the steering axis of wheel i . |
| I_x Vehicle moment of inertia with respect to x axis. | Mz_i Self-aligning torque of tire i . |
| $I_{antiroll\ f}$ Front anti-roll bar inertia. | $Mz_{i_wo_rlx}$ Tire self-aligning torque without taking into account relaxation length. |
| $I_{antiroll\ r}$ Rear anti-roll bar inertia. | P_{servo} Servo assistance pressure. |
| I_z Vehicle moment of inertia with respect to z axis. | $P_{b,f}$ Front brake pressure at master cylinder. |
| J Steering wheel and column inertia. | $P_{b,r\ limit}$ Rear brake limit pressure at master cylinder. |
| J_{sw} Steering wheel moment of inertia. | $P_{b,r}$ Rear brake pressure at master cylinder. |
| K_{pitch} Pitch axis torsion stiffness. | R_{nom} Tire nominal radius. |
| $K_{roll\ f}$ Front axle roll stiffness. | $Roll\ st_f$ Front wheels roll steer compliance. |
| $K_{roll\ r}$ Rear axle roll stiffness. | $Roll\ st_r$ Rear wheels roll steer compliance. |
| $K_{0\ f}$ Stiffness of the spring of front suspensions in normal operative area. | |
| K_{TB} Torsion bar stiffness. | |
| $K_{antiroll\ f}$ Front anti-roll bar torsion stiffness. | |

| | |
|---|---|
| <i>SAL</i> Steering arm lever length. | <i>T_{sw}</i> Steering wheel torque. |
| <i>S_i</i> Tire combined slip. | <i>T_{TB}</i> Torque acting on the torsion bar. |
| <i>S_{xi}</i> Tire longitudinal slip. | <i>T_{engine,int}</i> Internal variable in the transmission model. |
| <i>S_{yi}</i> Tire lateral slip. | <i>T_{engine,max}</i> Maximum engine torque. |
| <i>T_{bi}</i> Braking torque at wheel i. | <i>T_{engine,min}</i> Minimum engine torque. |
| <i>T_{di}</i> Driving torque at wheel i. | <i>T_{engine}</i> Engine torque. |
| <i>T_f</i> Steering wheel friction torque. | <i>T_{input}</i> Throttle position. |

Roman lower case letter

| | |
|---|---|
| <i>a_y</i> Vehicle lateral acceleration. | <i>m_{si}</i> Fraction of vehicle sprung mass laying on suspension i. |
| <i>a_x</i> Vehicle longitudinal acceleration. | <i>m_{ui}</i> Fraction of vehicle unsprung mass laying on wheel i. |
| <i>d_{roll}</i> Distance between CG and roll axis. | <i>m_{rack}</i> Rack mass. |
| <i>d_r</i> Rear anti-roll bar diameter. | <i>m_{GVi}</i> Fraction of the gross vehicle mass laying on suspension i. |
| <i>d_{pitch}</i> Distance between CG and pitch axis. | <i>r_p</i> Pinion radius. |
| <i>d_f</i> Front anti-roll bar diameter. | <i>r_{KP}</i> Scrub radius. |
| <i>d_{df}</i> Front brake disk diameter. | <i>r_c</i> caster trail. |
| <i>d_{dr}</i> Rear brake disk diameter. | <i>t_f</i> Front track. |
| <i>d_{piston}</i> Caliper piston diameter. | <i>t_r</i> Rear track. |
| <i>f_r</i> Rolling resistance coefficient. | <i>toe_f</i> Front wheels toe angle. |
| <i>f_{sw}</i> steering column filtering coefficient. | <i>toe_r</i> Rear wheels toe angle. |
| <i>g</i> Gravity acceleration. | <i>v_y</i> Absolute lateral velocity. |
| <i>h_{frc}</i> Front roll centre height. | <i>v_{xi}</i> Tire longitudinal velocity. |
| <i>h_{rrc}</i> Rear roll centre height. | <i>v_x</i> Absolute longitudinal velocity. |
| <i>h_{CG}</i> Centre of gravity (CG) height. | <i>ḡ_y</i> Absolute lateral acceleration. |
| <i>i_T</i> Total transmission ratio. | <i>ḡ_x</i> Absolute longitudinal acceleration. |
| <i>i_i</i> Transmission ratio of gear i. | <i>v_{yi}</i> Tire lateral velocity. |
| <i>i_{final}</i> Final gear transmission ratio. | <i>v_{si}</i> Tire slip velocity. |
| <i>l_{rx}</i> tire relaxation length absorber. | <i>v_{bump f}</i> Transition velocity between slow and fast bump for front shock absorber. |
| <i>m</i> Total vehicle mass. | |
| <i>m_s</i> vehicle sprung mass. | |
| <i>m_u</i> vehicle unsprung mass. | |

| | |
|---|---|
| <p>$v_{rebound f}$ Transition velocity between slow and fast rebound for front shock.</p> <p>$v_{bump r}$ Transition velocity between slow and fast bump for rear shock absorber.</p> <p>$v_{rebound r}$ Transition velocity between slow and fast rebound for rear shock absorber.</p> <p>x_{rack} Rack displacement.</p> <p>\dot{x}_{rack} Rack velocity.</p> <p>\ddot{x}_{rack} Rack acceleration.</p> <p>z_{si} Displacement of the sprung mass in the attachment point with suspension i.</p> <p>z_s Sprung mass displacement.</p> <p>\dot{z}_{si} Velocity of the sprung mass in the attachment point with suspension i.</p> | <p>\ddot{z}_{si} Acceleration of the sprung mass in the attachment point with suspension i.</p> <p>z_{ui} Displacements of the unsprung mass (wheel hub) of wheel i.</p> <p>z_u Unsprung mass displacement.</p> <p>\dot{z}_{ui} Velocity of the unsprung mass of wheel i.</p> <p>\ddot{z}_{ui} Acceleration of the unsprung mass of wheel i.</p> <p>z_{ri} Road profile under wheel i.</p> <p>z_{CG} CG vertical displacement.</p> <p>$z_{GVM i}$ Displacement of the spring of suspension i in full weight vehicle configuration.</p> <p>$z_{bump stop i}$ Maximum displacement of the spring of suspension i during the intervention of the bump stopper.</p> |
|---|---|

Greek lower case letters

| | |
|---|--|
| <p>α_{wheel} Wheel acceleration.</p> <p>γ King pin angle.</p> <p>δ Steering wheel angle.</p> <p>δ_{wi} Road angle of wheel i.</p> <p>δ_{int} Internal variable for steering model.</p> <p>η_{trans} Transmission efficiency.</p> <p>θ Roll angle.</p> <p>$\dot{\theta}$ Roll rate.</p> <p>$\ddot{\theta}$ Roll acceleration.</p> <p>$\dot{\theta}_{TB}$ Torsion bar angular velocity.</p> <p>θ_{road} Road bank angle.</p> <p>$\dot{\varphi}$ Pitch rate.</p> <p>$\ddot{\varphi}$ Pitch acceleration.</p> | <p>θ_{TB} Torsion bar angular displacement.</p> <p>μ_i Friction coefficient between road and tire i.</p> <p>μ_{vi} Sliding friction constant.</p> <p>ξ_i Brush model internal variable.</p> <p>ρ_{air} Air density.</p> <p>σ Dahl stiffness coefficient.</p> <p>τ Caster angle.</p> <p>φ Pitch angle.</p> <p>φ_{road} Road slope angle.</p> <p>ψ Yaw angle.</p> <p>$\dot{\psi}$ Yaw rate.</p> <p>$\ddot{\psi}$ Yaw acceleration.</p> <p>ω_{engine} Engine rotational velocity.</p> |
|---|--|

| | |
|----------------------------------|--|
| θ_p Pinion angle. | $\omega_{engine,int}$ Internal variable in the transmission model. |
| ω_{wheel} Wheel velocity. | |

Greek upper case letters

| |
|--|
| ΔFz_{rollr} Rear axle roll load transfer. |
| ΔFz_{rollf} Front axle roll load transfer. |
| ΔFz_{pitch} Pitch load transfer. |

1 Introduction

This report describes the activity devoted to refine an existing vehicle dynamic model (VDM) for driving simulators, used to compute in Real-time the dynamics of a passenger car. This mathematical model has been implemented in the *Sim IV*, an advanced driving simulator located at the Swedish Road and Traffic Research Institute, known also as VTI, in Göteborg.

As a research institute, VTI deals with different themes related to the automotive world such as: passive safety, roads and infrastructures maintenance, tyre testing, air quality and noise measurement, traffic and driving simulation. In particular, VTI has more than forty years of experience using driving simulators and is a leading authority both in conducting simulator experiments and in developing simulator technologies.

Driving simulator experiments are very important because they allow understanding the driver response in different conditions. For example, a simulator can be used both to investigate how the driver reacts to new technologies related to active safety (i.e. lane keeping devices, stability control systems, etc.) and to investigate the effect of drug, alcohol and tiredness on the driver. Since the main target of driving simulator is to analyse driver behaviour, the driving experience should be as close as possible to reality, in order to produce accurate and credible results.

1.1 Driving simulator

A driving simulator, whose structure is shown in *Figure 1.1*, is made by different subsystems, which must work in synchrony in order to guarantee the best performance of the simulation.

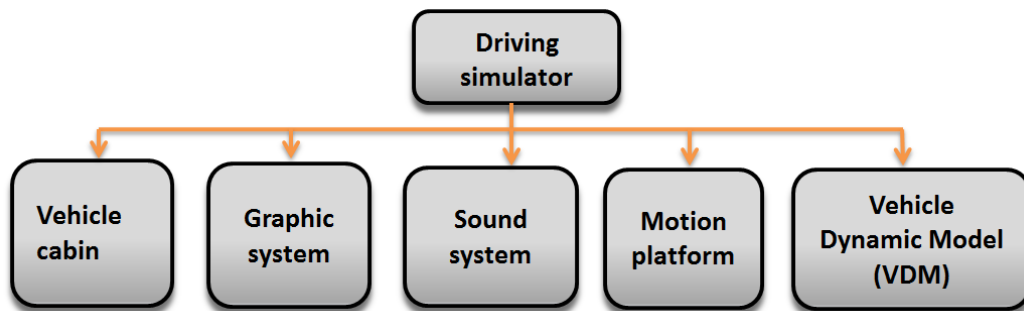


Figure 1.1: driving simulator structure.

The vehicle cabin is the main interface between the driver and the simulator. *Sim IV* can host both a car cabin (Volvo XC-60) and a truck cabin (Volvo FH 16-700): they are shown in *Figure 1.2*. The graphic system consists of a 180° screen surrounding the vehicle cabin and covering the entire driver vision field. The scenery is represented on the screen using projectors. Furthermore, all the rear view mirrors (both internal and external) have been replaced by LCD screens to represent the environment behind the vehicle, as shown in *Figure 1.3*.



Figure 1.2: vehicle cabin of Volvo XC-60 and Volvo FH 16-700.

The sound system is formed by several speakers inside the cabin. The sound model, used by the speakers, reproduces the car sound in function of different factors such as velocity, engine load, road characteristic etc. Furthermore, a microphone allows the communication between driver in the simulator and engineers in the control room.



Figure 1.3: graphic system.

The motion system is the responsible of reproducing the vehicle dynamic states, present in real driving, through several actuators. The cabin is mounted over a motion platform through a Hexapod architecture. The motion platform can move both in longitudinal and lateral directions, to generate longitudinal and lateral accelerations. Vertical displacement, yaw, pitch and roll are generated by the Hexapod system, shown in *Figure 1.4*. The aforementioned structure allows simulating both lateral and longitudinal accelerations for a maximum value of 0.6g. The VDM is the file containing the set of equations describing vehicle physics. It is used by the simulator to reproduce the dynamic of the vehicle, depending on inputs coming both from the driver (i.e. throttle position, steering wheel angle etc.) and from the road (i.e. road profile, road-tire friction coefficient, etc.).



Figure 1.4: Hexapod system.

1.2 Project definition

VTI and Chalmers University of Technology developed in 2012 a VDM for driving simulator using Modelica® as programming language.[11] The model works well, but it can be improved in different areas. The aim of this thesis is to refine this existing VDM. In particular, the work is focused on:

- Developing vertical dynamics in order to get vehicle response from road roughness.
- Improve the model to compute in a more accurate way roll and pitch response in quick transient manoeuvres.
- Developing a new steering system model to improve the steering feel provided by the VDM.

The refined model has then to be validated using the *Sim IV*.

1.3 Model characteristics

The refined model must satisfy the following characteristics:

- It must compute the vehicle motion considering 14 degrees of freedom. In particular the sprung mass has 6 degrees of freedom: 3 rotations (yaw, pitch and roll) plus 3 translations. Each wheel has 2 degrees of freedom: 1 rotation and 1 vertical translation.
- It must provide a more realistic steering feel.
- It must be parameterized in a realistic and flexible way, so that it can be used to represent different cars.
- The model must be as simple as possible (according to the targets that it has to reach), in order to be easily modified and to avoid numerical problems that cause instability while tested.

1.4 Model limitations

The VDM developed in this Master's thesis has some limitations, which are listed below:

- It is validated to perform in linear conditions because this is the range of usage of the simulator. So it represents the behaviour of a car driven in normal conditions, but it is not reliable in representing car behaviour in non-linear conditions, that is when the vehicle is driven up to its limits.
- It is developed assuming the hypothesis that the wheels are always in contact with the ground. So, wheel lift phenomenon is not captured by the model. Furthermore, camber angle is not considered.
- Wheels can move only in vertical direction, since the suspension geometry has been neglected.
- The work of this thesis does not involve a NVH (*Noise, vibration and harshness*) analysis for the vertical dynamic model.
- The steering model developed in this work has some limitations itself: it does not represent steering dynamics in parking conditions, the rack friction is constant over rack displacement and the rack damping is assumed to be linear.
- The refined model uses the previous driveline, brakes and tire models, with their own limitations.

All these limitations can be seen as a starting point for future works devoted to improve the model.

2 Background

This section aims to give an overview on the previous work, done in 2012 to develop the VDM used as a starting point of this thesis. In particular, the motivations that led to the development of the VDM are explored. Furthermore a brief description of the model is given.

2.1 Motivations

The vehicle dynamic model currently used in the simulator was initially developed in 1984 and it was implemented using FORTRAN 77 as programming language. This is a complete vehicle model which has been validated in different conditions and the results correspond well with field test data. The drawbacks of this model are several: first of all the programming language, which has a code that becomes more and more difficult to read when the model is updated or some changes are applied, if compared with newer programming languages. (For example the FORTRAN 77 code allows a maximum length of the variable name of 8 characters). Furthermore this model has been parameterized using the data of an old Volvo (V40), which has a dynamic behaviour that differs from more recent cars.

The use of FORTRAN code was probably the best option in 1984, but a lot of new programming languages have been developed in the last 25 years. Most of them provide simpler codes and more user friendly environment.

Since VTI performs a wide range of experiments in its simulator, the vehicle dynamic model should describe contemporary cars and should be easy to adjust properly, to perform different experiments. These are the reasons that led to the development of a new VDM, using a new programming language.

2.2 Programming language

Nowadays there are different programming languages for Real-Time applications. One of the most used software is Matlab Simulink[®]. It is a well-known tool for multi-domain simulation and model-based design for dynamic and embedded systems and it has extensions to run in Real-time simulations, like XPC Target available in *Sim IV*. But its block-oriented programming language has limitations in term of flexibility and ease of use. Furthermore the model implementation requires some initial mathematical work to obtain the required variables in the proper order. For these reasons Modelica[®] has been chosen as programming language. It is a non-proprietary, object-oriented and equation-based language developed by a non-profit organization. It is used to model complex physical systems and there are different commercial software using it, such as: CATIA Systems, Dymola, JModelica, AMEsim, MapleSim, MathModelica, OpenModelica, SimulationX, etc. The one used in this thesis is Dymola 2013, developed by Dassault system. A physical system can be modelled in Dymola by simply writing the equations describing it and the software deals internally with the system of equations to obtain a conventional form that can be solved numerically. Furthermore, Dymola provides feature that allow exporting the model in Simulink to run it in Real-time. So the vehicle dynamic model can be edited and modified easily and quickly in Dymola environment and can be exported to Simulink whenever it has to perform a Real-time simulation. *Figure 2.1* shows the workflow of this thesis and the software used in each step:

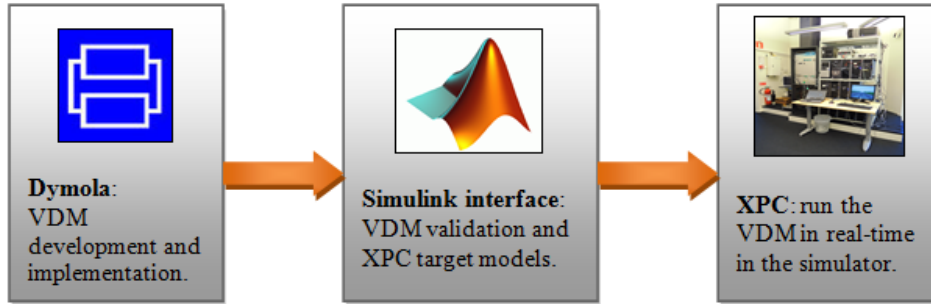


Figure 2.1: Thesis workflow.

So, the objective of VTI is to have a complete vehicle model, written in Modelica, that can be used to replace FORTRAN model in the *Sim IV*. In 2012 the first Modelica VDM was implemented at VTI by *Jorge Gómez Fernández*, [11]. It has been implemented in the *Sim IV* and it has been parameterized according to the data of a Saab 9.3 vehicle. Now there is the need to refine this model, to make it closer (in terms of completeness) to the FORTRAN one. This is the context in which this Master's thesis is written in.

2.3 Description of the starting VDM

A vehicle dynamic model is made by different subsystems: chassis, wheels, tires, suspensions, steering system, driveline and brakes. In the following paragraphs only the chassis, suspension and the steering models are described, because these are the areas on which the refinement is focused. The remaining subsystems are described in the Appendix B.

2.3.1 Chassis

The equations describing chassis motion are reported below. They are computed using as a reference *Figure 2.5*.

The equilibrium along x direction gives:

$$\begin{aligned}
 & Fx_1 \cdot \cos(\delta_{w1}) - Fy_1 \cdot \sin(\delta_{w1}) + Fx_2 \cdot \cos(\delta_{w2}) - Fy_2 \cdot \sin(\delta_{w2}) \\
 & + Fx_3 \cdot \cos(\delta_{w3}) - Fy_3 \cdot \sin(\delta_{w3}) + Fx_4 \cdot \cos(\delta_{w4}) \\
 & - Fy_4 \cdot \sin(\delta_{w4}) + F_{drag} + F_{rolling} + F_{slope} + F_{ext,x} \\
 & = m \cdot a_x
 \end{aligned} \tag{2.1}$$

The longitudinal acceleration is computed as:

$$a_x = \dot{v}_x - v_y \cdot \dot{\psi} \tag{2.2}$$

The aerodynamic resistant force is:

$$F_{drag} = -\frac{1}{2} \cdot \rho_{air} \cdot C_x \cdot v_x^2 \cdot sign(v_x) \tag{2.3}$$

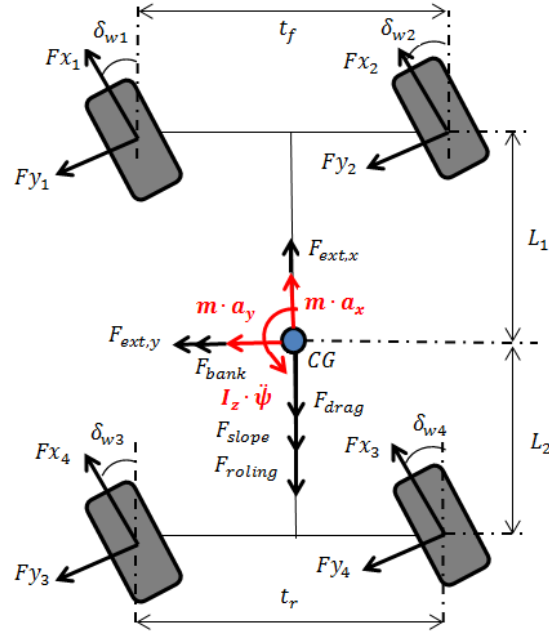


Figure 2.5: external forces acting in the X-Y plane.

The force generated by tire rolling resistance is expressed by:

$$F_{rolling} = -f_r \cdot m \cdot g \cdot \min(1, v_x) \cdot \text{sign}(v_x) \quad (2.4)$$

The longitudinal force due to gravity when a road slope is present is given by:

$$F_{slope} = -m \cdot g \cdot \sin(\varphi_{road}) \quad (2.5)$$

The equilibrium along y direction gives:

$$\begin{aligned} Fx_1 \cdot \sin(\delta_{w1}) + Fy_1 \cdot \cos(\delta_{w1}) + Fx_2 \cdot \sin(\delta_{w2}) + Fy_2 \cdot \cos(\delta_{w2}) \\ + Fx_3 \cdot \sin(\delta_{w3}) + Fy_3 \cdot \cos(\delta_{w3}) + Fx_4 \cdot \sin(\delta_{w4}) \\ + Fy_4 \cdot \cos(\delta_{w4}) + F_{bank} + F_{ext,y} = m \cdot a_y \end{aligned} \quad (2.6)$$

The lateral acceleration is computed as follows:

$$a_y = \dot{v}_y + v_x \cdot \dot{\psi} \quad (2.7)$$

The lateral force due to gravity when a road bank is present is given by:

$$F_{bank} = -m \cdot g \cdot \sin(\theta_{road}) \quad (2.8)$$

The equilibrium to rotation around z axis gives:

$$\begin{aligned}
& [Fx_1 \cdot \sin(\delta_{w1}) + Fy_1 \cdot \cos(\delta_{w1})] \cdot L_1 \\
& + [Fx_2 \cdot \sin(\delta_{w2}) + Fy_2 \cdot \cos(\delta_{w2})] \cdot L_1 \\
& - [Fx_3 \cdot \sin(\delta_{w3}) + Fy_3 \cdot \cos(\delta_{w3})] \cdot L_2 \\
& - [Fx_4 \cdot \sin(\delta_{w4}) + Fy_4 \cdot \cos(\delta_{w4})] \cdot L_2 \\
& - [Fx_1 \cdot \cos(\delta_{w1}) - Fy_1 \cdot \sin(\delta_{w1})] \cdot \frac{t_f}{2} \\
& + [Fx_2 \cdot \cos(\delta_{w2}) - Fy_2 \cdot \sin(\delta_{w2})] \cdot \frac{t_f}{2} \\
& - [Fx_3 \cdot \cos(\delta_{w3}) - Fy_3 \cdot \sin(\delta_{w3})] \cdot \frac{t_r}{2} \\
& + [Fx_4 \cdot \cos(\delta_{w4}) - Fy_4 \cdot \sin(\delta_{w4})] \cdot \frac{t_r}{2}
\end{aligned} \tag{2.9}$$

$$+Mz_1 + Mz_2 + Mz_3 + Mz_4 = I_z \cdot \ddot{\psi}$$

Newton notation will be used for time derivatives. So, the yaw acceleration and the yaw rate are expressed as follows:

$$\ddot{\psi} = \frac{d\dot{\psi}}{dt} \tag{2.10}$$

$$\dot{\psi} = \frac{d\psi}{dt} \tag{2.11}$$

The equilibrium to rotation around x axis allows computing roll angle. In particular, if the roll angle is small enough, it can be assumed:

$$\cos(\theta) \sim 1 \quad \text{and} \quad \sin(\theta) \sim \theta \tag{2.12}$$

$$\begin{aligned}
(I_x + m \cdot d_{roll}^2) \cdot \ddot{\theta} + m \cdot d_{roll} \cdot a_y + (K_{rollf} + K_{rollr} - m \cdot g \cdot d_{roll}) \cdot \theta \\
+ (D_{rollf} + D_{rollr}) \cdot \dot{\theta} = 0
\end{aligned} \tag{2.13}$$

The equilibrium to rotation around y axis allows calculating pitch angle. Again, pitch angle is assumed to be small:

$$\cos(\varphi) \sim 1 \quad \text{and} \quad \sin(\varphi) \sim \varphi \tag{2.14}$$

This gives:

$$\begin{aligned}
(I_y + m \cdot d_{pitch}^2) \cdot \ddot{\varphi} - m \cdot d_{pitch} \cdot a_x + (K_{pitch} + m \cdot g \cdot d_{pitch}) \cdot \varphi \\
+ D_{pitch} \cdot \dot{\varphi} = 0
\end{aligned} \tag{2.15}$$

The vertical displacement of vehicle CG is expressed by:

$$z = h_{CG} + d_{pitch} \cdot [\cos(\varphi) - 1] + d_{roll} \cdot [\cos(\theta) - 1] \tag{2.16}$$

Limitations

For sake of simplicity, aerodynamic drag is the only aerodynamic force considered in the model. It generates a longitudinal resistance force, which is not applied to the centre of pressure, but to vehicle CG. The vehicle rolls around the roll axis, defined as the axis joining the front and rear roll centres. Roll motion is studied considering suspensions as two torsion springs located in the front and rear roll centres, and so the roll angle is determined through vehicle rotational (roll) stiffness, according to *Equation 2.13*. Pitch is studied in a similar way, *Equation 2.15*, by considering a pitch axis with a torsion spring, located on it, generating pitch stiffness. The pitch axis is located below vehicle CG. Vertical dynamics is only affected by pitch and roll, since the road is considered as a smooth surface, horizontal or sloped. No heave is considered. Furthermore the model adopts both linear springs and dampers in the suspensions.

2.3.2 Suspensions

The suspension system is made by solid axle suspensions. Each wheel has only the rotational degree of freedom. Roll and pitch dynamics are modelled using pitch and roll axis. The distance between vehicle CG and the roll centre is:

$$d_{roll} = h_{CG} - \left\{ h_{rrc} + L_2 \cdot \sin \left[\tan^{-1} \left(\frac{h_{frc} - h_{rrc}}{L_1 + L_2} \right) \right] \right\} \quad (2.17)$$

Figure 2.9 shows the roll axis in the vehicle plan:

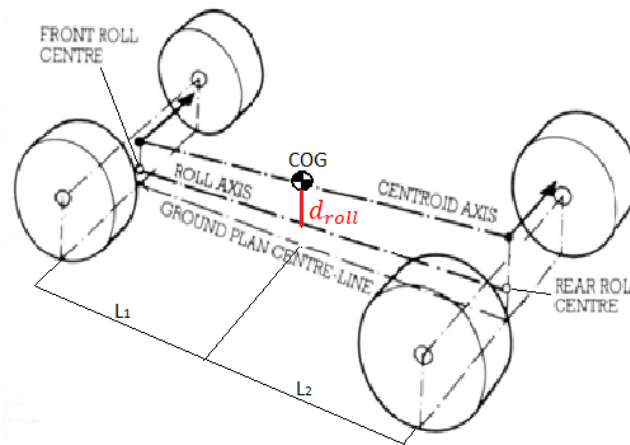


Figure 2.9: roll axis representation, adapted from Jorge Gómez Fernández (2012).

The equivalent roll stiffness of the front axle is the sum of the contribution of the springs and of the torsion bar.

$$K_{roll f} = \frac{K_{sf} \cdot t_f^2}{2} + K_{antiroll f} \quad (2.18)$$

The anti-roll bar stiffness is given by:

$$K_{antiroll f} = \frac{G \cdot I_{antiroll f} \cdot L_{antiroll f}}{L_{lever f}^2} \quad (2.19)$$

$$I_{antiroll f} = \frac{\pi \cdot d_f^4}{32} \quad (2.20)$$

The equivalent roll stiffness produced by the rear axle is computed in the same way:

$$K_{roll r} = \frac{K_{sr} \cdot t_r^2}{2} + K_{antiroll r} \quad (2.21)$$

The rear anti-roll bar provides a roll stiffness computed as:

$$K_{antiroll r} = \frac{G \cdot I_{antiroll r} \cdot L_{antiroll r}}{L_{lever r}^2} \quad (2.22)$$

$$I_{antiroll r} = \frac{\pi \cdot d_r^4}{32} \quad (2.23)$$

The equivalent roll damping of the two axles is computed as follows. This variable depends mainly on the value of the damping coefficient of the shock absorbers in the suspension system.

$$D_{roll f} = D_{shock f} \cdot t_f^2 \quad (2.24)$$

$$D_{roll r} = D_{shock r} \cdot t_r^2 \quad (2.25)$$

The lateral load transfer due to roll is computed, both for front and rear axle with *Equations 2.26* and *2.27*:

$$\Delta F_{Z_{roll f}} = \frac{\frac{K_{roll f} \cdot m \cdot d_{roll}}{t_f}}{K_{roll f} + K_{roll r} - m \cdot g \cdot d_{roll}} \quad (2.26)$$

$$\Delta F_{Z_{roll r}} = \frac{\frac{K_{roll r} \cdot m \cdot d_{roll}}{t_r}}{K_{roll r} + K_{roll f} - m \cdot g \cdot d_{roll}} \quad (2.27)$$

The pitch stiffness and damping generated by the suspensions are computed in a similar way with respect to roll stiffness and damping. *Figure 2.10* shows the pitch axis, located at a distance d_{pitch} below vehicle CG.

The pitch stiffness generated by the front and rear axles, is computed through an equivalent torsion spring located on the pitch centre:

$$K_{pitch} = \frac{K_{sf} \cdot L_1^2 + K_{sr} \cdot L_2^2}{2} \quad (2.28)$$

In a similar way, the pitch equivalent damping is computed:

$$D_{pitch} = \frac{D_{shock f} \cdot L_1^2 + D_{shock r} \cdot L_2^2}{2} \quad (2.29)$$

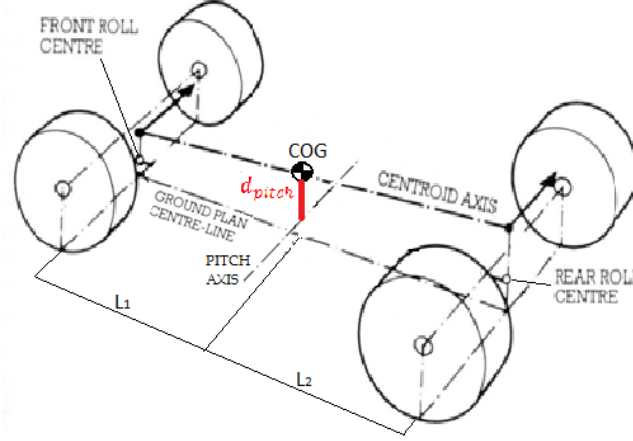


Figure 2.10: pitch axis representation, adapted from Jorge Gómez Fernández (2012).

The vertical forces acting on each tire are then computed, using *Equations 2.30 to 2.33*. They are function of the load transfer in static condition and of the load transfer due to road slope, road banking, pitch and roll.

$$Fz_1 = \frac{m \cdot g}{2} \cdot \frac{L_2 \cdot \cos(\varphi_{road}) + R_{nom} \cdot \sin(\varphi_{road}) - h_{CG} \cdot \sin(\varphi_{road})}{L_{tot} \cdot \cos(\varphi_{road})} \cdot \frac{1 - h_{CG} \cdot \tan(\theta_{road})}{t_f} - \Delta Fz_f \cdot a_y - \frac{\frac{K_{sf}}{2} \cdot L_1 \cdot \tan(\varphi) + D_{shock f} \cdot L_1 \cdot \dot{\varphi}}{2} \quad (2.30)$$

$$Fz_2 = \frac{m \cdot g}{2} \cdot \frac{L_2 \cdot \cos(\varphi_{road}) + R_{nom} \cdot \sin(\varphi_{road}) - h_{CG} \cdot \sin(\varphi_{road})}{L_{tot} \cdot \cos(\varphi_{road})} \cdot \frac{1 + h_{CG} \cdot \tan(\theta_{road})}{t_f} + \Delta Fz_f \cdot a_y - \frac{\frac{K_{sf}}{2} \cdot L_1 \cdot \tan(\varphi) + D_{shock f} \cdot L_1 \cdot \dot{\varphi}}{2} \quad (2.31)$$

$$\begin{aligned}
Fz_3 = & \\
\frac{m \cdot g}{2} \cdot & \left[1 - \frac{L_2 \cdot \cos(\varphi_{road}) + R_{nom} \cdot \sin(\varphi_{road}) - h_{CG} \cdot \sin(\varphi_{road})}{L_{tot} \cdot \cos(\varphi_{road})} \right] \\
& \cdot \frac{1 - h_{CG} \cdot \tan(\theta_{road})}{t_r} - \Delta Fz_r \cdot a_y \\
& + \frac{\frac{K_{sr}}{2} \cdot L_2 \cdot \tan(\varphi) + D_{shock r} \cdot L_2 \cdot \dot{\varphi}}{2}
\end{aligned} \tag{2.32}$$

$$\begin{aligned}
Fz_4 = & \\
\frac{m \cdot g}{2} \cdot & \left[1 - \frac{L_2 \cdot \cos(\varphi_{road}) + R_{nom} \cdot \sin(\varphi_{road}) - h_{CG} \cdot \sin(\varphi_{road})}{L_{tot} \cdot \cos(\varphi_{road})} \right] \\
& \cdot \frac{1 + h_{CG} \cdot \tan(\theta_{road})}{t_r} + \Delta Fz_r \cdot a_y \\
& + \frac{\frac{K_{sr}}{2} \cdot L_2 \cdot \tan(\varphi) + D_{shock r} \cdot L_2 \cdot \dot{\varphi}}{2}
\end{aligned} \tag{2.33}$$

Limitations

The geometry of the suspension has been simplified to the maximum and the vertical displacement of the wheels is not considered. No camber angle is present. The tire is considered always in contact with the ground with ideal camber angle. With a similar description of the suspension system, the front and rear roll centres are considered as fixed points, while actually they move according to the suspension geometry.

2.3.3 Steering system

The actual steering system model describes a rack and pinion steering. The pinion angle θ_p is computed through an internal variable δ_{int} .

$$\dot{\delta}_{int} = \frac{1}{f_{sw}} \cdot (\delta - \delta_{int}) \tag{2.34}$$

Equation 2.34 is basically a first order filter that models the steering column compliance. Then the pinion angle is computed:

$$\theta_p = \delta_{int} + D_{sw} \cdot \dot{\delta} \tag{2.35}$$

The road wheel angles δ_i are function of the pinion angle, the steering ratio, the compliance introduced by lateral force and self-aligning torque and of the roll steer.

$$\delta_{w1} = -toe_f + \frac{\theta_p}{SR} - CompFy_f \cdot Fy_1 + CompMz_f \cdot Mz_1 + Rollst_f \cdot \theta \tag{2.36}$$

$$\delta_{w2} = toe_f + \frac{\theta_p}{SR} - CompFy_f \cdot Fy_2 + CompMz_f \cdot Mz_2 + Rollst_f \cdot \theta \tag{2.37}$$

$$\delta_{w3} = -toe_r - CompFy_r \cdot Fy_3 + CompMz_r \cdot Mz_3 + Rollst_r \cdot \theta \quad (2.38)$$

$$\delta_{w4} = -toe_r - CompFy_r \cdot Fy_4 + CompMz_r \cdot Mz_4 + Rollst_r \cdot \theta \quad (2.39)$$

The torque on the steering wheel is computed as function of the front tire self-aligning torque, on the steering wheel damping and on the steering system friction. The effect of the servo assistance is also taken into account, through the coefficient C_{servo} . As a result:

$$T_{sw} = [(Mz_1 + Mz_2) \cdot SAL \cdot r_p - D_{sw} \cdot \dot{\delta} + T_f] \cdot C_{servo} \quad (2.40)$$

$$T_f = -\tanh 20 \cdot \delta \cdot \min\left(1.75, \frac{1.75}{0.18} \cdot |\delta|\right) \quad (2.41)$$

Figure 2.11 shows the friction torque in function of the steering wheel angle:

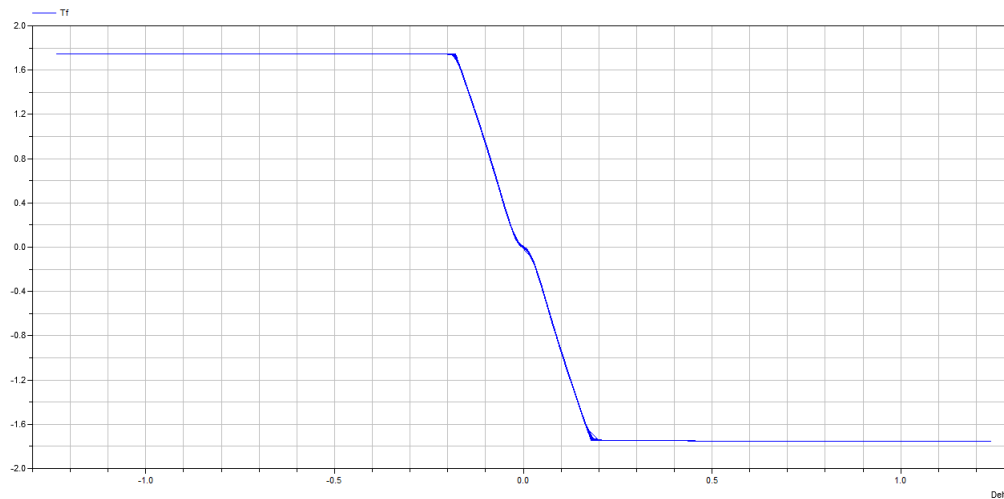


Figure 2.11: friction torque in function of the steering wheel angle.

Limitations

This steering model is very simple, but it has some limitations. So the “feel” that it provides, can be enhanced. First of all the steering resistant torque is computed only in function of the self-aligning torque. Neither the contribution of the longitudinal force nor of the vertical forces is taken into account. The steering axis inclination is not taken into account in the model, in fact neither King-pin nor caster angles are present. The friction torque computed through Equation 2.41 does not take into account hysteresis, but it rather describes friction in term of elasticity. The effect of servo assistance is simplified. Actually neither torque dependence nor speed dependence of the assistance are modelled. The way in which the pinion angle is computed, does not relate it with the resistant forces coming from the tires. It is only a function of the steering wheel angle (which is an input) and of the intermediate variable δ_{int} . Furthermore, it is true that Equation 2.34 has been introduced to take into account steering column compliance, but the same equation implies that in steady-state the steering wheel angle δ is equal to the pinion angle θ_p , but this is not true if compliance is taken into account (for example by modelling a torsion bar on the steering column).

2.4 Summary

The vehicle dynamic model used as a starting point for this thesis has been briefly analysed. As it has been said, the aim of this Master's thesis is to improve this model in different areas. The focus on the limitations has been made, essentially, for two reasons:

- In order to better understand the work of refinement behind this thesis
- To have an overview of the ways in which the model can be improved with future works.

From now on the author will refer to this starting model with the acronym VDM-10 (vehicle dynamic model with 10 degrees of freedom), to distinguish it from the refined model developed in this thesis, which will be identified as VDM-14 (vehicle dynamic model with 14 degrees of freedom). In the next chapter the work will be analysed, from the development of new mathematical models for vertical dynamics and steering system up to the validation of the model.

3 Model for Non-Linear Vertical Dynamics

The development of a non-linear vertical dynamics model is described in this section. The aim of this work is to add four degrees of freedom to the VDM-10, in order to take into account the vertical displacements of the automobile due to road irregularities, *Figure 3.1*.

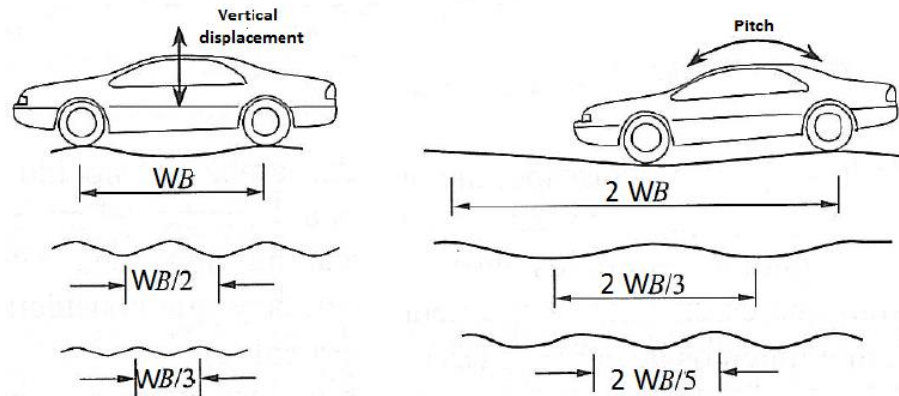


Figure 3.1: displacements of the car due to road irregularities. Adapted from Jorge Gómez Fernández (2012).

3.1 Vertical dynamics: an overview

The aim of vertical dynamics is to determine the response of the vehicle, both in terms of vibrations (not analyzed in this thesis) and in terms of exchanged forces, induced by the road irregularities. Vertical dynamics is important in the design of a ground vehicle because it affects the controllability and the stability of the automobile. In studying vehicle dynamics, three essential components are considered for typical ground vehicle:

- Sprung mass (m_s): is the mass of all the parts of the vehicle that lean on the suspension system (i.e. chassis, engine, transmission, etc.)
- Unsprung mass (m_u): is the mass of all the parts of the vehicle that can be considered as “concentrated” in the wheel hub (i.e. wheel hub, brake disk and caliper, axle, tire, wheel rim, etc.).
- The suspension system: it is the set of components connecting the sprung mass to the unsprung mass (i.e. spring, shock absorber, bump stopper, elastic bushings, etc.). The suspension plays an important role both in terms of comfort and handling. In the first case it helps to isolate vehicle cabin from the vibrations coming from road disturbances. In the second case the suspension has the task of both keeping the tire in contact with the ground and controlling wheel kinematics, to guarantee that the tire is positioned properly with respect to the road surface.

The vehicle’s kinematics and dynamics can be described from the interaction among those elements. The incorporation of road-tire interaction is also an essential part of vehicle dynamics. All the cars have non-linear characteristics of the suspension, both for comfort and handling reasons: a non-linear spring which always include a bump

stopper, and a non-linear shock absorber, with different characteristics in bump and rebound stroke. Therefore, it is important to construct a mathematical model that includes the nonlinear characteristics of the system, the general three dimensional motion of the sprung and unsprung masses and the required inertial coupling between sprung and unsprung masses. Many vehicle models have been developed and their governing equations were derived by considering energy equilibrium or dynamic equilibrium. In general, these models can be classified into three types: the quarter-car models, the half-car models, and the full-car models.

3.1.1 The quarter car models

The simplest representation of a ground vehicle is a quarter-car model. Actually, different quarter-car models with different degrees of freedom have been developed. The quarter car model is used only when the heave motion needs to be considered. The aim of this section is to give an overview on these models.

The first one, which is also the simplest, is the quarter-car model with one degree of freedom. The hypotheses at the base of this model are several:

- Since the tire vertical stiffness is much higher than the one of the suspension, connecting wheel hub to the sprung mass, it is possible to neglect the vertical displacements of the four wheel hubs (unsprung mass).
- Tire compliance is not taken into account. Tire is stiff and massless.
- The roll and pitch motions are considered negligible with respect to the vertical motion due to road irregularities. This is true, with a good approximation, for the roll motion, which is not excited by road irregularities, but it does not always hold for the pitch motion, which cannot always be neglected.

With these hypotheses the vehicle is described by the system in *Figure 3.2*:

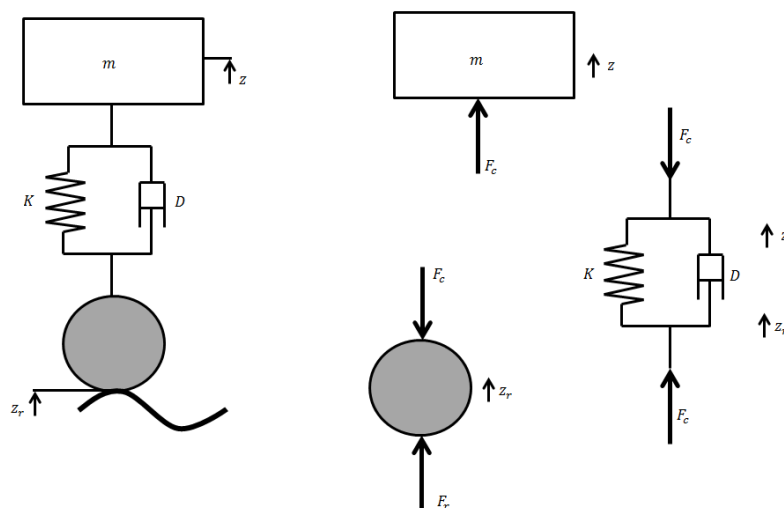


Figure 3.2: quarter car model with one degree of freedom.

The vertical equilibrium for the sprung mass gives:

$$m \cdot \ddot{z} = F_c \quad (3.1)$$

$$F_r - F_c = 0 \quad (3.2)$$

The force exerted by the suspensions on the chassis is:

$$F_c = K \cdot (z_r - z) + D \cdot (\dot{z}_r - \dot{z}) \quad (3.3)$$

This model works well in describing motions that take place at low frequencies, in the range of the sprung mass natural frequency (in most cases up to 3÷5 Hz, so in the range defined as *ride* by SAE) [7].

The quarter car model with two degrees of freedom is used to describe the motions taking place at frequencies up to the natural frequency of the unsprung mass and slightly over (up to 30÷50 Hz including *ride* and *shake* according to SAE) [7]. The hypotheses at the base of this model are:

- Tire is not considered as stiff anymore. The compliance between road and unsprung mass is modeled. Tire is considered as a massless suspension, made by a spring and a damper in parallel.
- The displacement of the four wheel hubs are taken into account.
- The roll and pitch motion are considered negligible with respect to the vertical motion of the due to road irregularities.

In the vertical dynamic models (quarter cars, half car and full car) with more than one d.o.f, usually the tire is modeled as a massless suspension, i.e. as a spring with a damper in parallel. The damping coefficient of the tire is usually very small, if compared to the one of the suspension. The VDM is thought to be run in real time at 200 Hz, and at that frequency the tire damping does not affect very much the dynamic behavior of the vehicle. For this reason it has been neglected in the original suspension model developed in this thesis. Actually, the refined model is being tested at 1 KHz: at that frequency the presence of the tire damping affects tire oscillations, which need to be damped. So, a version of the VDM with tire damping has been prepared internally at VTI, to study vehicle dynamic by running the VDM in real time at 1 KHz.

The 2 d.o.f. model is shown in *Figure 3.3*. The sprung mass vertical equilibrium is expressed through:

$$m_s \cdot \ddot{z}_s = F_c \quad (3.4)$$

The unsprung mass vertical equilibrium:

$$m_u \cdot \ddot{z}_u = F_r - F_c \quad (3.5)$$

The forces F_c , and the ones exerted by the tire due to road irregularities F_t , are expressed by *Equations 3.6* and *3.7*.

$$F_t = K_t \cdot (z_r - z_u) \quad (3.6)$$

$$F_c = K \cdot (z_u - z_s) + D \cdot (\dot{z}_u - \dot{z}_s) \quad (3.7)$$

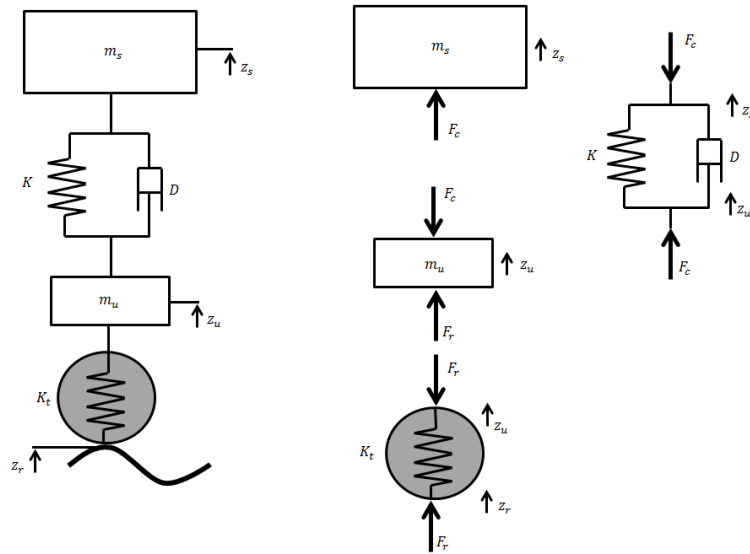


Figure 3.3: quarter car model with two degrees of freedom.

The last quarter car model analyzed is the one with three degrees of freedom. It is shown in *Figure 3.4*.

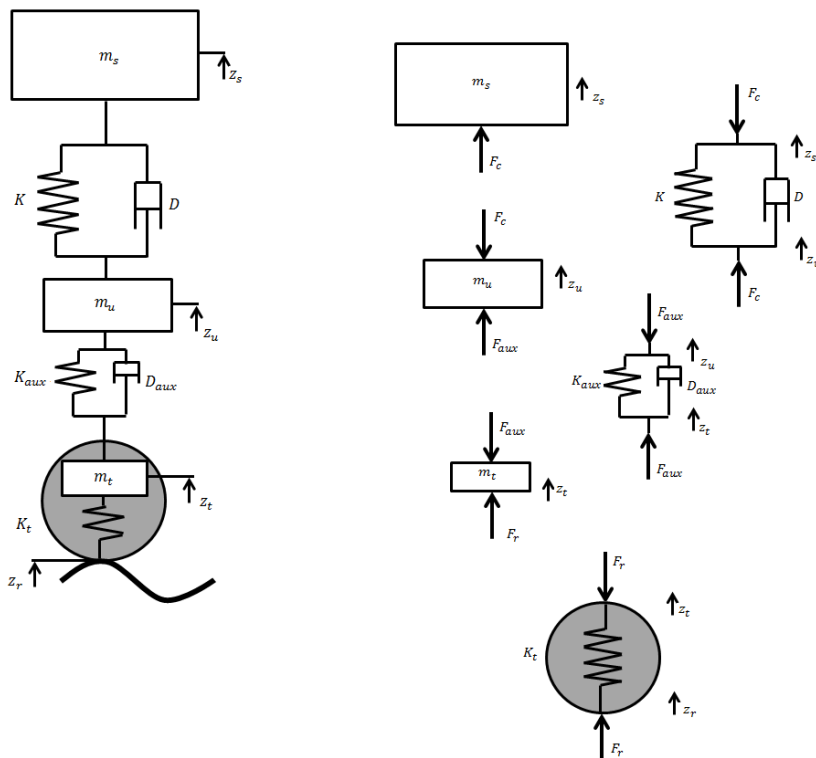


Figure 3.4: quarter car model with three degrees of freedom.

The hypotheses at the base of this model are:

- The roll and pitch motion are considered negligible with respect to the vertical motion of the due to road irregularities.
- Tire is not considered massless anymore, but it is modeled by a mass-spring-damper system. Furthermore, tire damping is not considered.
- It takes into account the compliance of the frame that connects the suspension system to the body. In fact, in many vehicles, the suspensions are not directly assembled to the body, but they are mounted on a secondary frame with a non-negligible mass. This auxiliary frame is then connected to the chassis with a secondary suspension, made with elastomeric mounts.

The equation governing the dynamics of the tire is:

$$m_t \cdot \ddot{z}_t = F_t - F_{aux} \quad (3.8)$$

Tire force F_t is still expressed by *Equation 3.6*. F_{aux} is the force exerted by the auxiliary frame both on the tire and on the unsprung mass.

$$F_{aux} = K_{aux} \cdot (z_t - z_u) + D_{aux} \cdot (\dot{z}_t - \dot{z}_u) \quad (3.9)$$

The vertical equilibrium for unsprung mass gives:

$$m_u \cdot \ddot{z}_u = F_{aux} - F_c \quad (3.10)$$

For the sprung mass equilibrium *Equation 3.4* holds.

This model is used to study the behavior of the system at frequencies higher than the first natural frequency of the tires (up to 120÷150 Hz in the range of *harshness*) [7].

3.1.2 Half car model

All the models that have been introduced up to now, take only into account the vertical displacement of the sprung/unsprung mass, while they don't take into account the effect of pitch, which is not negligible for vehicle comfort. Actually, the heave motion of the vehicle is strictly coupled with pitch motion. A model for studying the heave-pitch coupling is the half car model. Also in this case, different models are used on the basis of the variables one wants to take into account. The simplest half car model is the one shown in *Figure 3.5*. The vehicle body is considered as rigid, its dimensions are not negligible and it lies on two suspensions. The hypotheses behind this model are:

- The overturning moment due to weight $-m_s \cdot g \cdot d_{pitch}$ has been neglected, because no assumption has been made on the height of the pitch center with respect to the ground.
- Tires are considered stiff. No compliance is considered.
- The longitudinal position of the springs and of the shock absorber is assumed to be the same.
- No aerodynamic forces are considered.
- The values of stiffness K_{axi} and damping D_{axi} are the ones referring to the whole axle and so they are of a single spring or shock absorber.
- Mass m_s and moment of inertia I_y are referred to the whole sprung mass.

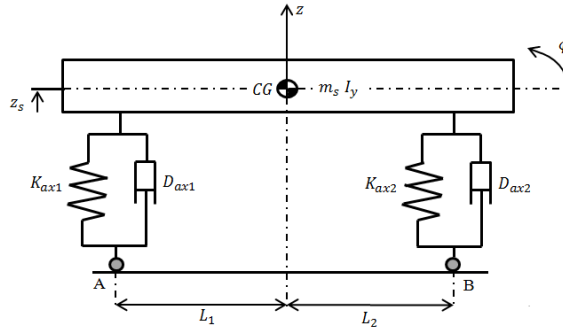


Figure 3.5: half car model.

The equation of motion describing the physics of the system is that of a beam on two elastic and damped supports.

$$\begin{aligned}
 \begin{bmatrix} m_s & 0 \\ 0 & I_y \end{bmatrix} \cdot \begin{Bmatrix} \ddot{z}_s \\ \ddot{\varphi} \end{Bmatrix} + \begin{bmatrix} D_{ax1} + D_{ax2} & -L_1 \cdot D_{ax1} + L_2 \cdot D_{ax2} \\ -L_1 \cdot D_{ax1} + L_2 \cdot D_{ax2} & L_1^2 \cdot D_{ax1} + L_2^2 \cdot D_{ax2} \end{bmatrix} \cdot \begin{Bmatrix} \dot{z}_s \\ \dot{\varphi} \end{Bmatrix} \\
 + \begin{bmatrix} K_{ax1} + K_{ax2} & -L_1 \cdot K_{ax1} + L_2 \cdot K_{ax2} \\ -L_1 \cdot K_{ax1} + L_2 \cdot K_{ax2} & L_1^2 \cdot K_{ax1} + L_2^2 \cdot K_{ax2} \end{bmatrix} \cdot \begin{Bmatrix} z_s \\ \varphi \end{Bmatrix} \\
 = \begin{Bmatrix} F_{c1} \\ F_{c2} \end{Bmatrix}
 \end{aligned} \quad (3.11)$$

Where:

$$\begin{Bmatrix} F_{c1} \\ F_{c2} \end{Bmatrix} = \begin{Bmatrix} D_{ax1} \cdot \dot{z}_A + D_{ax2} \cdot \dot{z}_B + K_{ax1} \cdot z_A + K_{ax2} \cdot z_B \\ -L_1 \cdot D_{ax1} \cdot \dot{z}_A + L_2 \cdot D_{ax2} \cdot \dot{z}_B + L_1 \cdot K_{ax1} \cdot z_A + L_2 \cdot K_{ax2} \cdot z_B \end{Bmatrix} \quad (3.12)$$

The relationship between the coordinates z_s, φ, z_A, z_B is expressed by:

$$\begin{Bmatrix} z_s \\ \varphi \end{Bmatrix} = \frac{1}{(L_1 + L_2)} \cdot \begin{bmatrix} L_2 & -L_1 \\ -1 & 1 \end{bmatrix} \cdot \begin{Bmatrix} z_A \\ z_B \end{Bmatrix} \quad (3.13)$$

The different kind of mode shapes for heave and pitch are shown in *Figure 3.6*:

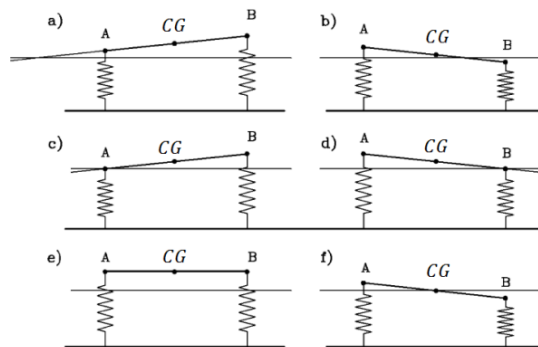


Figure 3.6: heave and pitch mode shapes, adapted from Genta, Morello (2009)

For cases *a, b, c* and *d* pitch and heave motion are coupled. If the displacements of nodes A and B have the same sign, the node (the point with zero displacement) lies outside the wheelbase and the motion is primarily translational (*a*). If the displacements of nodes A and B have opposite signs, the node is inside the wheelbase. The motion is mainly rotational, but the rotation is not about vehicle CG (*b*). Cases *c* and *d* represent two particular cases of motion mainly translational (*c*) and mainly rotational (*d*) that occur when:

$$m_s \cdot \frac{L_2}{(L_1 + L_2)} = m_s \cdot \frac{L_1}{(L_1 + L_2)} \quad (3.14)$$

But it is still impossible to distinguish between pure bounce and pure pitch. This can be done in a particular case, when:

$$L_1 \cdot K_{ax1} = L_2 \cdot K_{ax2} \quad (3.15)$$

In this case bounce and pitch uncouples, and the resulting motion is shown in case *e* and *f*.

If the tire compliance has to be taken into account the model must contain also the unsprung masses. So the heave-pitch half car model becomes the one of *Figure 3.7*. The models described in this section do not allow taking into account the effect of roll. It can be taken into account by introducing a full car model. By the way, roll rotations have a minor effect on the comfort with respect to pitch ones. For a deeper description of this topic the author suggests to refer to [7].

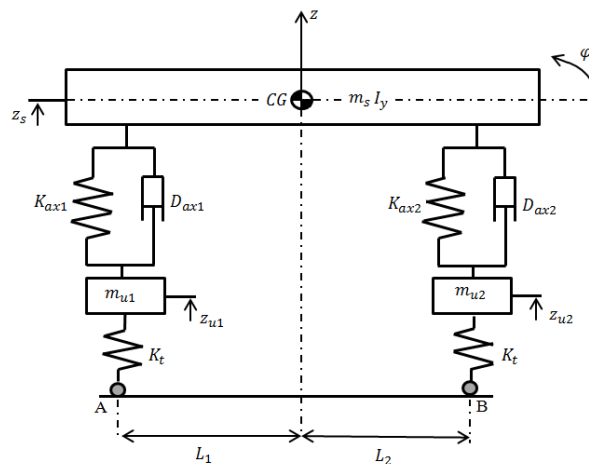


Figure 3.7: half car model with tire compliance.

3.1.3 Full car model

A more complex model is the full vehicle model, which is a four wheel model with seven degrees of freedom done for studying the heave, pitch and roll motions. It is shown in *Figure 3.8*. The vehicle body is represented by a three degree of freedom rigid cuboid. The heave, pitch and roll motions of the sprung mass are also considered. The four unsprung masses are connected to each corner of the rigid cuboid and they are assumed to be free to bounce vertically.

The model developed in this thesis is a full car model equipped with non-linear springs and dampers. It will be described in details in the following paragraphs.

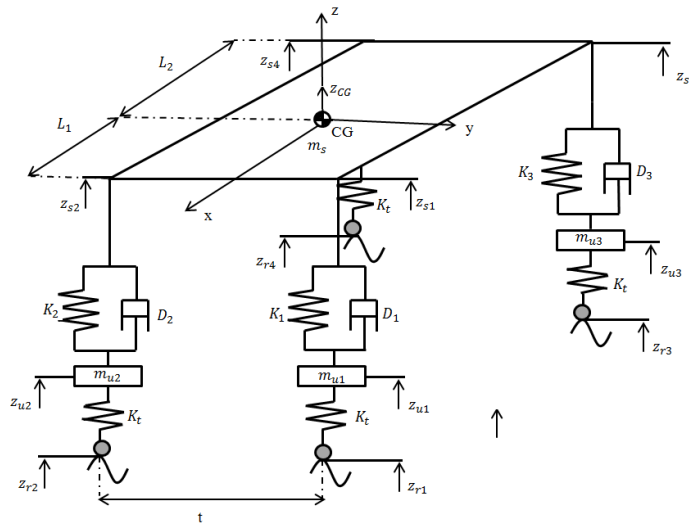


Figure 3.8: full car model.

3.2 Non-linear vertical dynamics model

Taking into account the limitations of VDM-10 described in *Sections 2.3.1* and *2.3.2*, a non-linear vertical dynamics full vehicle model has been developed, in order to take into account the effect of road irregularities and the coupling between vertical heave, pitch and roll. The model adopted is similar to the one described in *Section 3.1.3*, but with the further addition of front and rear torsion bar. It is shown in *Figure 3.9*. The hypotheses at the base of this model are:

- Each independent suspension is modelled using the quarter car model with two degrees of freedom, with all the annexed hypotheses.
- Each wheel has two degrees of freedom: a rotation and a vertical translation.
- The assumption of symmetry between left and right suspensions holds and this places the roll center symmetrically between the wheels.
- Suspension geometry is unknown and the springs are considered applied to the centre of the wheels.
- The unsprung mass is considered located at the height of the wheel hub, so at a distance R_{nom} from ground level.
- Springs and dampers in each suspension have non-linear characteristics. The wheels are assumed to be always in contact with ground with ideal camber. No camber angle is considered.
- No wheel lift phenomenon is considered.
- Roll and pitch angles are considered small enough to linearize their trigonometric functions.
- The roll axis is located at a distance d_{roll} under CG and this distance varies according the vertical displacement of the centre of gravity, and so of the suspensions. The same for the pitch axis, located at a distance d_{pitch} .

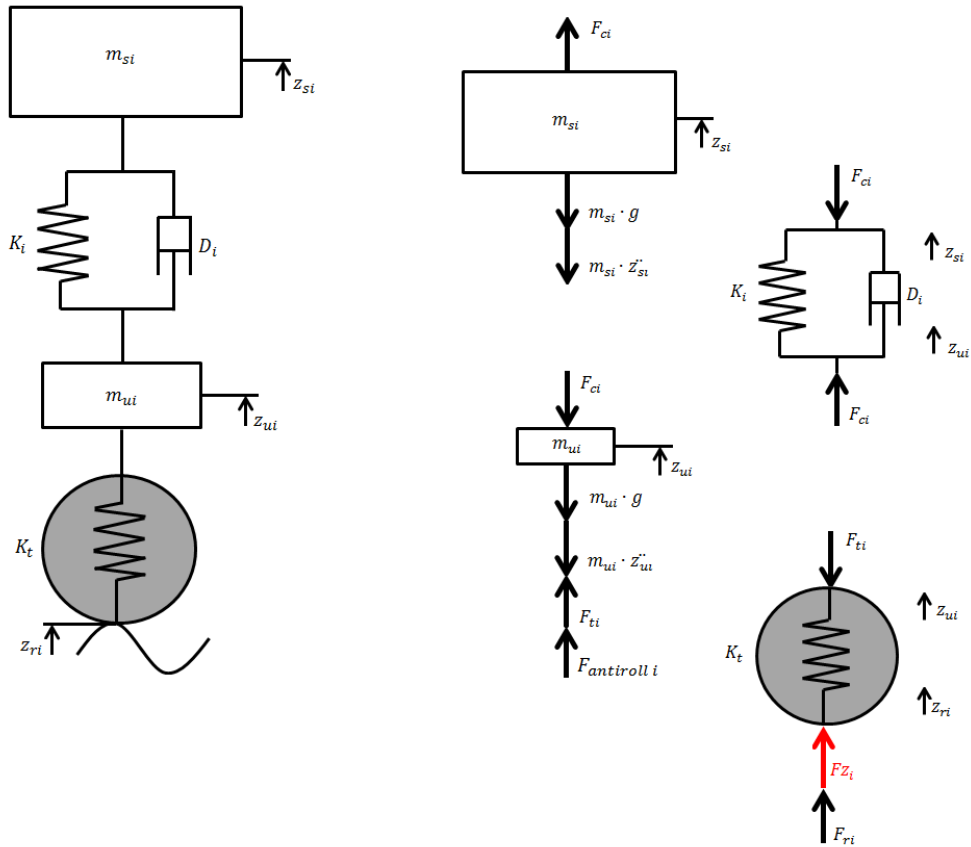


Figure 3.10: free body diagram of the suspension.

For the rear suspensions m_{si} and m_{ui} are computed as:

$$m_{s3} = m_{s4} = m_s \cdot \frac{L_1}{2 \cdot L_{tot}} \quad (3.20)$$

And:

$$m_{u3} = m_{u4} = m_u \cdot \frac{L_1}{2 \cdot L_{tot}} \quad (3.21)$$

The free body diagram of *Figure 3.10* shows that the tire is subjected to the vertical load Fz_i , due to vehicle weight. The effect of Fz_i is to generate a preload on the suspension springs due to the weight of the car. This preload “affects” both the sprung and the unsprung mass positions, and must be taken into account. In order to understand how to do it, it is useful to introduce *Figure 3.11*, where a generic system made of two springs and two masses is represented:

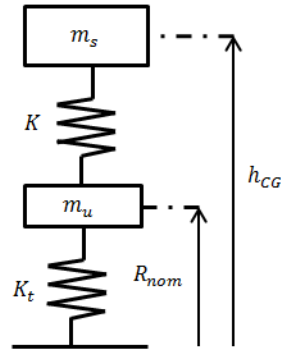


Figure 3.11: generic suspension in static condition

This system represents the suspension in static condition, i.e. when the car is stopped and its wheels are in contact with ground. In this situation, the unsprung mass is at a distance from the ground equal to the tire nominal radius R_{nom} , while the sprung mass is at a distance equal to the centre of gravity height h_{CG} . It is important to understand, that when the car is leaning on the ground the springs in the system of *Figure 3.11* have experienced a compression due to the vehicle weight and as a result have shortened. So a preload is present on these springs. Its effect on the tire spring, is shown in *Figure 3.12*.

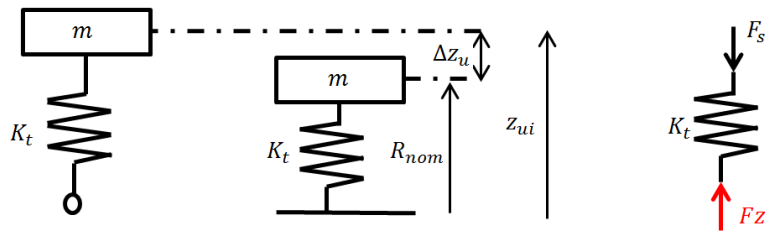


Figure 3.12: effect of the pre-load on the unsprung mass

First of all it is important to notice that the tire spring “feels” a mass which is the sum of sprung and unsprung mass. When the wheels of the car are not in contact with the road, the tire spring is in an initial position equal to z_{ui} . When the wheel is placed on the ground, the tire spring shortens of a quantity Δz_u due to the effect of F_z . If the road is completely flat, and neither banking nor slope are present:

$$F_z = \frac{m \cdot g}{K_t} \quad (3.22)$$

Otherwise F_z includes terms that describe the load transfer due to road banking and slope. From the tire spring equilibrium one gets:

$$F_z = F_s \rightarrow F_z = K_t \cdot \Delta z_u \quad (3.23)$$

Where F_s is the spring force. When the spring reaches it equilibrium under the compression of F_z it is located on a distance R_{nom} with respect to the ground.

$$\Delta z_u = z_{ui} - R_{nom} \quad (3.24)$$

Substituting *Equation 3.23* in *3.24* the initial position of the spring is computed:

$$z_{ui} = \frac{Fz}{K_t} + R_{nom} \quad (3.25)$$

The initial position of the suspension spring (and so of the sprung mass laying on it) can be computed in a similar way, starting from *Figure 3.13*.

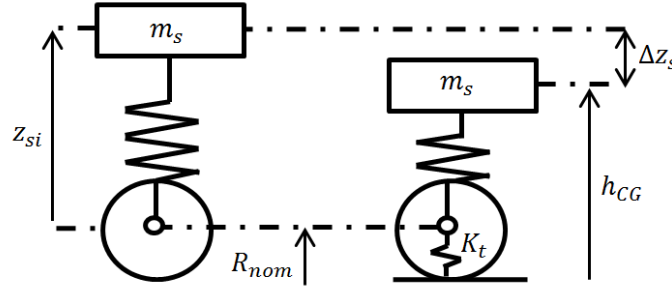


Figure 3.13: effect of the pre-load on the sprung mass.

Again, when the wheels are not in contact with the ground, the suspension spring (of stiffness K) is at its initial position z_{si} . Once the wheels are placed on the ground the suspension spring shortens of a quantity Δz_s due to sprung mass weight. The sprung mass at the static equilibrium is located at a distance h_{CG} from the ground. It is important to notice that this spring “feels” only the sprung mass weight. It is also important to notice that the lower extremity of the suspension spring is connected to the unsprung mass (located in the wheel hub), so is at a distance R_{nom} from the ground in static equilibrium condition. As a result:

$$z_{si} + R_{nom} = \frac{m_s \cdot g}{K} + h_{CG} \quad (3.26)$$

And so:

$$z_{si} = \frac{m_s \cdot g}{K} + h_{CG} - R_{nom} \quad (3.27)$$

Now that the sprung and unsprung masses lying on each suspension have been computed and their initial positions are known, it is possible to write the vertical equilibrium at the four wheel hubs.

$$F_{ci} = -m_{ui} \cdot \ddot{z}_{ui} + K_t \cdot \left[(z_{ri} - z_{ui}) + \left(\frac{Fz_i}{K_t} + R_{nom} \right) \right] - m_{ui} \cdot g \quad (3.28)$$

with $i = 1, \dots, 4$.

According to *Equation 3.29*, the total force acting on each tire is:

$$F_{ti} = K_t \cdot \left[(z_{ri} - z_{ui}) + \left(\frac{Fz_i}{K_t} + R_{nom} \right) \right] \quad \text{with } i = 1, \dots, 4 \quad (3.29)$$

So, the total force coming from the tires acting on the unsprung mass is the sum of two contributions: the term $K_t \cdot (z_{ri} - z_{ui})$ represents the force generated by the tire, F_{ri} , considered as a spring, when counteracting the displacements coming from road irregularities. The term $K_t \cdot z_{ui}$ that describes the preload to which the spring are subjected in static equilibrium conditions.

The forces F_{ci} are the forces applied by the suspension system to the chassis. They are the sum of the forces coming from springs (F_{si}), dampers (F_{di}) and anti-roll bars ($F_{antiroll\ f/r}$).

$$F_{ci} = F_{si} + F_{di} \pm F_{antiroll\ f} \quad \text{with } i = 1, 2 \quad (3.30)$$

$$F_{ci} = F_{si} + F_{di} \pm F_{antiroll\ r} \quad \text{with } i = 3, 4 \quad (3.31)$$

The anti-roll bar force is:

$$F_{antiroll\ f} = K_{antiroll\ f} \cdot (z_{s1} - z_{s2}) \quad (3.32)$$

$$F_{antiroll\ r} = K_{antiroll\ r} \cdot (z_{s3} - z_{s4}) \quad (3.33)$$

Now that the vertical forces acting over the chassis have been computed, it is possible to rewrite the equations of roll, pitch and vertical equilibrium along z axis, in a way that takes into account the presence of the suspensions and their dynamics due to road irregularities. For what concerns vertical equilibrium along z axis, *Equation 2.20*, which does not take into account heave, is replaced by *Equation 3.34*.

$$F_{c1} + F_{c2} + F_{c3} + F_{c4} - m_s \cdot g = m_s \cdot \ddot{z}_{CG} \quad (3.34)$$

Now, the displacement of the centre of gravity depends on heave, pitch and roll (according to *Equations 3.16* and *3.17*) and can be calculated integrating twice \ddot{z}_{CG} . *Equations 2.13* and *2.15* for describing roll and pitch motions do not hold anymore. The basic assumption behind *Equation 2.13*, in fact is that:

$$z_{si} = \frac{t_{f/r}}{2} \cdot \theta \quad \text{with } i = 1, \dots, 4 \quad (3.35)$$

And for *Equation 2.17* is that:

$$z_{si} = L_{1/2} \cdot \varphi \quad \text{with } i = 1, \dots, 4 \quad (3.36)$$

As a consequence all the equivalent stiffness and damping of the axles used in *Equations 2.13* and *2.17* cannot be used anymore. Now *Equations 3.16* to *3.17* hold.

The difference with respect to VDM-10 is that the roll centres move due to vertical displacements of the wheels, and so the distance between the vehicle CG and the roll axis is no more constant. *Figure 3.14* shows this concept:

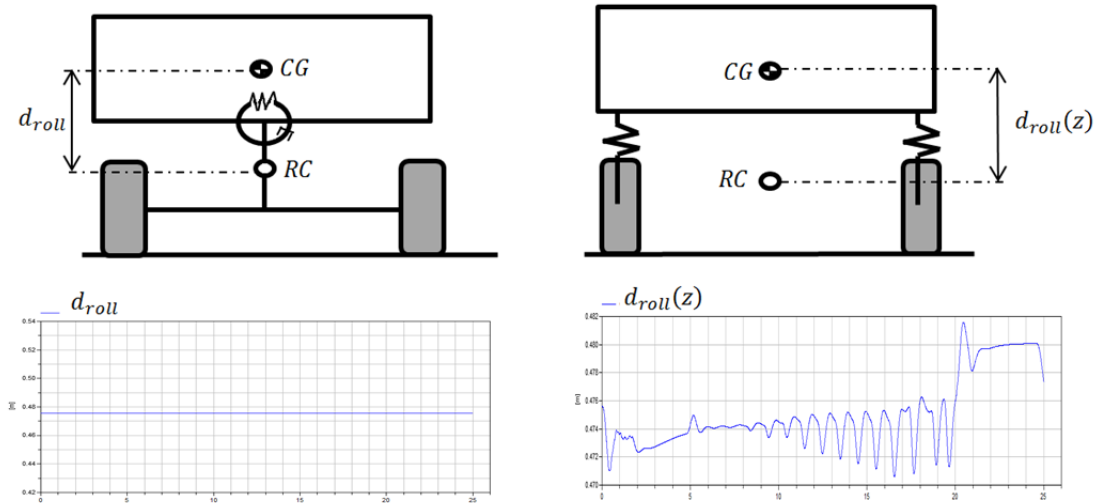


Figure 3.14: difference in the suspension model between VDM-10 and VDM-14.

As a consequence Equation 2.56 must be rewritten:

$$d_{roll}(z_{CG}) = z_{CG} - \left\{ h_{rrc} + L_2 \cdot \sin \left[\tan^{-1} \left(\frac{h_{frc} - h_{rrc}}{L_1 + L_2} \right) \right] \right\} \quad (3.37)$$

The sprung mass still rotates around the roll axis, so the new equations describing roll can be obtained starting from *Figure 3.15*. This figure represents the roll free body diagram for the front axle. In a similar way the free body diagram of the rear axle can be obtained. Once all the forces and the constraining reactions are known, the equations of motion can be written.

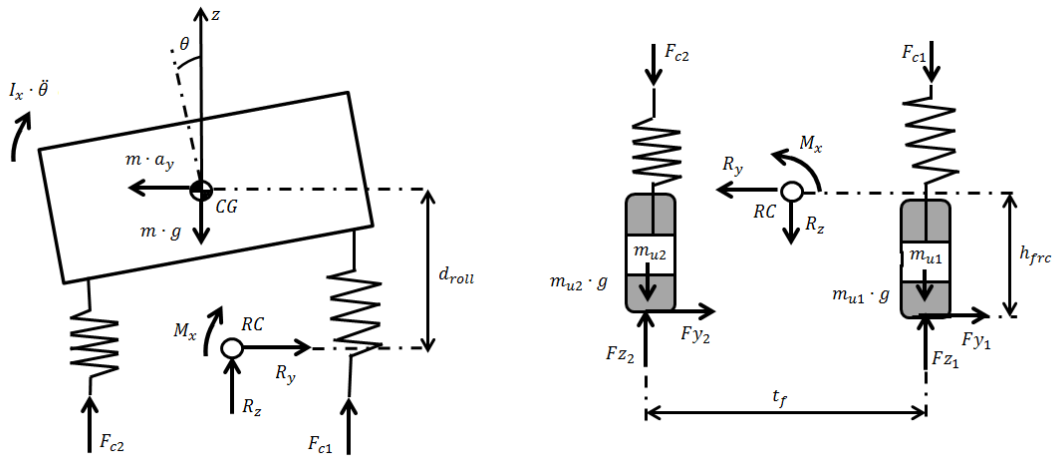


Figure 3.15: roll free body diagram.

The mass m for the front axle is the sprung mass laying over it:

$$m = m_{sf} = m_{s1} + m_{s2} \quad (3.38)$$

So the equilibrium to rotation around the roll centre for the front axle gives:

$$M_x + (F_{c2} + m_{u2} \cdot g - F_{z2}) \cdot \frac{t_f}{2} + (-F_{c1} - m_{u1} \cdot g + F_{z1}) \cdot \frac{t_f}{2} + (Fy_1 + Fy_2) \cdot h_{frc} = 0 \quad (3.39)$$

Knowing that:

$$F_{ci} = F_{zi} - m_{ui} \cdot g \quad (3.40)$$

The *Equation 3.39* becomes:

$$M_x = -(Fy_1 + Fy_2) \cdot h_{rc} \quad (3.41)$$

Once that the constraining torque M_x is known it is possible to write the equilibrium to rotation for the sprung mass:

$$M_x + (I_x + m \cdot d_{roll}^2) \cdot \ddot{\theta} + (F_{c2} - F_{c1}) \cdot \frac{t_f}{2} - m_{sf} \cdot a_y \cdot d_{roll} - m_{sf} \cdot g \cdot d_{roll} \cdot \theta = 0 \quad (3.42)$$

Substituting *Equation 3.41* into *3.42* one gets:

$$(I_x + m \cdot d_{roll}^2) \cdot \ddot{\theta} = \left[(F_{c1} - F_{c2}) \cdot \frac{t_f}{2} + (Fy_1 + Fy_2) \cdot h_{rc} \right] + m_{sf} \cdot a_y \cdot d_{roll} + m_{sf} \cdot g \cdot d_{roll} \cdot \theta \quad (3.43)$$

The total torque generated by the front axle to counteract roll is then:

$$M_{roll,f} = (F_{c2} - F_{c1}) \cdot \frac{t_f}{2} - (Fy_1 + Fy_2) \cdot h_{frc} \quad (3.44)$$

With a similar procedure the roll resistant torque generated by the rear axle can be computed:

$$M_{roll,r} = (F_{c4} - F_{c3}) \cdot \frac{t_r}{2} - (Fy_3 + Fy_4) \cdot h_{rrc} \quad (3.45)$$

Now it is possible to write the equilibrium equation to roll for the whole vehicle:

$$(I_x + m_s \cdot d_{roll}^2) \cdot \ddot{\theta} = \left[(F_{c1} - F_{c2}) \cdot \frac{t_f}{2} + (Fy_1 + Fy_2) \cdot h_{frc} + (F_{c3} - F_{c4}) \cdot \frac{t_r}{2} + (Fy_3 + Fy_4) \cdot h_{rrc} \right] + m_s \cdot g \cdot d_{roll} + m_s \cdot g \cdot d_{roll} \cdot \theta \quad (3.46)$$

This equation now replaces *Equation 2.13*. In fact *Equation 3.46* allows computing the roll angle in function of the forces that the suspensions exchange with the chassis, so the relation between roll angle and heave is now modelled.

In a similar way the new pitch equilibrium equation can be computed, starting from considering that the pitch distance varies according to the vertical displacements of the vehicle:

$$d_{pitch}(z_{CG}) = z_{CG} - h_{PC} \quad (3.47)$$

Figure 3.16 shows the free body diagram for pitch (considering half of the car). Starting from this figure one gets:

$$M_y + (F_{c1} + m_{u1} \cdot g - F_{z1}) \cdot L_1 + (F_{z3} - F_{c3} - m_{u3} \cdot g) \cdot L_2 + (F_{x1} + F_{x3}) \cdot (h_{PC}) = 0 \quad (3.48)$$

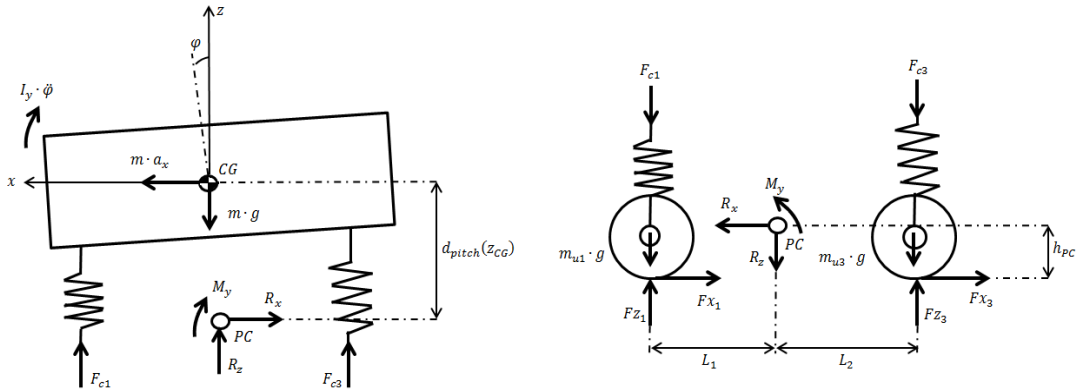


Figure 3.16: pitch free body diagram.

Substituting Equation 3.40 into 3.48 the constraining torque M_y on the pitch centre is known.

$$M_y = -(F_{x1} + F_{x3}) \cdot (h_{PC}) \quad (3.49)$$

Equation 3.48 refers to one half of the vehicle. If the total vehicle is considered and the expression of M_y is rewritten, the pitch resistant torque is computed.

$$M_{pitch} = (F_{c1} + F_{c2}) \cdot L_1 - (F_{c3} + F_{c4}) \cdot L_2 + (F_{x1} + F_{x2} + F_{x3} + F_{x4}) \cdot (h_{PC}) \quad (3.50)$$

And the equilibrium of the sprung mass gives:

$$(I_y + m_s \cdot d_{pitch}^2) \cdot \ddot{\phi} = -(F_{c1} + F_{c2}) \cdot L_1 + (F_{c3} + F_{c4}) \cdot L_2 + (F_{x1} + F_{x2} + F_{x3} + F_{x4}) \cdot (h_{PC}) \quad (3.51)$$

$$+ m_s \cdot a_x \cdot d_{pitch} + m_s \cdot g \cdot d_{pitch} \cdot \phi$$

This equation replaces Equation 2.15.

The load transfer due to roll is computed as:

$$\Delta F_{Z_{roll f}} = \frac{M_{roll f}}{t_f} \quad (3.52)$$

$$\Delta F_{Z_{roll,r}} = \frac{M_{roll,r}}{t_r} \quad (3.53)$$

In this way the load transfer takes into account also the heave motion of the wheels. For what concerns pitch, the load transfer is:

$$\Delta F_{Z_{pitch}} = \frac{M_{pitch}}{L_{tot}} \quad (3.54)$$

According to these changes in the models, also *Equations 2.30 to 2.33* have been rewritten. Now the vertical loads on the tires are computed as follows:

$$F_{Z_1} = \frac{m \cdot g}{2} \cdot \frac{L_2 \cdot \cos(\varphi_{road}) + R_{nom} \cdot \sin(\varphi_{road}) - h_G \cdot \sin(\varphi_{road})}{L_{tot} \cdot \cos(\varphi_{road})} \cdot \frac{1 - h_G \cdot \tan(\theta_{road})}{t_f} - \Delta F_{Z_{roll,f}} + L_2 \cdot \frac{\Delta F_{Z_{pitch}}}{L_{tot}} \quad (3.55)$$

$$F_{Z_2} = \frac{m \cdot g}{2} \cdot \frac{L_2 \cdot \cos(\varphi_{road}) + R_{nom} \cdot \sin(\varphi_{road}) - h_G \cdot \sin(\varphi_{road})}{L_{tot} \cdot \cos(\varphi_{road})} \cdot \frac{1 + h_G \cdot \tan(\theta_{road})}{t_f} + \Delta F_{Z_{roll,f}} + L_2 \cdot \frac{\Delta F_{Z_{pitch}}}{L_{tot}} \quad (3.56)$$

$$F_{Z_3} = \frac{m \cdot g}{2} \cdot \left[1 - \frac{L_2 \cdot \cos(\varphi_{road}) + R_{nom} \cdot \sin(\varphi_{road}) - h_G \cdot \sin(\varphi_{road})}{L_{tot} \cdot \cos(\varphi_{road})} \right] \cdot \frac{1 - h_G \cdot \tan(\theta_{road})}{t_r} - \Delta F_{Z_{roll,r}} - L_1 \cdot \frac{\Delta F_{Z_{pitch}}}{L_{tot}} \quad (3.57)$$

$$F_{Z_4} = \frac{m \cdot g}{2} \cdot \left[1 - \frac{L_2 \cdot \cos(\varphi_{road}) + R_{nom} \cdot \sin(\varphi_{road}) - h_G \cdot \sin(\varphi_{road})}{L_{tot} \cdot \cos(\varphi_{road})} \right] \cdot \frac{1 + h_G \cdot \tan(\theta_{road})}{t_r} + \Delta F_{Z_{roll,r}} - L_1 \cdot \frac{\Delta F_{Z_{pitch}}}{L_{tot}} \quad (3.58)$$

3.3 Non-linear springs

In this paragraph the implementation of a non-linear spring is analysed. The springs connect the wheel to the body elastically and store the energy produced by an uneven road profile. They also determine body position as a function of payload entity. Non-

linear springs have been modelled in the suspension system in order to take into account the presence of the bump stoppers.

The bump stopper serves as a buffer in both cases of bump and roll and is designed to control the maximum height of the bump. It also supplements the function of a spring to absorb shocks when an excessive load from the road surface is transferred to the suspension. In the case of a vehicle's turn, it controls roll of the vehicle. To this end, conventional suspension has a bump stopper in the upper end of a shock absorber damper. The introduction of a bump stop generates a force-displacement characteristic in the suspension which is no more linear, but it similar to the one in *Figure 3.17*.

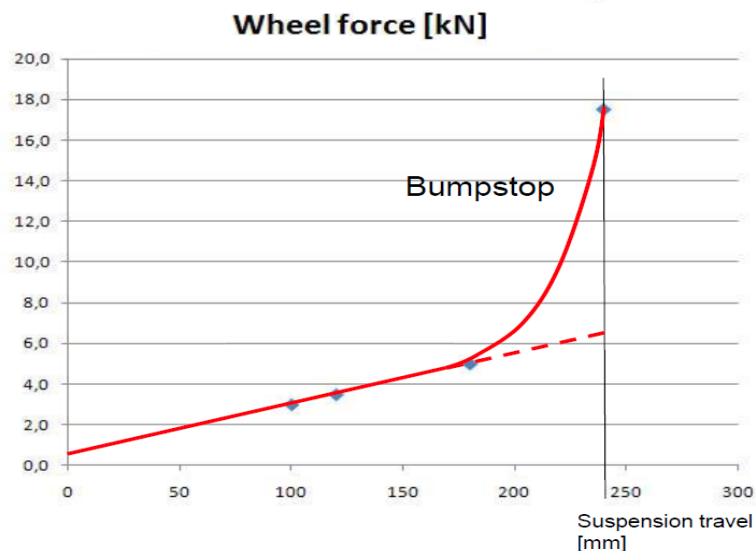


*Figure 3.17: characteristic curve of a spring with bump stopper.
Adapted from Olsson, Jacobson (2013)*

The stiffness of the spring is computed by imposing certain values of spring displacement in different load conditions. In particular three conditions are considered:

- Curb weight: is the total weight of a vehicle with standard equipment, all necessary operating consumables (e.g., motor oil and coolant), a full tank of fuel, while not loaded with either passengers or cargo. This definition may include or not the driver. According to European Union manufacturers the weight of a 75 kilogram driver is added, to follow European Directive 95/48/EC.
- Gross vehicle weight rating, known also as gross vehicle mass (GVM): is the maximum operating weight/mass of a vehicle as specified by the manufacturer including the vehicle's chassis, body, engine, engine fluids, fuel, accessories, driver, passengers and cargo but excluding any trailers.
- Full rebound: it is the condition in which the bump stopper acts.

So, for each of this load condition it is possible to compute the force acting on the suspension, and by imposing a maximum value of displacement, the spring stiffness is obtained.

3.3.1 Front springs

In this paragraph the characteristic curve F-z for the front suspensions is computed. The starting condition of the vehicle is exactly the curb weight condition (the total mass, driver included, is 1750 Kg. This is the configuration used for this simulation). So, the sprung mass acting on each of the front springs is known, and it has been computed with *Equation 3.18*. Also the force on each spring is known (preload). So each spring of the front axle has shortened of a quantity Δz_{si} with respect to the free length condition (i.e. when the wheels are not in contact with ground).

$$\Delta z_{si} = \frac{m_{si} \cdot g}{K_i} \text{ with } i = 1,2 \quad (3.59)$$

This configuration is set as a reference condition and the displacements of the spring under a full weight and during full rebound are computed relatively to the curb weight displacement (which is set to 0, since it is a reference condition, see *Figure 3.18*).

The gross vehicle weight is given by adding 4 passengers (each of them weighting 75 Kg) and 150 Kg of luggage to the curb weight. So the GVM is 2200 Kg. Using GVM instead of m_s in *Equation 3.18*, it is possible to compute the fraction of weight ($m_{GV i}$) and the force ($F_{GVM i}$) acting on each front spring in the full load condition. The maximum displacement allowed in this condition is set to z_{GVM} .

The full rebound condition is computed starting from the GVM condition and considering a vertical acceleration of 3g. With such acceleration, the wheel vertical displacement is too high to be counteracted only by the ordinary spring and the stop spring intervenes. So:

$$F_{bump\ stop\ i} = 3 \cdot g \cdot m_{GV i} \text{ with } i = 1,2 \quad (3.60)$$

The maximum displacement allowed in this case is assumed to be $z_{bump\ stop}$. *Figure 3.18* helps to understand better.

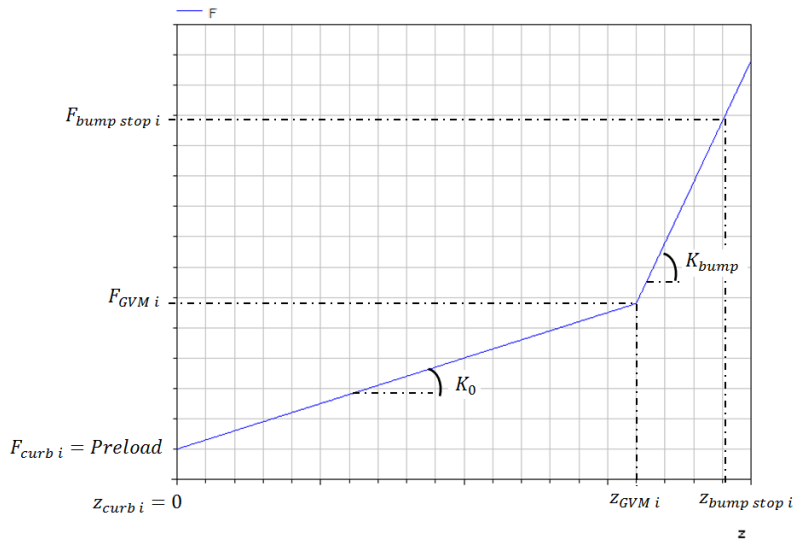


Figure 3.18: spring curve with different values of payload.

The ability of the human body to withstand vibration and related discomfort has been the object of studies and several standards on the subject have been stated. ISO 2631 standard, shown in *Figure 3.19*, distinguishes among vibrations with a frequency in the range between 0.5 Hz and 80 Hz.

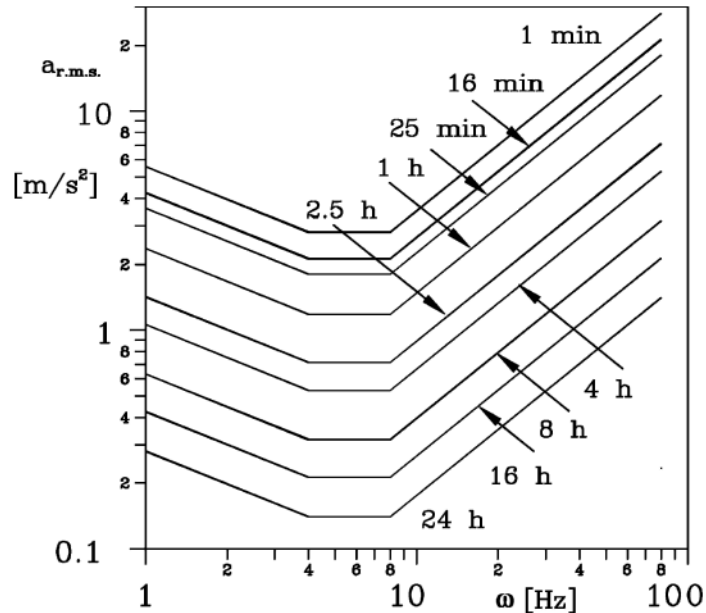


Figure 3.19: root mean square value of vertical acceleration in function of frequency. Adapted from Genta, Morello (2009).

Standards refer to the acceleration due to vibration and suggest weighting functions of the frequency to compute the root mean square values of the acceleration. Such functions depend both on the point of the body where the acceleration is applied and the direction along which it acts. The r.m.s. value of the acceleration causes, in a given time, a reduction of physical efficiency. From the plot it is clear that the frequency range in which humans are more affected by vibrations lies between 4 and 8 Hz. Frequencies lower than 0.5 – 1 Hz produce sensations that may be associated with motion sickness. Between 8 and 80 Hz this tolerance increases again in a practically linear law with frequency. In practice, what creates discomfort in that range, is not so much acceleration, but the ratio between acceleration and frequency. [7]

As a result the lower natural frequencies, those linked with the motion of the sprung mass, and so related with spring stiffness of the suspension, must be high enough to avoid motion sickness, but low enough to be well below 4 Hz. A common choice is to locate them in the range between 1.2 and 1.6 Hz.

So, the stiffness of the front springs in normal operating conditions can be computed by imposing a certain frequency of the sprung mass, as shown in *Equation 3.61*.

$$K_{0f} = m_{si} \cdot (2 \cdot \pi \cdot f_{front})^2 \quad \text{with } i = 1, \dots, 4 \quad (3.61)$$

And:

$$z_{GVM f} = \frac{F_{GVM f}}{K_{0 f}} \quad (3.62)$$

The value of $z_{bump stop f}$ is imposed by knowing some values for experience (*Table 3.1*). Typically, a wheel in full bump has an absolute displacement which is not higher than 250 mm.

The stiffness in the region where bump stopper intervenes is given by:

$$K_{bump f} = \frac{F_{bump stop} - F_{GVM}}{z_{bump stop} - z_{GVM f}} \quad (3.63)$$

Once the two stiffness coefficients are known, it is possible to compute the expression of the force generated by each spring F_{si} .

$$F_{si} = \mathbf{if} \ z_i < z_{GVM f} \quad (3.64)$$

$$\mathbf{then} \ K_{0 f} \cdot \left(z_{ui} - R_{nom} - z_{si} + \frac{m_{si} \cdot g}{K_{0 f}} + h_{CG} \right) \mathbf{else}$$

$$K_{bump f} \cdot \left(z_{ui} - R_{nom} - z_{si} + \frac{m_{si} \cdot g}{K_{bump f}} + h_{CG} - z_{GVM, f} \right) + K_{0 f} \cdot z_{GVM, f}$$

with $i = 1, 2.$

3.3.2 Rear springs

The stiffness of the rear springs can be computed in a similar way. The curb mass laying over each spring is expressed by *Equation 3.20*. Starting from this point, the procedure to compute all the forces and the masses in the different load conditions is the same as the one used with the front springs. The only difference is in the natural frequency used to compute rear springs stiffness. In fact the natural frequency of the rear suspension should be higher than that of the front, at least if the weight distribution is not such that the rear wheels are far more loaded than those in front. The importance of having a lower natural frequency for the front suspension may be explained by observing that any road input reaches the front suspension first and then, only after a certain time, the rear one. If the natural frequency of the latter is higher, when the vehicle rides over a bump the rear part quickly ‘‘catches up’’ to the motion of the front and, after the first oscillation, the body of the vehicle moves in bounce rather than pitch, a favorable factor for ride comfort.

$$K_{0 r} = m_{si} \cdot (2 \cdot \pi \cdot f_{frear})^2 \quad (3.65)$$

with $i = 3, 4$ and $f_{frear} > f_{ffront}$

$$z_{GVM r} = \frac{F_{GVM r}}{K_{0 r}} \quad (3.66)$$

$$K_{bump\ r} = \frac{F_{bump\ stop} - F_{GVM}}{z_{bump\ stop\ r} - z_{GVM\ r}} \quad (3.67)$$

And finally:

$$F_{si} = \mathbf{if} \ z_i < z_{GVM\ r} \\ \mathbf{then} \ K_{0\ r} \cdot \left(z_{ui} - R_{nom} - z_{si} + \frac{m_{si} \cdot g}{K_{0\ r}} + h_{CG} \right) \ \mathbf{else} \quad (3.68) \\ K_{bump\ r} \cdot \left(z_{ui} - R_{nom} - z_{si} + \frac{m_{si} \cdot g}{K_{bump\ r}} + h_{CG} - z_{GVM,r} \right) + K_{0\ r} \cdot z_{GVM,r} \\ \mathbf{with} \ i = 3,4$$

Figure 3.20 shows an example of characteristic curves of the front and of the rear springs:

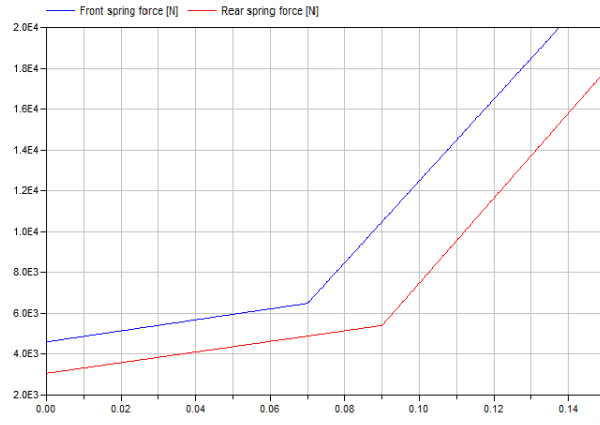


Figure 3.20: characteristic curve of the suspension implemented in Modelica for VDM-14.

3.3.3 Spring tuning

Table 3.1 resumes the value used to tune the spring stiffness. The values of displacements related to full bump conditions are computed relatively to the curb position displacement, starting from data available in [2].

Table 3.1: spring model parameters.

| PARAMETER | VALUE |
|----------------------------|---------------|
| f_{front} | [1.2,1.3 Hz] |
| f_{rear} | [1.5,1.6 Hz] |
| $z_{bump\ f}, z_{bump\ r}$ | [0.12,0.15 m] |

3.4 Non-linear shock absorber

This paragraph describes the development of non-linear shock absorbers. Apart from the nonlinearities in the behavior of the shock absorbers and those due to the geometry of the suspension, along with asymmetries purposely built in, other unwanted nonlinear effects, such as dry friction and cavitation, are often present in a real shock absorber. The latter phenomenon is primarily felt at high temperature, and consists in the vaporization of the fluid or the expansion of the gasses dissolved in it. Moreover, even in cases where shock absorbers are assumed to act in the same direction as other forces, some deviations may occur in practice, introducing further nonlinearities that should be accounted for. The model of shock absorber developed in this thesis takes into account only the non-linearities coming from the different damping coefficients in bump and rebound. Neither cavitation effects nor dry friction are taken into account. Shock absorbers are provided to absorb the elastic energy stored by the elastic members and to allow the oscillation damping of the vehicle body, avoiding stationary vibrations or resonances. This means that they are employed both to improve handling and comfort, but these two exigencies are in contrast: to increase handling a stiffer shock absorber is needed, in order to reduce the variation of the dynamic component of the tire force. But too high damping coefficients penalize comfort. So a compromise is found between handling and comfort, in tuning the force-velocity (F-V) curve of a shock absorber. In particular, shock absorbers work in two conditions: bump (compression) and rebound (extension). In extension, the damper dissipates the high values of energy stored in the spring in order to reduce oscillations of the sprung mass. In compression, the damper has the task of reducing the velocity of the wheel during its motion over an obstacle. The non-linearity of the F-V curve comes from the fact that shock absorbers have a different damping coefficient in bump and rebound. During compression, the spring and the damper act “together”, both producing a force directed “upwards” on the frame. The damping force should not be high, in order to avoid an excessive load on the suspension when the wheel travels on an obstacle, especially at high speeds. During the extension the main contribution for reducing the wheel movement comes from the damper, while the spring mainly works in compression. This causes the damping coefficient to be higher in rebound and lower in bump.

A typical characteristic of a non-linear damper is shown in *Figure 3.21*:

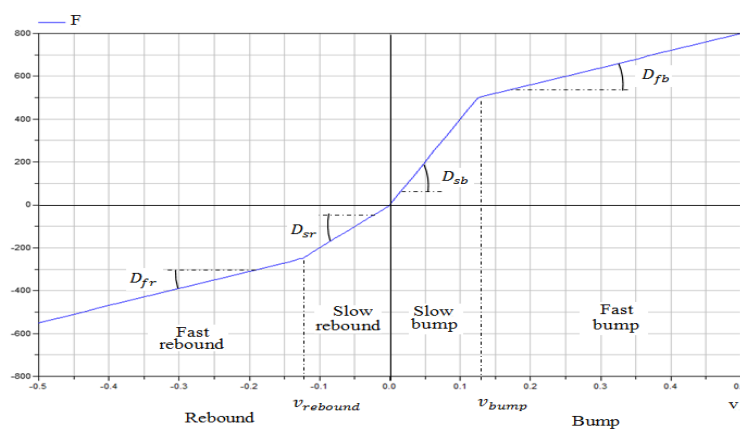


Figure 3.21: characteristic curve of non-linear damper.

Four main areas can be identified:

Fast Bump: controls the rapid upward movement of the suspension following bumps and curbs. This Bump is described as “fast” because the damper is moving up (compressing) in a rapid motion, usually above 0.100 m/s. So this adjustment controls how the suspension conforms to the road as the car it’s negotiating a bump or road undulation (in compression). The fast bump damping coefficient is D_{fb} .

Slow Bump: controls the mild upward movement of the suspension corner caused by a driver input (steering, braking, throttle, etc.). In other words, it controls the velocity at which the suspension will compress under turning, braking, and/or acceleration. This Bump is described as “slow” because the damper is moving up (compressing) in a slow motion, usually below 0.100 m/s. The slow bump damping coefficient is D_{sb} .

Slow Rebound: acts in the same way of the slow bump, but when suspension is extended due to a road profile or a pothole. The slow rebound damping coefficient is D_{sr} .

Fast Rebound: acts in the same way of the fast bump, but when suspension is extended due to a road profile or a pothole. The fast rebound damping coefficient is D_{fr} .

v_{bump} is the velocity at which there is the transition between slow and fast bump.

$v_{rebound}$ is the velocity at which there is the transition between slow and fast rebound.

The bump setting determines how fast the damper absorbs the spring energy when the spring compresses. With a soft setting, the damper allows the spring to compress more, and it takes longer to absorb all the spring energy. With a hard one, it doesn’t allow the spring to compress as much and absorbs its energy quicker.

The rebound setting determines how fast the damper absorbs the spring energy on the extension stroke. So a soft rebound setting will allow the spring to extend quickly (or push the wheel back down), this can give the car a bouncy feeling as the spring extends to quickly. A hard rebound setting will not allow the spring to extend too quickly and will absorb the spring energy quicker. This can give the car a more stable feeling.

Basically, the value of the force generated by the shock absorber depends on the shape of the curve F-V. There are several ways to model F-V curves, as *Figure 3.22* shows:

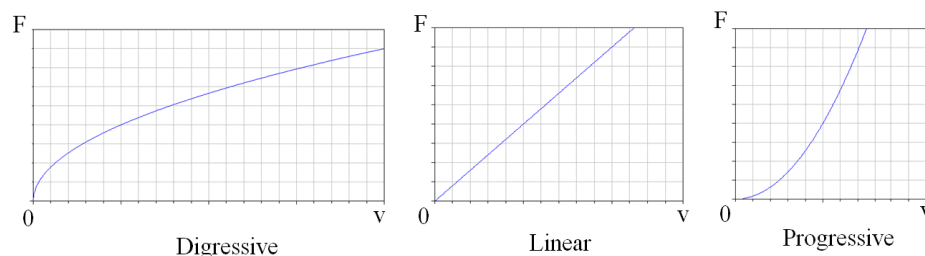


Figure 3.22: different F-V curves.

3.4.1 Shock absorber modeling

The modeling of the shock absorber F-V characteristic has been done by linearizing the curve in the different areas, i.e. fast and slow bump and fast and slow rebound, as shown in *Figure 3.21*. In this way, by simply tuning the damping coefficients in the different areas, it is possible to obtain a progressive, linear or digressive characteristic curve. Since the characteristic curves of Saab 9.3 shock absorber were not available, the reference values of damping (and of velocities) in the different areas were taken from [2], [3], [7], [12], and then they were tuned in order to improve the realism of the model. It is known from experience that the damping coefficient in rebound D_{sr} is from 1 to 5 times higher than the bump damping coefficient D_{sb} . Also this rule has been taken into account while tuning the shock absorber. *Table 3.2* resumes the range of values used in this thesis:

Table 3.2: parameters of the shock absorber model.

| PARAMETER | VALUE |
|---------------|---|
| v_{bump} | $\left[0.07, 0.2 \frac{m}{s}\right]$ |
| $v_{rebound}$ | $\left[-0.07, -0.2 \frac{m}{s}\right]$ |
| D_{sr} | $\left[800, 9000 \frac{N \cdot s}{m}\right]$ |
| D_{sb} | $\frac{1}{\Gamma} \cdot D_{sr} \quad \text{with } \Gamma = 1,5$ |
| D_{fr} | $\leq D_{sr}$ |
| D_{fb} | $\leq D_{sb}$ |

Once having imposed the values of the parameters in *Table 3.2* both for the front and rear shock absorbers, it is possible to compute the force produced by each damper, F_{di} . The four shock absorber velocities are expressed as:

$$v_i = (\dot{z}_{ui} - \dot{z}_{si}) \quad \text{with } i = 1, \dots, 4 \quad (3.69)$$

The four forces are given by:

$$\begin{aligned}
 & \mathbf{If } v_i < v_{rebound f} \mathbf{ then} \\
 F_{di} &= D_{fr f} \cdot (v_i - v_{rebound f}) + D_{sr f} \cdot v_{rebound f} \\
 & \mathbf{else if } v_{rebound f} \leq v_i < 0 \mathbf{ then} \\
 F_{di} &= D_{sr f} \cdot v_i \\
 & \mathbf{else if } 0 \leq v_i < v_{bump f} \mathbf{ then} \\
 F_{di} &= D_{sb f} \cdot v_i \\
 & \mathbf{else} \\
 F_{di} &= D_{fb f} \cdot (v_i - v_{bump f}) + D_{sb f} \cdot v_{bump f} \\
 & \mathbf{with } i = 1,2
 \end{aligned} \tag{3.70}$$

$$\begin{aligned}
 & \mathbf{If } v_i < v_{rebound r} \mathbf{ then} \\
 F_{di} &= D_{fr r} \cdot (v_i - v_{rebound r}) + D_{sr r} \cdot v_{rebound r} \\
 & \mathbf{else if } v_{rebound r} \leq v_i < 0 \mathbf{ then} \\
 F_{di} &= D_{sr r} \cdot v_i \\
 & \mathbf{else if } 0 \leq v_i < v_{bump r} \mathbf{ then} \\
 F_{di} &= D_{sb r} \cdot v_i \\
 & \mathbf{else} \\
 F_{di} &= D_{fb r} \cdot (v_i - v_{bump r}) + D_{sb r} \cdot v_{bump r} \\
 & \mathbf{with } i = 3,4
 \end{aligned} \tag{3.71}$$

Figure 3.23 shows the curves F-V for the front (blue) and rear (red) shock absorber adopted for the model, according to the parameters of Table 3.2:

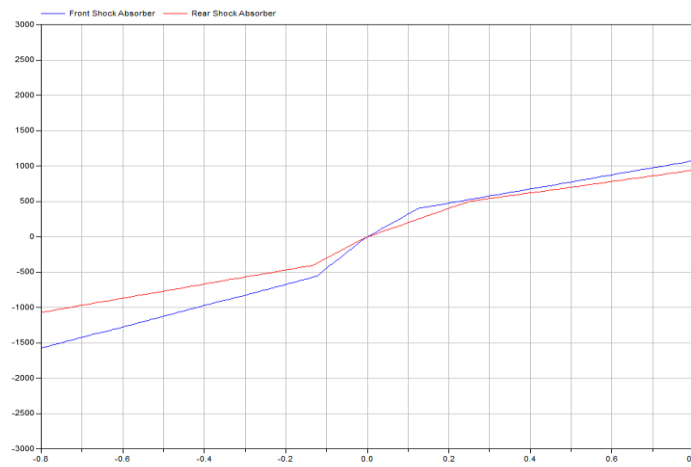


Figure 3.23: characteristic curve of front and rear shock absorbers implemented in Modelica for VDM-14.

3.5 Suspension model: summary

A vertical dynamics model has been added to the VDM-10, allowing it to take into account also heave motion. As a result, now the vehicle motion is influenced by the road profile and has 14 degrees of freedom. *Figure 3.24* shows an example of how VDM-14 reacts to a road disturbance, in particular when wheel 1 is excited by a sinusoidal disturbance.

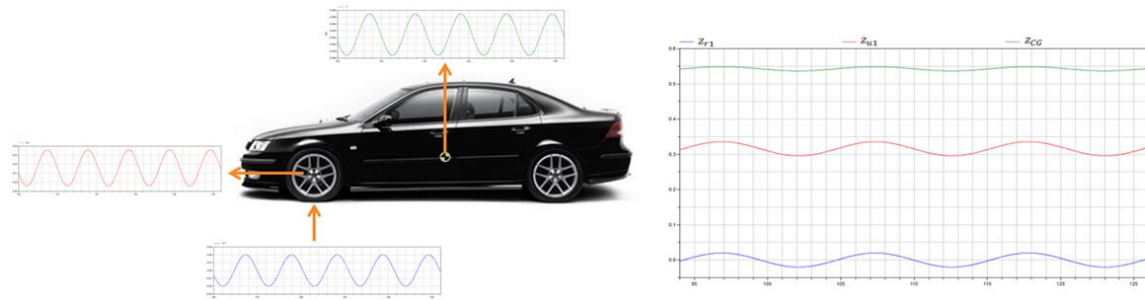


Figure 3.24: response of VDM-14 due to road irregularities.

Table 3.3 and 3.4 show an overview on the main variables and parameters used in the suspension model.

Table 3.3: main variables in the suspension model.

| SUSPENSION VARIABLES | |
|---------------------------------------|---|
| F_{ci} | Force transmitted by the suspensions to the chassis |
| F_{si} | Spring force |
| F_{di} | Damper force |
| $F_{antiroll}$ | Anti-roll bar force |
| $z_{si}, \dot{z}_{si}, \ddot{z}_{si}$ | Displacement, velocity and acceleration of the sprung mass |
| $z_{ui}, \dot{z}_{ui}, \ddot{z}_{ui}$ | Displacement, velocity and acceleration of the unsprung mas |
| z_{ri} | Road profile at wheel i |
| z_i | Displacement of the spring |
| v_i | Velocity of compression/extension of the damper |
| ΔFz_{roll} | Roll load transfer |

| | |
|--|---|
| $\Delta F Z_{pitch}$ | Pitch load transfer |
| $\theta, \dot{\theta}, \ddot{\theta}$ | Roll angle, roll rate and roll acceleration |
| $\varphi, \dot{\varphi}, \ddot{\varphi}$ | Pitch angle, pitch rate, pitch acceleration |
| θ_{road} | Road banking |
| φ_{road} | Road slope |
| d_{roll}, d_{pitch} | Distances between vehicle CG and roll and pitch axis respectively |

Table 3.4: main parameters of the suspension model.

| SUSPENSIONS PARAMETERS | |
|--------------------------|--|
| m_s | Vehicle sprung mass |
| m_u | Vehicle unsprung mass |
| m_{curb} | Vehicle curb mass |
| m_{GV} | Gross vehicle mass |
| h_{frc}, h_{rrc} | Front and rear roll centers heights |
| h_{PC} | Pitch center height |
| L_1, L_2 | Distances between vehicle CG and front and rear axles respectively |
| t_f, t_r | Front and rear track |
| f_f, f_r | Heave natural frequencies of front and rear sprung masses |
| $Z_{GVM f}, Z_{GVM r}$ | Maximum vertical displacements of front and rear suspensions in full load condition. |
| $Z_{bump f}, Z_{bump r}$ | Maximum vertical displacements of front and rear suspensions in full bump condition. |
| $F_{bump stop}$ | Maximum load on the suspension during full bump |
| F_{GVM} | Maximum load on the suspension in full |

| | |
|----------------------------|---|
| | load condition |
| v_{bump} | Transition velocity between slow and fast bump |
| $v_{rebound}$ | Transition velocity between slow and fast rebound |
| $D_{sr\ f/r}, D_{fr\ f/r}$ | Slow and fast rebound damping coefficients for front and rear shock absorbers |
| $D_{sb\ f/r}, D_{fb\ f/r}$ | Slow and fast bump damping coefficients for front and rear shock absorbers |
| $K_{0\ f/r}$ | Stiffness of front and rear springs |
| $K_{bump\ f/r}$ | Stiffness of front and rear bump stoppers |

4 Steering system

In this section the modeling of a new steering system, which replaces the one described in *Section 2.3.3*, is analyzed. The model receives as input the angular position of the steering wheel and provides as output the reaction torque on the steering wheel. The aims of the work are:

- To develop a more realistic steering model
- To improve the steering feel

The first point implies the development of a model that overcomes the limitations described in *Section 2.3.3*. For what concerns the second point, the steering model of VDM-10 was compared last year with the FORTRAN one, considered as a reference, showing a lack of steering feel and so an improvement in this area is needed. A very important part of this activity has been played by *Sim IV*: a strong correlation between modeling and simulation is required. In fact, a key point for this work is to test the steering model in the simulator in order to tune it properly. Furthermore, simulations help to find bugs that cannot be seen while working on Dymola environment.

4.1 Steering: an overview

The main function of the steering system in a vehicle is to assure directional control, by converting the steering angle into wheel angle. The steering wheel angle is transmitted to the steerable wheels through a mechanical system composed by a series of linkages rods, pivots and gears. The steering linkages, connecting the steering box and the wheels, usually conform to a variation of Ackermann-Jeantaud steering geometry, shown in *Figure 4.1*

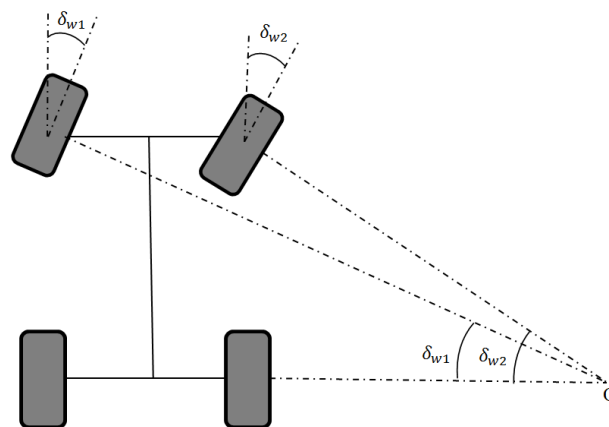


Figure 4.1: Ackermann-Jeantaud geometry.

In a turn, the inner wheel is actually travelling a path of smaller radius than the outer wheel, and so:

$$\delta_{w2} > \delta_{w1} \quad (4.1)$$

But modern cars do not use pure Ackermann-Jeantaud steering architecture, mainly because it ignores important dynamic and compliant effects that can affect road wheel angles.

For what concerns steering compliance, many efforts have been made to minimize it; nevertheless it must be considered that:

- A wheel side slip angle is always present, by steering.
- Most suspensions cause an additional steer angle with roll.
- In most cases steering wheels must have a slight toe-in angle.
- Additional steering angles are caused by suspension stroke and deformation.

In a road car, both front and rear axles are always set with a small toe angle (see *Figure 4.2*). This characteristic improves the vehicle stability when driving straight and also has an influence in the vehicle response when entering in a turn. Typically, the toe-out for the front wheel is used for front wheel drive vehicles (like the Saab 9.3 used to parameterize the VDM) and a toe-in for rear wheel drive vehicle.

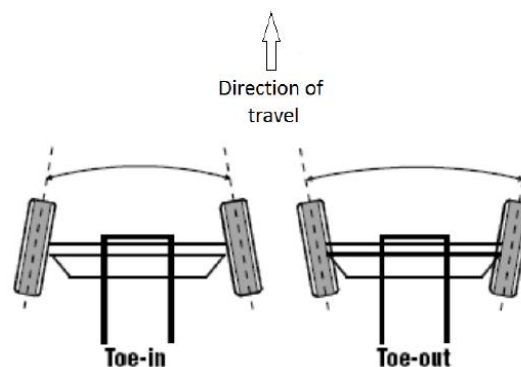


Figure 4.2: toe angles, adapted from Jorge Gómez Fernández (2012).

The suspension compliance comes from the fact that the wheels of the car are mounted to the body through the suspension linkage which is not a completely stiff system, but it presents a compliance due to the flexion of the suspension arms, the rubber bushes and ball joints used to connect the different links, generating additional (added or subtracted) steering angles in the wheels, *Figure 4.3*.

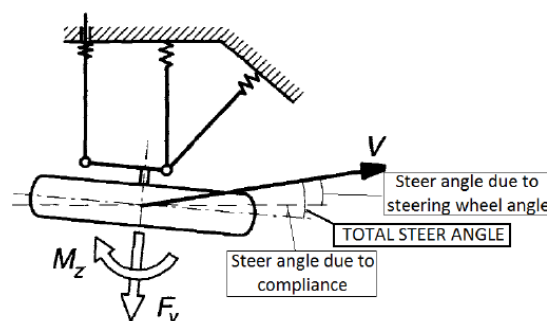


Figure 4.3: suspension compliance, adapted Nordmark S., (1984).

An effective way to evaluate the suspension compliance is to consider the steering angles generated by compliance proportional to the forces and aligning torques

produced by the tires. An additional term added to the suspension compliance is the usually called roll steer or bump steer. Roll steer is the change in the steering angle of a wheel when the wheel moves in its 3D movement of bump and rebound. This change in the steering angle with the wheel vertical displacement can be considered as a function of the vehicle's roll angle and definitely has an influence in the vehicle behaviour.

For what concerns the dynamic effects, the Ackerman-Jeantaud model doesn't take into account that, if the steering occurs at a speed which is not vanishingly small, the wheels must move with suitable sideslip angles to generate cornering forces in order to balance the centripetal force. As a result, Ackerman-Jeantaud model works for very low speeds (kinematic steering), but when the velocity increases it does not provide an accurate description of steering dynamic. In fact, during dynamic steering, the point O of *Figure 4.1* is not anymore aligned with rear axle, but it moves depending on the side slip angles, as shown in *Figure 4.4*:

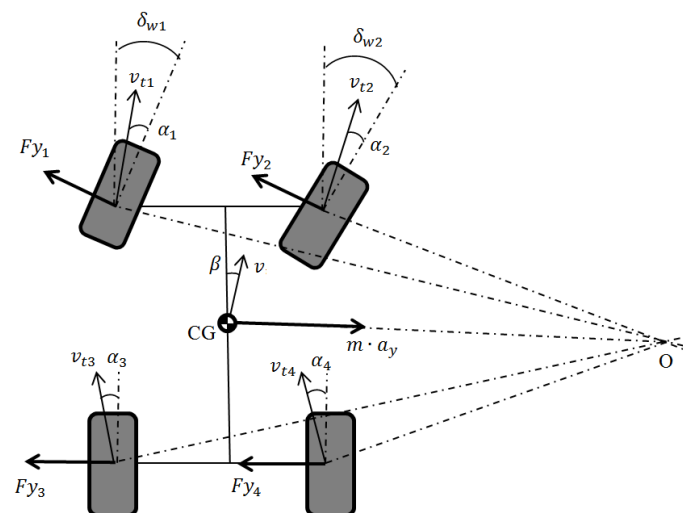


Figure 4.4: dynamic steering.

This means that when designing the steering wheel architecture, it must be taken into account that the minimum radius of curvature available in normal driving depends mainly on the road wheel angles, and so on the steering system geometry. But at higher speeds the limit of path curvature is rather related to the maximum centripetal force that can be generated then to the road wheel angles. This is governed by the limiting friction coefficient between road and tires, μ_i . For typical passenger car, the region in which geometry dominates the steering behavior is small, until 20 Km/h, [13].

The steering model developed in this thesis takes into account all these phenomena, and the road wheel angles depend on suspension compliance, roll steer and toe angles, as expressed by *Equations 2.36 to 2.39*.

The other important function of the steering system is to provide to the driver a good “feel” of the behaviour of the car on a road. Subjectively, impressions of vehicle behaviour are gathered to a significant extent through the hand wheel, whether consciously or subconsciously. A great deal effort is concentrated in modern cars on the manner in which torque is transmitted back to the driver up the steering column.

Steering feel is correctly given a great deal of importance in road car design since it is the primary mean by which the driver comprehends the dynamics of the vehicle. Accurate modelling of the steering feel is difficult and requires a great deal of data about friction in the individual joints plus a good characterization of the electrical or hydraulic power assist. In particular steering torque feedback helps the driver reduce steering variability and locate on centre position more quickly following a manoeuvre. It is also thought that the driver can respond more quickly to kinaesthetic cues than those perceived through vision [13].

Changes in the steering torque are a primary input for drivers to detect vehicle behaviour. When driving normally, the tires generate forces by distortions in the contact patch that result in a moment attempting to return the tire to zero slip angle condition. As the front tires get close to their frictional limit (i.e. when the lateral forces are maximized), the deformed shape of the patch changes so that the self-aligning torque falls to its minimum, *Figure 4.6*.

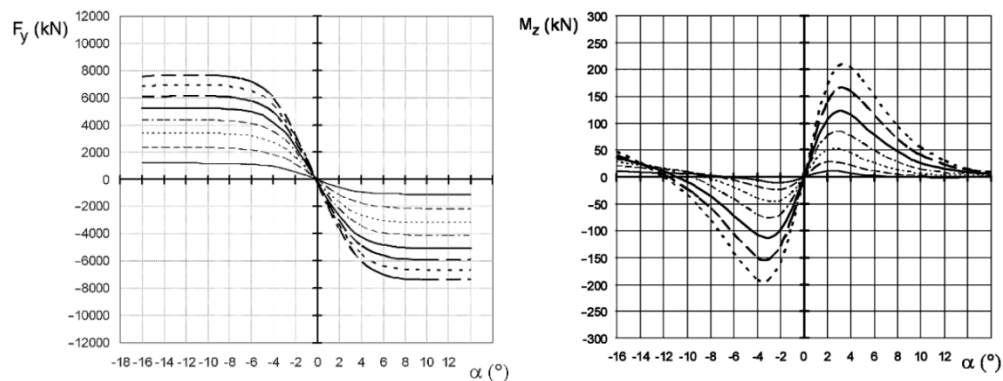


Figure 4.6: Self-aligning torque and lateral force. Adapted from Genta, Morello (2009).

This phenomenon generates some changes in the resistant torque perceived by the driver, who is then aware of the fact that the car is reaching limit conditions. If this drop in the self-aligning torque occurs abruptly the driver can have the impression of losing control of the vehicle. For a more detailed description of these topics, see [6],[7], [13] and [14].

4.2 Rack and pinion model

The steering system modelled in this thesis is a rack and pinion one. This steering mechanism is widely used on nowadays cars: its advantages are:

- It tends to be more precise because there are fewer parts and pivot points. Because of this, the steering is more responsive and easier to control.
- The reduced number of components reduces the weight and makes it easy to repair.
- It gives a good "road feel" not only in terms of "feedback", but also in terms of quickness of response.

Figure 4.7 shows the rack and pinion steering system with all the main components:

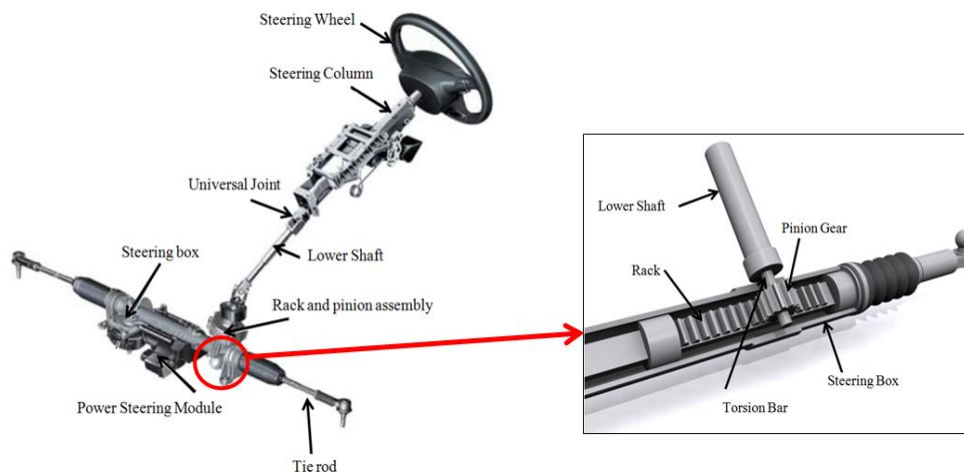


Figure 4.7: rack and pinion steering model.

The system comprises of a steering wheel turning a steering column. The steering column is connected to an intermediate shaft through a universal joint. The universal joint transmits torque to a lower shaft. It is mainly used for “packaging” reasons. In fact, thanks to the fact that it allows transmitting a torque to an inclined shaft, the lower shaft can be properly arranged in order to optimize the space in the engine compartment. A pinion at the end of the lower shaft mates with the rack and converts the column rotary motion into translatory motion of the rack. In power assisted steering usually a torsion bar is present. It is connected between the lower shaft and the pinion. Its torsion is used to compute the degree of assistance needed by the driver. A ball joint is used to connect the end of the rack to the tie rod, which is connected, on the other end, to the steering arm lever (SAL). The steering axis is the axis around which the wheels rotate during steering. It is defined by the line that runs through the upper and lower steering pivots, depending on the geometry of the suspension. Generally, the steering axis is inclined in the space. This inclination is important because it affects the entity of the torque perceived by the driver, and is defined by two angles: the king pin and the caster, as shown in *Figure 4.8*.

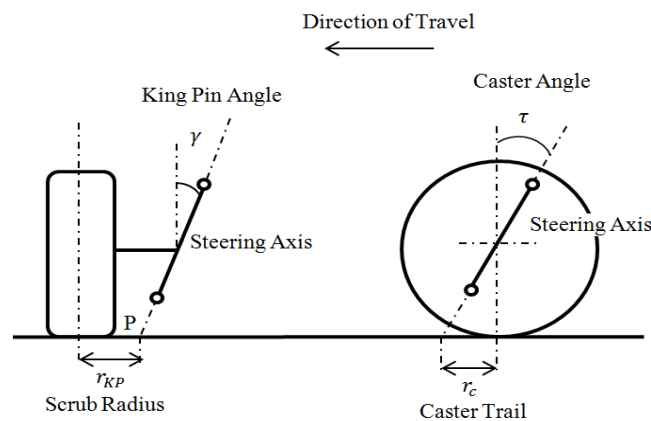


Figure 4.8: steering axis inclination.

The main purpose of the caster angle is to create a self-centring effect in the steering.

The consequence of a caster angle different from zero is the presence of a caster trail which can be positive or negative. The caster trail can be:

- Zero: when caster angle is equal to zero.
- Positive: if the centre of the tire contact patches lies between the steering axis projection and the frame, on side view.
- Negative: if the projection of the steering axis on the ground lies between the frame and the centre of the tire contact patch, on side view.

Caster affects directly the steering feel in terms of toughness of steering and self-aligning torque. If the caster trail is positive, when the wheel is steered, the lateral forces will generate a torque around the steering axis, counteracting the wheel movement. As a result the self-aligning torque of the steering will be higher and the steering wheel will align quickly. This worsens a little the behaviour of the vehicle while entering in a turn, but reduces understeering in the exit and the vehicle will maintain the turning trajectory better. The drawback is that the steering wheel will be tougher to move. Vice versa, with a negative caster trail, when the wheels are steered, the lateral forces will produce a torque that helps them steering. As a result, the entry of the turn is improved as well as the directionality in low-speed turns, but more oversteering will be present while exiting from a turn. Furthermore the steering will become more unstable at high speed. The advantage is that the steering wheel will be less tough to move. One can say that the first solution improves handling while the second comfort. The value of the caster trail is a compromise between these two exigencies.

The purpose of a kingpin angle is to set the scrub radius of the steered wheel. This is the offset between the tire's contact point with the road surface and the projection of the steering axis on the ground. The value of the scrub radius is generally on the order of some millimetres. In particular, the scrub radius can assume three values:

- Zero: when the distance between the central point of the tire contact patch and the point P is equal to zero (Point P is given by the intersection of steering axis projection with ground).
- Positive: when the central point of the tire contact patch is external to the steering axis (with respect to the frame).
- Negative: when the central point of the tire contact patch is internal to the steering axis (with respect to the frame).

A zero scrub radius doesn't transmit any reaction to the steering, improving the comfort. But this configuration is never used. In fact, since no reaction is transmitted to the steering, the driver is not able to perceive the change of attitude of the vehicle, which becomes "undrivable".

In case of negative scrub radius, when the wheel is steered, the longitudinal forces will produce a torque that "helps" the wheel to steer more. As a result the vehicle becomes more "oversteering". This configuration can be used on front wheel drive vehicles in order to attenuate their natural understeering behaviour. The comfort is improved, but the drawback is that the steering is less reactive, in particular in terms of self-aligning torque.

If the scrub radius is positive, the longitudinal forces will produce a torque around the steering axis that will counteract the steering of the wheel. As a result the vehicle

becomes more "understeering". This configuration is used on rear wheel drive vehicles, in order to improve their natural tendency to oversteering. With this configuration the steering becomes more reactive, especially in terms of self-aligning torque. This helps the driver to understand and evaluate better the limits of the vehicle, but it reduces comfort, because the steering becomes more sensitive to tire forces.

The value of the scrub radius is defined during the design phase. Its value is a compromise between the aforementioned exigencies and depends on the desired level of sensibility of the steering with respect to the forces exchanged between tire and ground during motion.

4.3 Mathematical modelling

The steering system shown in *Figure 4.7* has been modelled on the base of the following hypotheses:

- The variation of angular ratio of all universal joints has been neglected.
- The torsion bar is modelled as a massless spring.
- Both rack (D_{rack}) and torsion bar (D_{tb}) damping are considered,
- The length of the steering arm lever is considered constant.
- The damping and the inertia of steering wheel and of the steering column are included in the terms J_{sw} and D_{sw} .

With these assumptions the model can be represented as the one in *Figure 4.9*

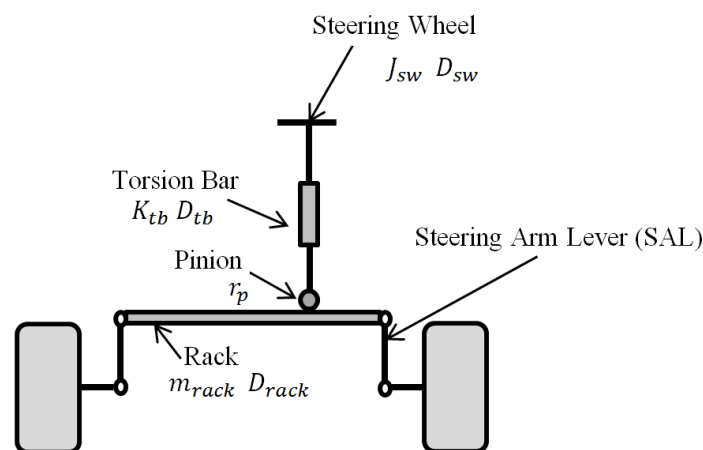


Figure 4.9: mathematical model of the steering system.

The starting point is to compute the resistant torque produced by the tire forces around the steering axis, taking into account both caster and king pin angles. This has been done by following *ISO 8855* regulation.

The total forces acting along x direction in the front tires are:

$$FX_i = (Fx_i - F_{rollingi}) \cdot \cos(\delta_{wi}) - Fy_i \cdot \sin(\delta_{wi}) \quad \text{with } i = 1,2 \quad (4.2)$$

The total forces along y direction are:

$$FY_i = Fy_i \cdot \cos(\delta_{wi}) + (Fx_i - F_{rollingi}) \cdot \sin(\delta_{wi}) \quad \text{with } i = 1,2 \quad (4.3)$$

The total torque produced around the steering axis by the generic force F_X can be computed starting from *Figure 4.10*:

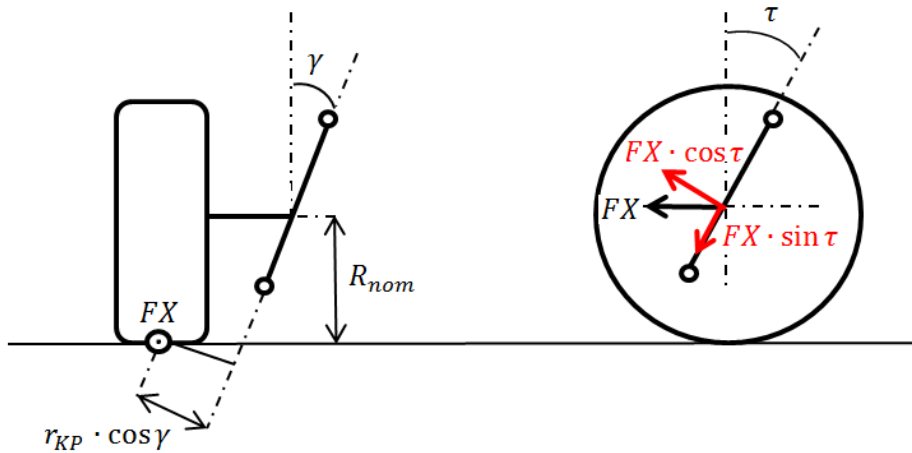


Figure 4.10: scheme used to compute the resistant torque produced by F_X .

So the resistant torque produced by force F_X is:

$$Mr_{FX} = FX \cdot \cos(\tau) \cdot [r_{KP} \cdot \cos(\gamma) + R_{nom} \cdot \sin(\gamma)] \quad (4.4)$$

The resistant torque due to F_Y is computed by taking into account that the lateral force is not applied directly to the centre of the tire contact patch, but at a distance t from it, as shown in *Figure 4.11*.

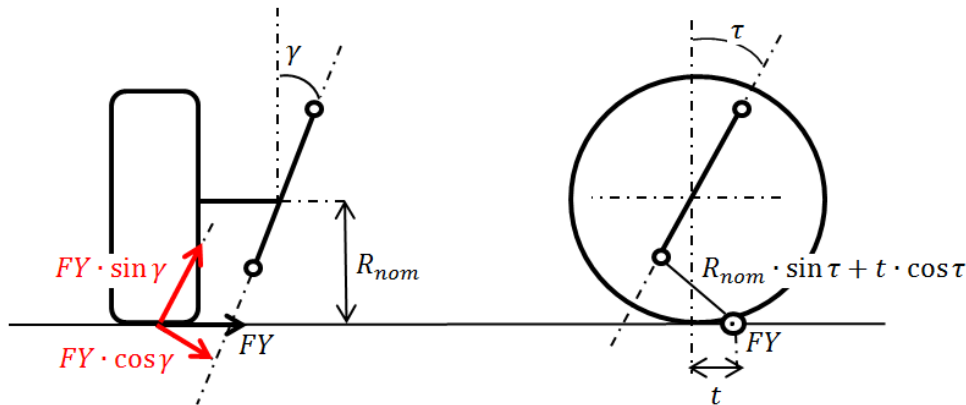


Figure 4.11: scheme used to compute the resistant torque produced by F_X .

This gives:

$$Mr_{FY} = FY \cdot \cos(\gamma) \cdot [R_{nom} \cdot \sin(\tau) + t \cdot \cos(\tau)] \quad (4.5)$$

The total torque produced by Fz is computed starting from *Figure 4.12* and adding the contribution due to caster and road wheel angle:

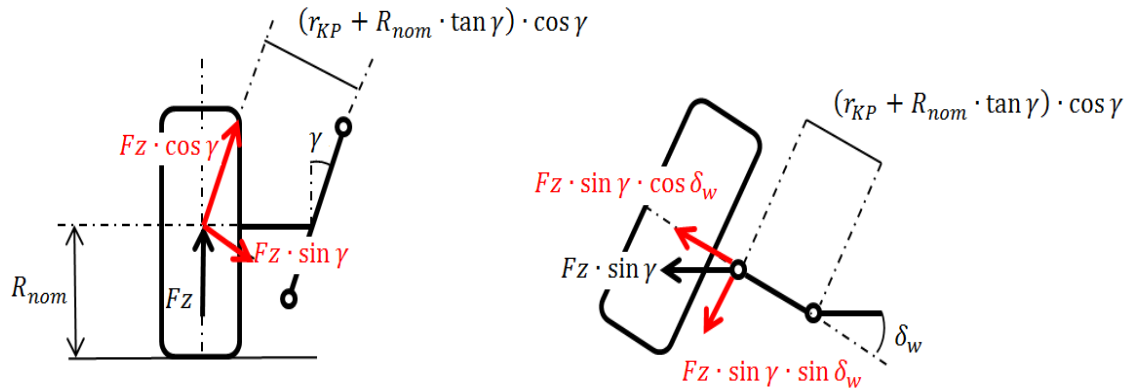


Figure 4.12: scheme used to compute the resistant torque produced by FZ .

As a result:

$$Mr_{Fz} = Fz \cdot \sin(\gamma) \cdot \sin(\delta_w) \cdot \cos(\tau) \cdot \{[r_{KP} + R_{nom} \cdot \tan(\gamma)] \cdot \cos(\gamma)\} \quad (4.6)$$

The total resistant torque produced by each wheel around the steering axis is then:

$$\begin{aligned} Mr_1 = & \\ -FX_1 \cdot \cos(\tau) \cdot [r_{KP} \cdot \cos(\gamma) + R_{nom} \cdot \sin(\gamma)] + FY_1 \cdot \cos(\gamma) & \quad (4.7) \\ \cdot [R_{nom} \cdot \sin(\tau) + t \cdot \cos(\tau)] + Fz_1 \cdot \sin(\gamma) \cdot \sin(\delta_{w1}) & \\ \cdot \cos(\tau) \cdot \{[r_{KP} + R_{nom} \cdot \tan(\gamma)] \cdot \cos(\gamma)\} & \end{aligned}$$

$$\begin{aligned} Mr_2 = & \\ FX_2 \cdot \cos(\tau) \cdot [r_{KP} \cdot \cos(\gamma) + R_{nom} \cdot \sin(\gamma)] + FY_2 \cdot \cos(\gamma) & \quad (4.8) \\ \cdot [R_{nom} \cdot \sin(\tau) + t \cdot \cos(\tau)] + Fz_2 \cdot \sin(\gamma) \cdot \sin(\delta_{w2}) & \\ \cdot \cos(\tau) \cdot \{[r_{KP} + R_{nom} \cdot \tan(\gamma)] \cdot \cos(\gamma)\} & \end{aligned}$$

The resistant forces acting on the rack are then:

$$Fr_i = \frac{Mr_i}{SAL} \quad \text{with } i = 1,2 \quad (4.9)$$

When the steering wheel is turned, the torsion bar twists of an angle equal to:

$$\theta_{TB} = \delta - \frac{x_{rack}}{r_p} \quad (4.10)$$

The twisting on the torsion bar produces a torque acting on the pinion, which makes the rack to translate of a quantity x_{rack} . This torque depends both on the stiffness of the torsion bar and on its damping properties and is equal to:

$$T_{TB} = K_{TB} \cdot \theta_{TB} + D_{TB} \cdot \dot{\theta}_{TB} \quad (4.11)$$

The rack-pinion free body diagram is shown in *Figure 4.13*.

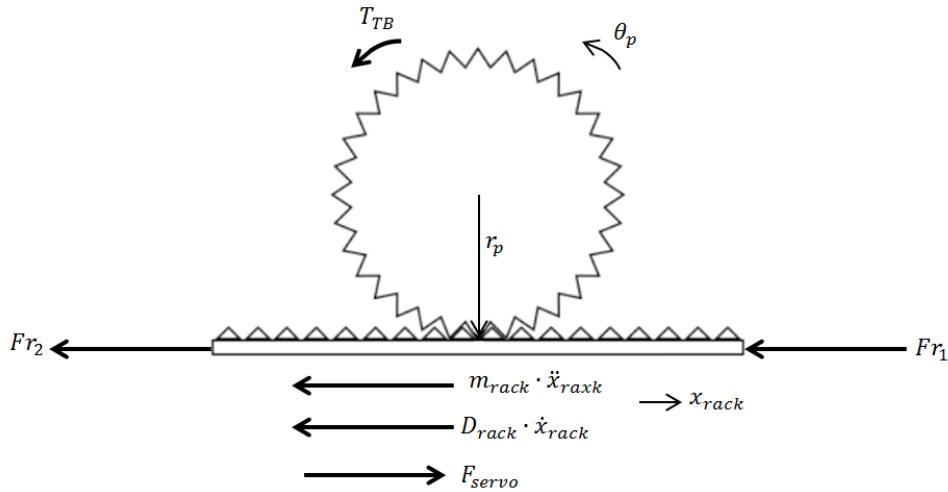


Figure 4.13: rack and pinion free body diagram.

The total force transmitted by the pinion to the rack is equal to:

$$F_p = m_{rack} \cdot \ddot{x}_{rack} + D_{rack} \cdot \dot{x}_{rack} + (Fr_1 + Fr_2) - F_{servo} \quad (4.12)$$

From the free body diagram *Equation 4.13* holds:

$$F_p = \frac{T_{TB}}{r_p} \quad (4.13)$$

Now that the forces acting on the rack are known, it is possible to compute the torque acting on the steering wheel, which depends on the torsion bar torque, on the damping and inertia properties of the steering wheel and steering column and on the servo assistance.

$$T_{sw} = F_p \cdot r_p + T_f + D \cdot \dot{\delta} + J \cdot \ddot{\delta} \quad (4.14)$$

The pinion angle is:

$$\theta_p = \frac{x_{rack}}{r_p} \quad (4.15)$$

Equation 4.15 replaces *Equation 2.35*. Now the pinion angle is directly influenced by the forces coming from the tires. The road wheel angles are computed starting from *Equations 2.36* to *2.39* using the value of θ_p coming from *Equation 4.15*. So they are function of the pinion angle, of the roll steer and of the compliance produced by lateral force and self-aligning torque.

In the next sections the friction torque and the servo assistance forces are computed.

4.4 Friction modelling

Friction has an important influence on steering feel, especially in the so called on-centre driving. This driving condition is the one in which the vehicle is driven with small steering angle, for instance when it is driven in a straight line and a small

movement of steering is needed to change trajectory. Friction mainly comes from the rack-pinion contact and through the bearings of the different components and can be modeled in different ways. An overall view on this topic can be found in [19]. For this thesis a Dahl friction model has been adopted, mainly because it is simple, computationally fast and it offers a good description of the phenomenon.

The Dahl model was developed for the purpose of simulating control systems with friction. The starting point for Dahl's model is the stress-strain curve in classical solid mechanics. When subject to stress, the friction force increases gradually until rupture occurs. Dahl modeled the stress-strain curve by the following differential equation:

$$\dot{F}_f(t) = \sigma \cdot \left[1 - \frac{F_f(t)}{F_c} \cdot \text{sign}(x(\dot{t})) \right]^\lambda \cdot \text{sign} \left(1 - \frac{F_f(t)}{F_c} \cdot \text{sign}(x(\dot{t})) \right) \cdot \dot{x}(t) \quad (4.16)$$

Where:

$F_f(t)$ is the Dahl friction force

F_c is the Coulomb friction force

σ is the stiffness coefficient

λ is the shape parameter

$\dot{x}(t)$ is the relative velocity between the two surfaces

The Dahl friction model is a generalization of ordinary Coulomb friction and so it does not capture the Stribeck effect. Anyway, the Stribeck effect in a steering wheel is usually too low that the driver does not perceive it, so there is really no need to model it. What is important is to model the hysteresis in the system. This model expresses the friction force only in function of the displacement: this means that the force is position dependent. In the steering system, instead of having $F_f(t)$, F_c and $\dot{x}(t)$, the correspondent variables are the steering wheel friction torque $T_f(t)$, the steering wheel angular velocity $\dot{\delta}$ and the Coulomb friction torque level T_c . In particular, the Dahl model used in this thesis has, for sake of simplicity and for computational reasons, a shape parameter $\lambda = 0$. So Equation 4.16 becomes:

$$\dot{T}_f = \sigma \cdot \text{sign} \left(1 - \frac{T_f}{T_c} \cdot \text{sign}(\dot{\delta}) \right) \cdot \dot{\delta} \quad (4.17)$$

The *Sim IV* has a dedicate computer that controls steering wheel, reproducing friction, damping and vibrations. The Dahl friction model developed in Dymola has to reproduce the one used by the simulator: for this reason, K_s , D_{sw} and T_c were set to the same reference values used by *Sim IV* and then they were tuned around that values to find the proper steering feel. As a result, the stiffness coefficient is computed as:

$$\sigma = \frac{2 \cdot D_{sw} \cdot K_s}{\sqrt{\frac{K_s}{J_{sw}}}} \quad (4.18)$$

Table 4.1 resumes the parameters used in the friction model:

Table 4.1: parameters of friction model

| PARAMETER | VALUE |
|---|--------|
| Spring constant K_s | [5,40] |
| Steering wheel damping D_{sw} | 0.5 |
| Steering wheel moment of inertia J_{sw} | 0.05 |
| Coulomb friction torque level CF | [-5,5] |

The coulomb friction torque has been modeled in function of CF and $\dot{\delta}$:

$$T_c = CF \cdot \text{sign}(\dot{\delta}) \quad (4.19)$$

In order to reproduce hysteresis and saturation in Dymola, the following code was used to compute the friction torque:

$$\dot{T}_f = \text{if } T_f > T_c \text{ and } \dot{\delta} > 0 \text{ or } T_f < -T_c \text{ and } \dot{\delta} < 0 \text{ then } 0 \text{ else } K_d \cdot \dot{\delta} \quad (4.20)$$

This equation substitutes Equation 2.41. The trend of the friction torque in function of the steering wheel angle is no more the one shown in Figure 2.11 since now hysteresis has been introduced. As a result, the $T_f - \delta$ curve is shown in Figure 4.15:

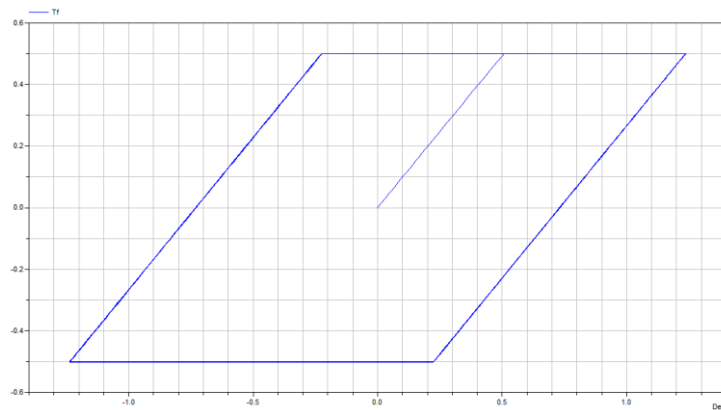


Figure 4.15: Dahl friction torque.

In Figure 4.16 the time trajectories of the steering wheel torque and the steering wheel angle are plotted against each other. In this way the relation between the steering wheel torque and the steering wheel angle can be seen.

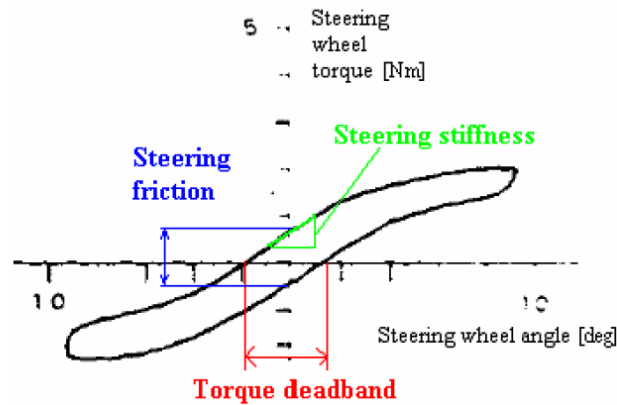


Figure 4.16: steering wheel torque in function of steering wheel angle. Adapted from Linden, Geluk, Nijmeijer (2007).

From this plot three parameters are determined: the steering friction, steering stiffness and torque deadband. The steering friction is the vertical distance between the two lines in the plot at a steering wheel angle of zero degrees. This is the torque that is required to overcome the (dry) friction in the steering system at a steering wheel angle of zero degrees. The steering stiffness is the average gradient of the upper line and the lower line over a range of + 10 % of the peak steering wheel angle [20]. In modern vehicles this stiffness is mainly determined by the characteristics of the torsion tube in the steering gear. The torque deadband is defined as the horizontal distance between the two lines at a steering wheel torque of zero Nm. *Figure 4.17* shows some different $T_{SW} - \delta$ characteristics of VDM-14, varying CF:

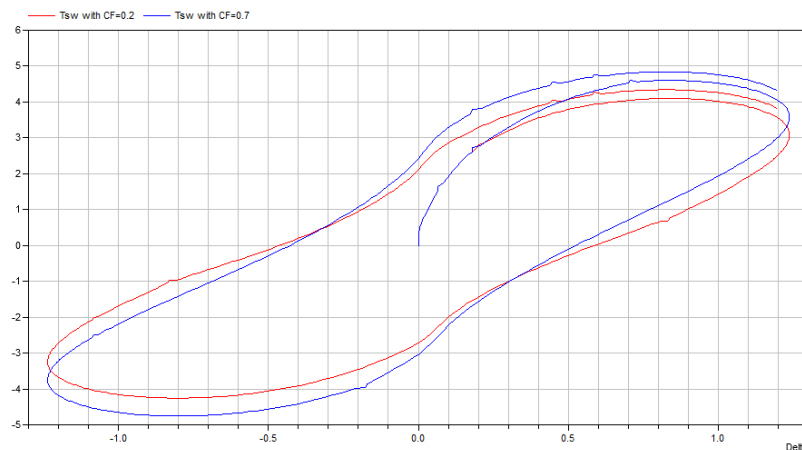


Figure 4.17: steering wheel torque in function of steering wheel angle, for different values of friction, implemented in Modelica for VDM-14.

The value of CF has to be carefully chosen, because not only it affects the global friction torque perceived by the driver, but also the deadband. In particular, the driving condition in *Sim IV* require for the majority of the time an on-centre driving, so it is important to find a value of CF which is a good compromise between friction torque and torque deadband.

4.5 Power steering modelling

The reason for which power steering is needed is mainly to take out the effort during parking and slow speed manoeuvring, and to reduce efforts when completing a severe cornering or correction of a car's attitude at medium speeds. Power steering has now become a positive necessity on many large modern cars which have high front axle weights, large section tyres, and now more frequently, front wheel drive. It also improves safety by enabling the car to be rapidly manoeuvred out of difficulties and helps the car to be controlled in unexpected situations. Good PAS reduces driver fatigue and contributes to safety in this sense also. It is obvious that power steering plays a key role in steering feel by limiting the maximum amount of torque exerted by the driver. There are several ways in which this additional power can be supplied, such as with a hydraulic system or an electric one. In this thesis, a hydraulic power steering has been modelled.

An engine driven hydraulic pump delivers fluid to a valve which is used to control this fluid and direct it to either side of a ram, which supplies the required steering assistance. To satisfy the conditions discussed above, it is necessary that the power should be available at all vehicle speeds and it is vital to introduce this power into the steering system in a way that is completely controllable by the driver, and without surges or fluctuations in the assistance torque as the power comes into, or goes out, of operation. The best way of exercising this control is by a servo valve which is operated by the driver through a direct mechanical linkage from the steering wheel. This is obtained by having one part of the valve directly operated by the steering column, though a torsion bar, thus putting the driver in direct control of its movement. A typical rotary valve is shown in *Figure 4.18*:

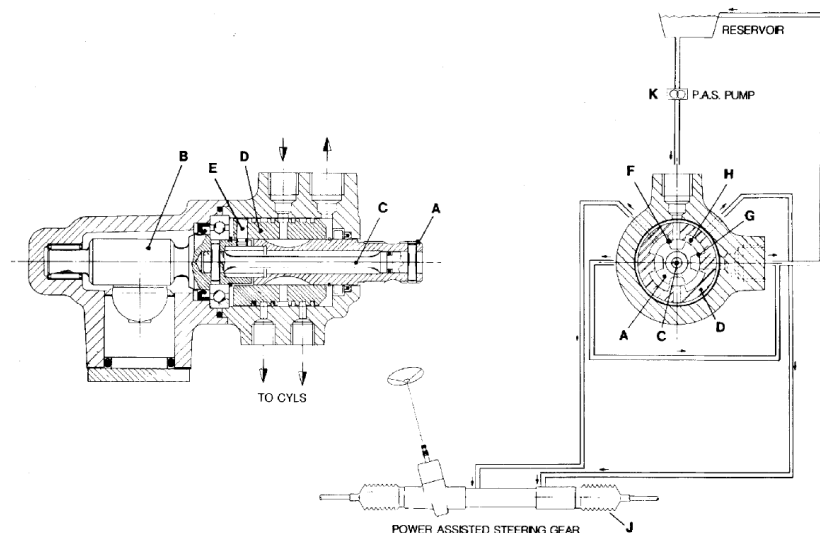


Figure 4.18: scheme of hydraulic power assisted steering system.

The inner member (A) is controlled directly by the steering column, and it therefore faithfully follows steering wheel movements. This input valve member is connected to the pinion (B) by the torsion bar (C) which transmits torque between the two members. Fluid taken from a power steering pump (K) is supplied to this. A typical characteristic of the rotary valve is shown in *Figure 4.19*, where the pressure is expressed in function of the input torque (coming from the driver).

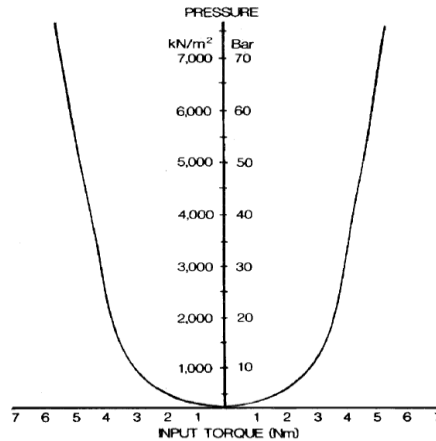


Figure 4.19: relation between servo pressure and steering wheel torque.

The fluid is then sent to a double-acting hydraulic cylinder, where a piston uses it to generate a force applied to the steering gear. The characteristic curve of *Figure 4.x* is the basis for determining the magnitude of assistant torque. So it is particularly important to tune it in order to get a proper steering feel. The tuning process is not easy, because the final characteristic curve will depend on many factors. Different vehicle types, different driving environments and different driving styles, etc. all tend to suggest that different ‘feels’ are required. For instance, a large vehicle that spends much of its “life” in town, at moderate speeds on straight roads can be satisfactorily steered with a system which uses large quantities of power and that only requires small forces from the driver to operate the valve. However, high speed straight line driving on highways or driving on twisting roads requires accurate placing of the car and demands a system which ‘tells’ the driver much more about the car’s response, enabling him to exercise the precise steering control that is necessary. At high speeds, in fact, the steering forces for corrections or lane changing maneuvers are quite low and power assistance is not necessary. So the characteristic curve is tuned trying to find a compromise between these exigencies and for these reasons a typical characteristic between boost pressure and steering wheel torque has the trend shown in *Figure 4.20*:

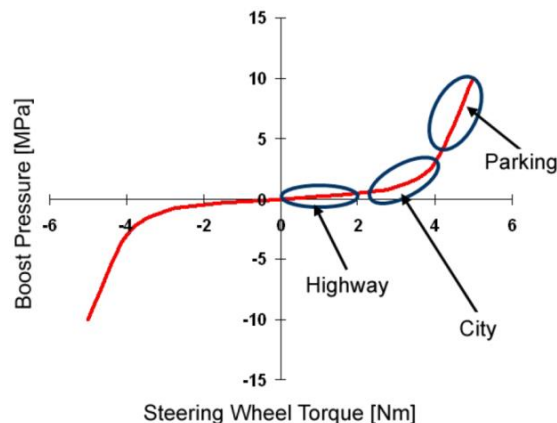


Figure 4.20: relation between servo pressure and steering wheel torque for different driving conditions.

In the “highway” interval the boost pressure is low and low power assist will be provided, making the steer more “direct”. Vice versa in “parking” interval, the boost pressure rises and the assistance torque provided since the main aim is to make the steering wheel as “soft” as possible, to reduce driver efforts..

The following characteristic has been implemented in Dymola, starting from the data available in [16].The relationship between boost pressure (or servo assistance pressure) P_{servo} and the steering wheel torque T_{sw} has been modeled using a polynomial function: after many attempts, it emerged that the best feel was given by a quadratic function, and so:

$$P_{servo} = A \cdot (T_{sw})^2 \cdot sign(T_{sw}) \quad (4.21)$$

The term $sign(T_{sw})$ was used instead of an “if preposition” because of computational reasons, in fact the “if statement” created some problems in Dymola. Knowing the boost pressure, the servo assistance force is computed as:

$$F_{servo} = P_{servo} \cdot A_{servo} \quad (4.22)$$

A_{servo} is the area of the piston inside the double-acting hydraulic cylinder.

The tuning process is the one in which the *Sim IV* has played an essential role. In fact, when defining a certain curve, it is impossible to know a priori which will be the feel provided. The only solution is to test it. Furthermore the feeling is always subjective, so it could be optimal for one driver and at the same time it can be inadequate for one other. Different parameters can be tuned, i.e. A_{servo} , K_{TB} and A . *Figure 4.21* shows different values of boost pressure by changing the servo assistance coefficient A :

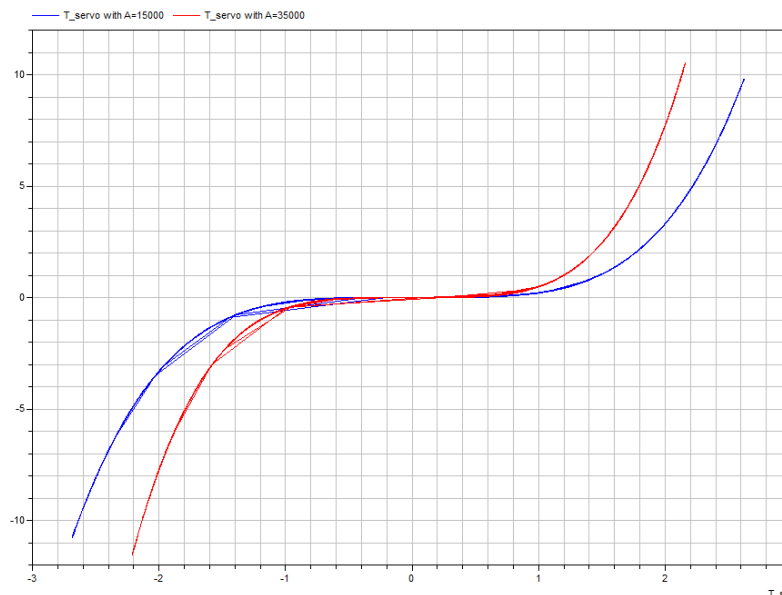


Figure 4.21: relation between servo pressure and steering wheel torque for different driving conditions.

Table 4.2 resumes the values of the parameter used for servo assistance:

Table 4.2: main parameters of the servo assistance model.

| PARAMETER | VALUE |
|-------------|---|
| A_{servo} | 0.001 m^2 |
| A | [10000,100000] |
| K_{TB} | $[90,170] \frac{\text{Nm}}{\text{rad}}$ |

4.6 Steering system model: summary

A new steering model has been developed for the VDM-14. It receives as an input the steering wheel angle and provides as output the steering wheel torque. Its aim is to give a better representation of reality both in terms of physics and in terms of steering feel. The model should also work as a “standalone” to study topics closely related to steering.

Table 4.3: main variables of the steering model.

| VARIABLES | |
|---|--|
| Mr_1, Mr_2 | Resistant torque produced by tire forces of wheel 1 and two around the steering axis |
| Fr_1, Fr_2 | Resistant forces acting on the rack due to resistant torques around steering axis |
| $\theta_{TB}, \dot{\theta}_{TB}$ | Torsion bar angular displacement and angular velocity |
| $\delta, \dot{\delta}, \ddot{\delta}$ | Steering wheel angle, velocity and acceleration |
| θ_p | Pinion angle |
| $x_{rack}, \dot{x}_{rack}, \ddot{x}_{rack}$ | Rack displacement, velocity and acceleration |
| F_p | Force acting on the pinion |
| F_{servo} | Servo assistance force |
| P_{servo} | Servo assistance pressure |
| δ_{wi} | Road wheel angles |
| T_{sw} | Steering wheel torque |
| T_f | Steering wheel friction torque |

Table 4.4: main parameters of the steering model.

| PARAMETERS | |
|----------------------|--|
| γ | King pin angle |
| τ | Caster angle |
| r_{KP} | Scrub radius |
| r_c | Caster trail |
| R_{nom} | Tire nominal radius |
| m_{rack}, D_{rack} | Rack mass and damping |
| r_p | Pinion radius |
| D, J | Steering wheel and column damping and inertia |
| K_s | Spring constant |
| D_{sw} | Steering wheel damping |
| J_{sw} | Steering wheel moment of inertia |
| CF | Coulomb friction torque level |
| σ | Dahl friction stiffness coefficient |
| A_{servo} | area of the piston inside the double-acting hydraulic cylinder |
| A | Assistance coefficient |
| K_{TB}, D_{TB} | Torsion bar stiffness and damping |

4.7 Refined VDM: an overview

The Vehicle dynamic model computes, as output, the vehicle response on the basis of inputs coming both from the driver and from the road. The inputs are listed in the *Table 4.5*:

Table 4.5: Refined VDM input.

| INPUT | DESCRIPTION |
|--|--|
| Steering wheel angle δ | Steering wheel position. Positive for left turn. $[-6, +6 \text{ rad}]$ |
| Steering wheel velocity $\dot{\delta}$ | Steering wheel angle derivative $[\frac{\text{rad}}{\text{s}}]$ |
| Steering wheel acceleration $\ddot{\delta}$ | Steering wheel angle derivative $[\frac{\text{rad}}{\text{s}^2}]$ |
| Throttle position | $[0,1]$ Where 1 is full throttle. |
| Clutch position | $[0,1]$ Where 1 for pedal fully pressed. |
| Brake pressure at master cylinder | Pressure generated by the driver when braking. $[0,17.000 \text{ KPa}]$ |
| Gear shift position | Gear selected by the driver. 0=neutral; 1,...,5 = gear selected. |
| Road slope | Measured in radians. Positive when driving uphill. |
| Road bank | Measured in radians. Positive when clockwise. |
| Road profile under each wheel | 4 functions describing road profile. |
| Tire-road friction coefficients | Friction coefficients between tires and road. Independent for each tire. |
| External forces applied to the centre of gravity | 3 components of the external force applied to vehicle CG |

Table 4.6 shows the outputs of the VDM need by the simulator to run an experiment. In addition to these, any variable or parameter of the VDM can be sent as an output, depending on the special requirements of the experiment in progress.

Table 4.6: Refined VDM outputs.

| OUTPUT | DESCRIPTION |
|--------------------------------|--|
| Vehicle velocities | 3 components of the vehicle velocity, according to vehicle coordinate system and measured in SI units, [$\frac{m}{s}$] |
| Vehicle accelerations | 3 components of the vehicle acceleration, according to vehicle coordinate system and measured in SI units, [$\frac{m}{s^2}$] |
| Vehicle angular velocities | 3 components of the vehicle angular velocity, according to vehicle coordinate system. [$\frac{rad}{s}$] |
| Vehicle angular accelerations | 3 components of the vehicle angular acceleration, according to vehicle coordinate system. [$\frac{rad}{s^2}$] |
| Steering wheel torque | Torque generated on the steering wheel [Nm] |
| Engine speed | Engine rotational speed [rpm] |
| Engine torque | [Nm] |
| Displacement of the wheel hubs | 4 vertical displacements of the wheel hubs due to road irregularities [m] |
| Secondary outputs | Outputs of interest for the experiment in progress. |

The final structure of VDM-14 can be shown in *Figure 4.22*:

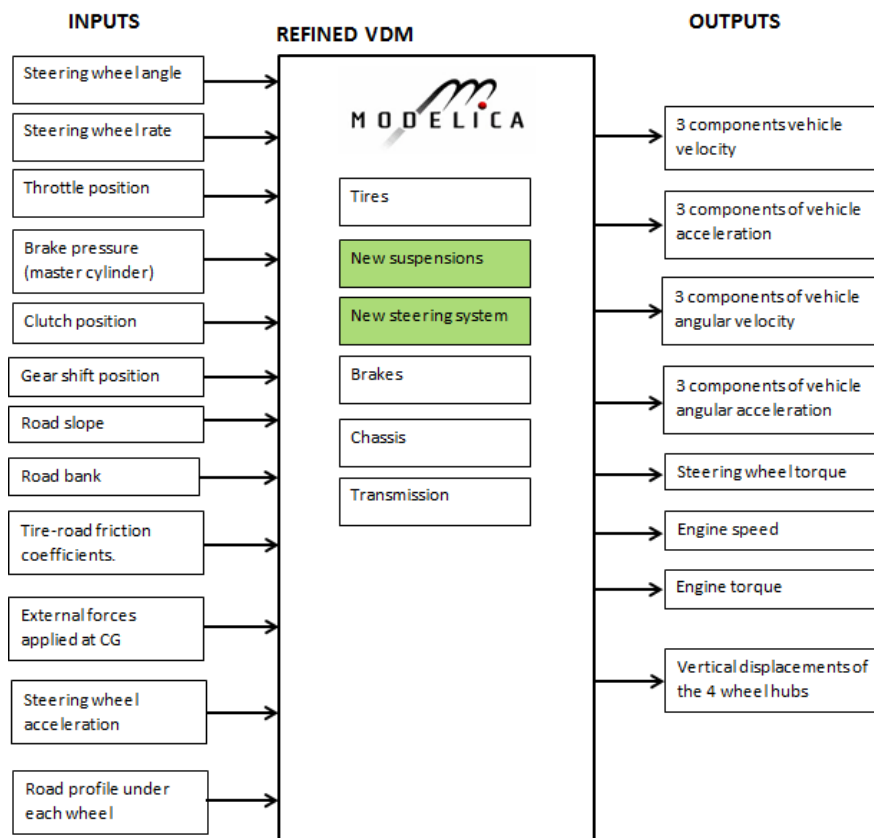


Figure 4.22: VDM-14 input-output scheme.

The new steering system model computes the resistant torque on the steering wheel taking into account the inertia, so the steering wheel acceleration is needed as an input. The refined suspension model, computes the forces transmitted by the suspensions on the chassis on the base of the road irregularities, so the functions describing the road profile under each wheel are an input to the VDM-14. In particular, there are 4 independent functions, one for each wheel.

5 Model validation

The final VDM-14 has been validated into two ways:

- by a comparison with real vehicle data coming from the test track
- by testing activity in the simulator

The parameters of the model have been tuned in order to find a good compromise between matching of the real data and “drivability” in the simulator.

5.1 Comparison with real data

Real data coming from test track were available thanks to the fact that they were recorded in the previous work to validate VDM-10. Data for different manoeuvres are available. In the following sections only the most significant results are shown, for sake of brevity. The other results can be found in [11]. The following paragraphs report the data in three different conditions: steady state driving, quick transient manoeuvres and straight driving. It must be noticed that the response generated by VDM-14 is related to a completely flat road, since it is very difficult and time consuming to reproduce the test track surface asperities.

5.1.1 Steady state driving

The vehicle’s response in steady-state conditions is studied. The car is driven along a constant radius circular path, starting from zero speed and slowly increasing until the stability limits are reached.

Figure 5.3 shows the lateral acceleration

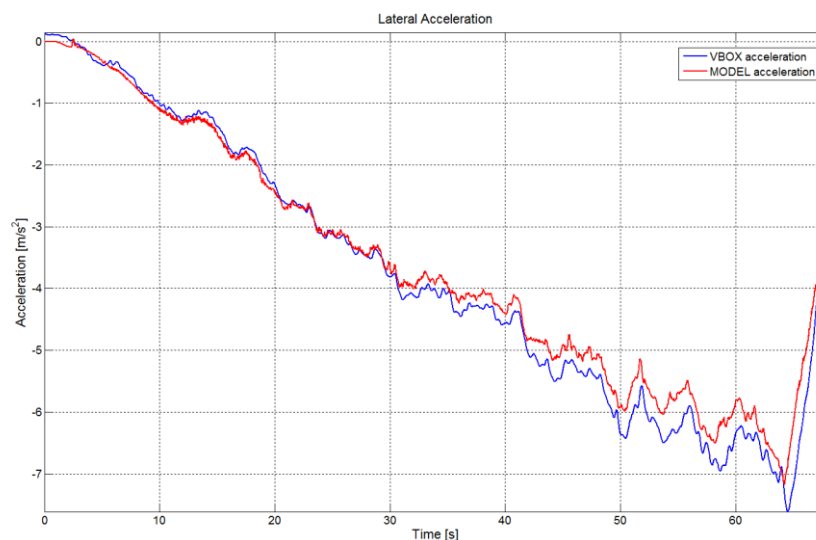


Figure 5.3: steady state lateral acceleration.

For values of lateral acceleration up to 5 m/s^2 the model (red curve) matches well the real data (blue curve). Then the real data show values which are a bit higher than the one coming from the model. The discrepancy reaches its maximum between 6 and 7 m/s^2 . There are mainly two reasons for these differences. The first one is related with the measurement equipment. As the vehicle speed is increasing and the lateral acceleration goes up, the vehicle tends to have a larger roll angle. The sensor used to measure vehicle

accelerations is attached to the vehicle body and when the body rolls, the sensor inclination introduces a component of the gravity in the measurement. The second reason is related with suspension and steering compliance in the VDM. It is necessary to find a balance between steady-state and transient response of the VDM and the compliances play an important role in the transient response, so probably the model presents a slightly more under steer behaviour than the real in steady-state cornering at high speed. Despite of these considerations, the differences between the test vehicle and the model are small and acceptable for this application. The frequency response is shown in *Figure 5.4*:

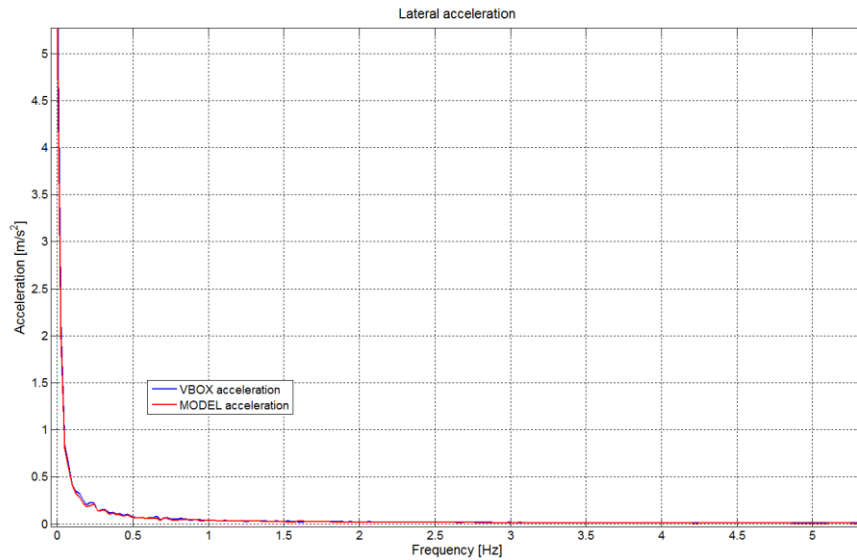


Figure 5.4: steady state frequency response of lateral acceleration.

The yaw rate matches quite well the trend of real data both in term of time response than in term of frequency response.

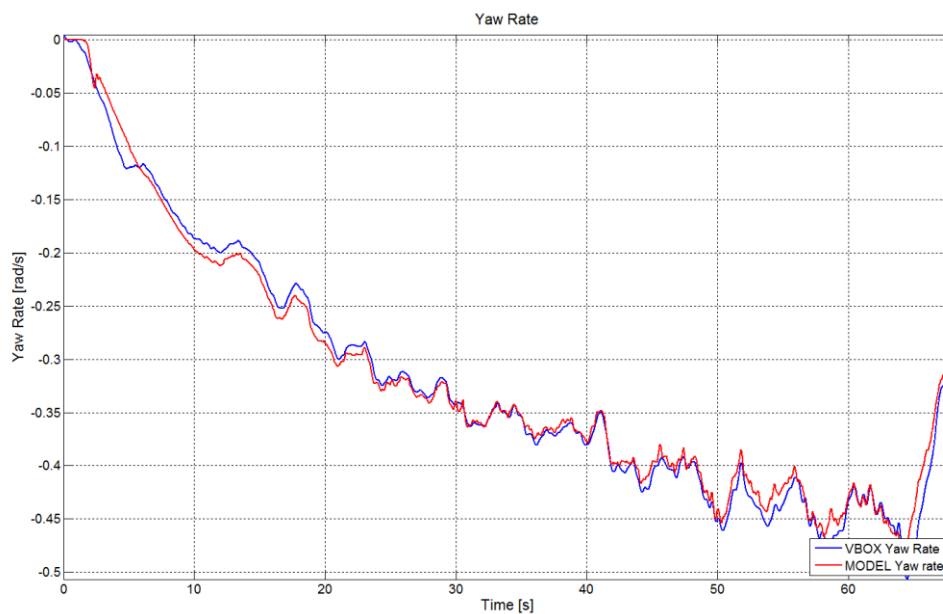


Figure 5.5: steady state yaw rate.

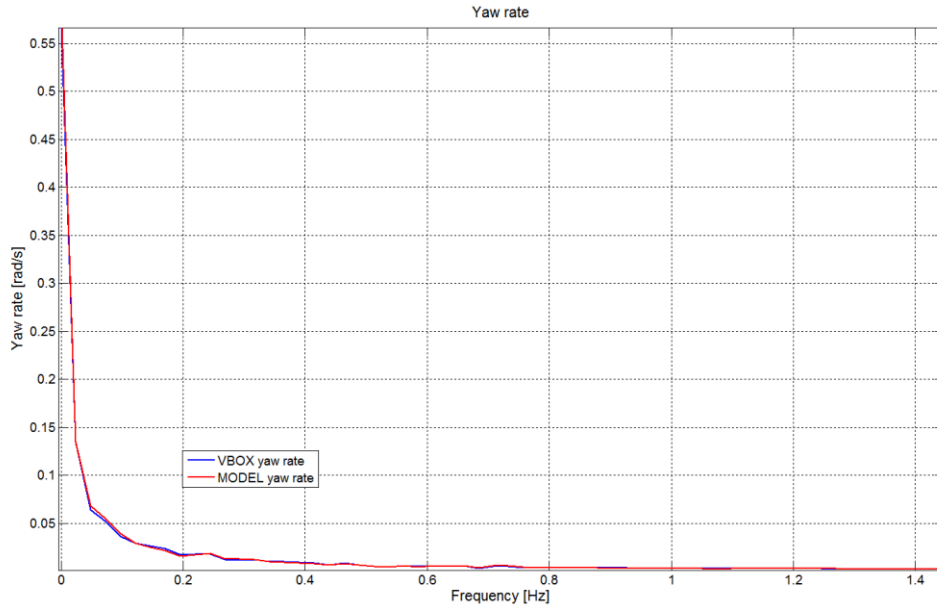


Figure 5.6: steady state yaw rate frequency response.

The pitch rate is shown by *Figure 5.7*:

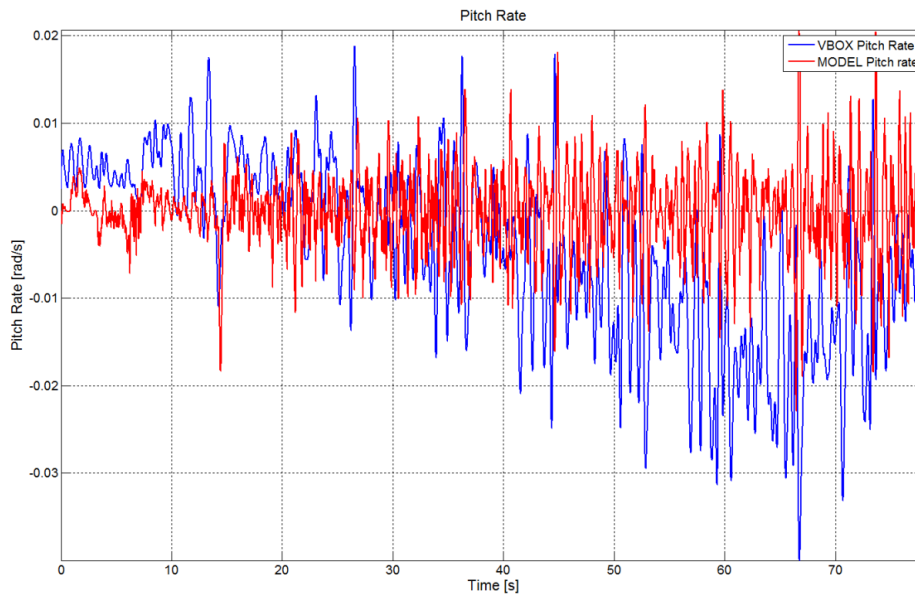


Figure 5.7: steady state pitch rate.

The pitch rate coming from the model has some small discrepancies with the one coming from real data. Despite of this, one can say that the model captures the pitch rate trend of the real car, but with a different magnitude. This difference in magnitude can be explained by the fact that the real track is not a completely flat surface and some road unevenness is always present, thus the pitch rate is affected by this. On the other side the model is tested on a completely flat surface, also because it is impossible to reproduce faithfully the road profile of the test track. Other differences can be due to suspension geometry. The pitch FRF is shown in *Figure 5.8* is useful to understand at which frequencies are located the main differences.

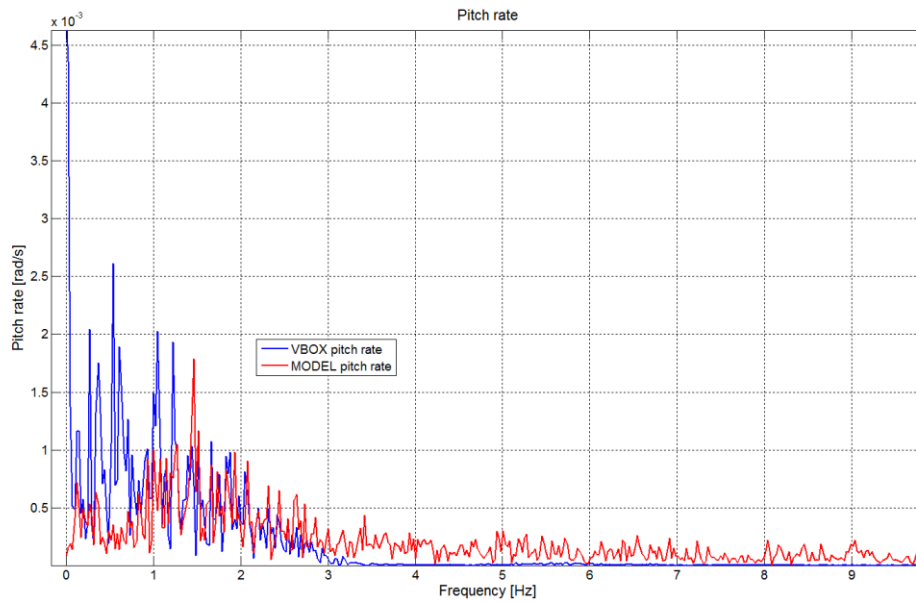


Figure 5.8: pitch rate steady state frequency response.

The main discrepancy lies in a range between 0 and 1 Hz. In the remaining part of the frequency spectrum the real trend is captured in a good way.

Similar considerations hold for roll rate, *Figure 5.9* (time response) and *Figure 5.10* (FRF)

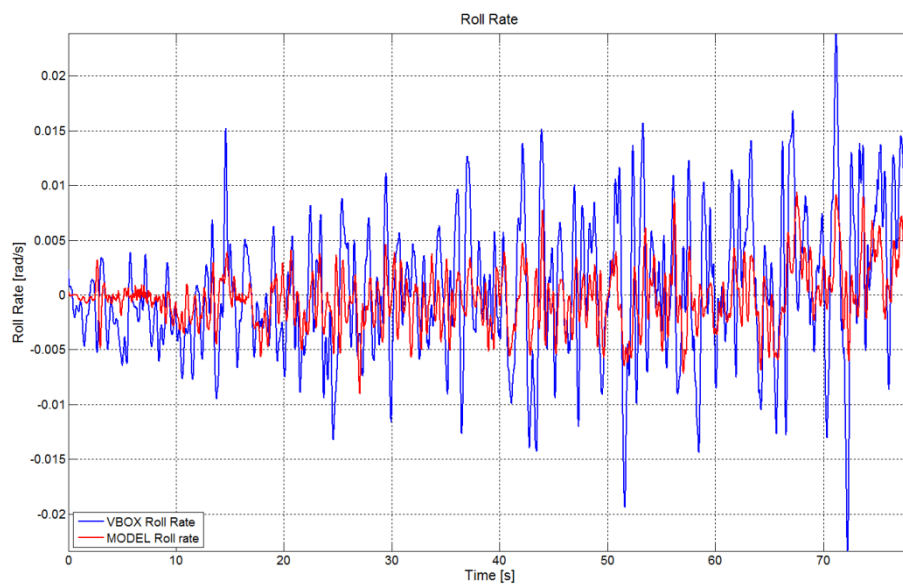


Figure 5.9: steady state roll rate.

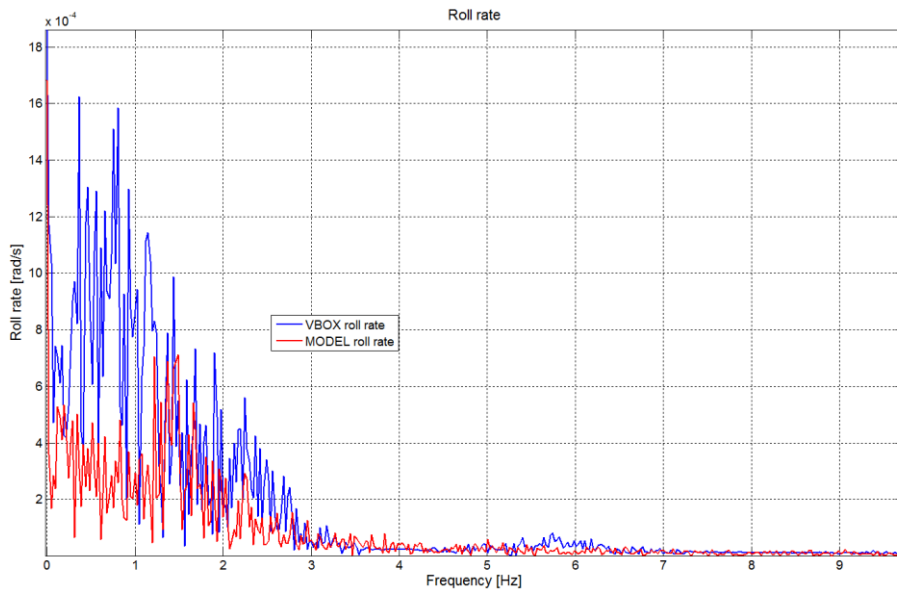


Figure 5.10: steady state roll rate frequency response.

Also the roll rate captures the trend of the model, but with different values of magnitude. Again the main differences are located between 0 and 1 Hz.

5.1.2 Transient response

The vehicle's response in transient conditions is evaluated by driving the car in a straight line at constant speed and by introducing sinusoidal steering wheel inputs of different frequencies, from small frequencies around 0.2 Hz to frequencies up to 2.5 Hz. The response of the vehicle due to a random input at 40 km/h is shown in the following images.

Figure 5.11 shows the lateral acceleration

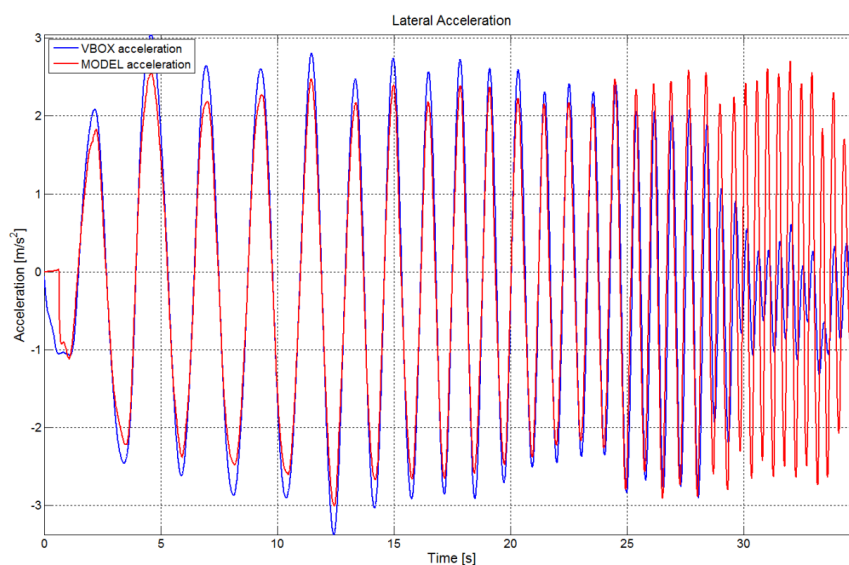


Figure 5.11: transient response of lateral acceleration, at 40 km/h.

The time response of the model shows a good matching with the real data, being also in phase with them, until a certain frequency, where the two curves diverge. According to reality, one can expect that the model response in terms of acceleration decreases with the increasing of frequency. This is true, in fact if the steering frequency increases the tire forces decrease, and so the overall roll and lateral acceleration should decrease. So, the model at a first sight seems not to capture correctly the trend of the real vehicle. But this is not true if the FRF is considered, *Figure 5.12*.

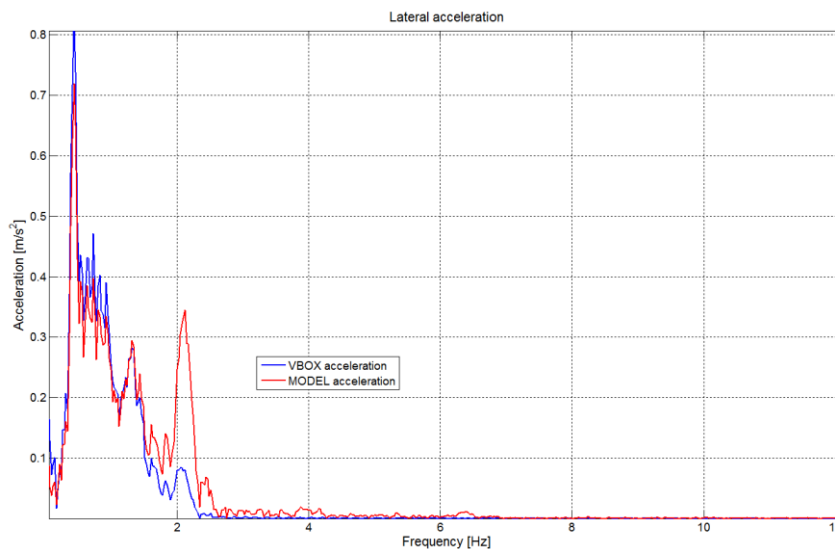


Figure 5.12: transient frequency response of lateral acceleration, at 40 km/h.

In fact, through the frequency response one can see that also the lateral acceleration of the model decreases while increasing the frequency. The VDM-14 matches well the real data in the whole frequency spectrum a part from a frequency interval around 2 Hz. For that particular frequency the VDM-14 presents a peak. This can be due to many causes: the actual tire behavior of the real car is more complex than the one described in the model, the suspension geometry can affect the values of tire force and the model does not take into account this. The steering geometry also affects the entity of the lateral forces (and so of the lateral accelerations) through the road wheels angles: even if the steering model of VDM-14 is a good approximation of reality, it has some limitations and the peak in correspondence of 2 Hz is due to higher order phenomena not represented by the model. Anyway, the response in terms of lateral acceleration of the model is acceptable.

The roll rate is shown in *Figure 5.13*: the model response tracks well the trend of the red curve being almost in phase with it. Only at higher frequencies there is a small delay, but the result is anyway satisfactory. The difference of magnitude that occurs at high frequencies can be explained in the same way of the lateral acceleration.

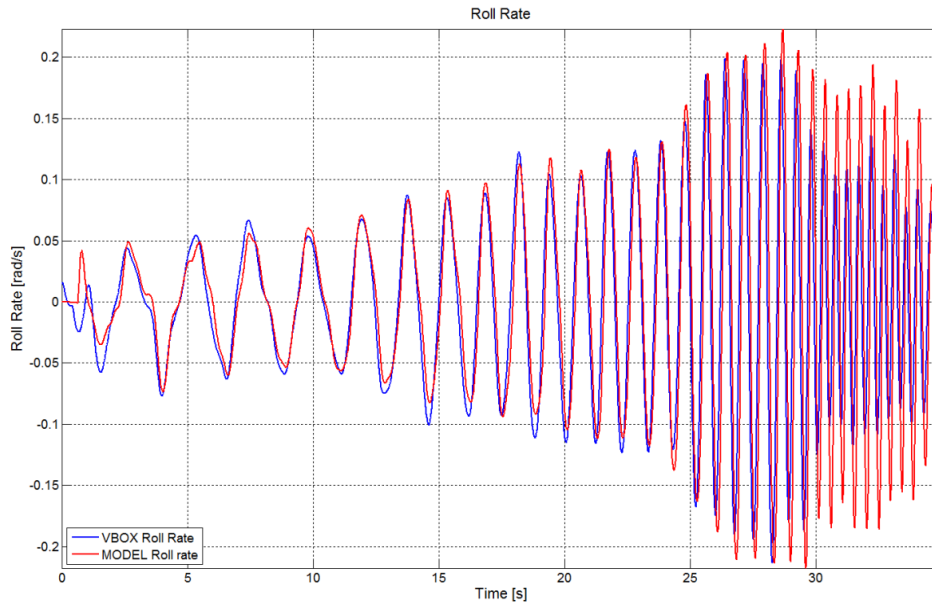


Figure 5.13: transient response of roll rate, at 40 km/h.

Figure 5.14 shows the roll rate FRF. The matching with real data is one more time emphasized. The roll rate magnitude of the VDM-14 differs from the real data around a frequency of 2 Hz, exactly as the lateral acceleration. But this is not a case: it is reasonable to expect a similar trend since the lateral acceleration is the cause of roll.

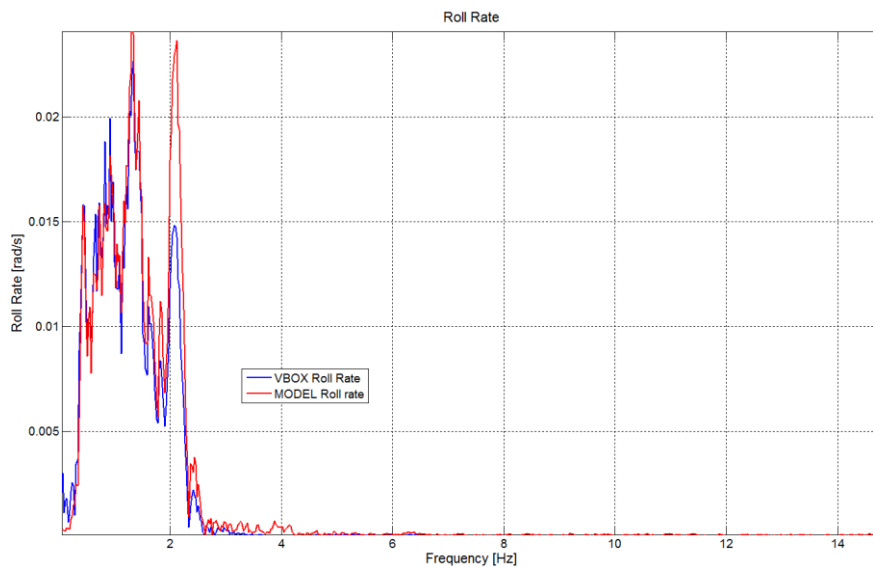


Figure 5.14: transient frequency response of lateral acceleration, at 40 km/h.

The yaw rate response is shown in *Figure 5.15*:

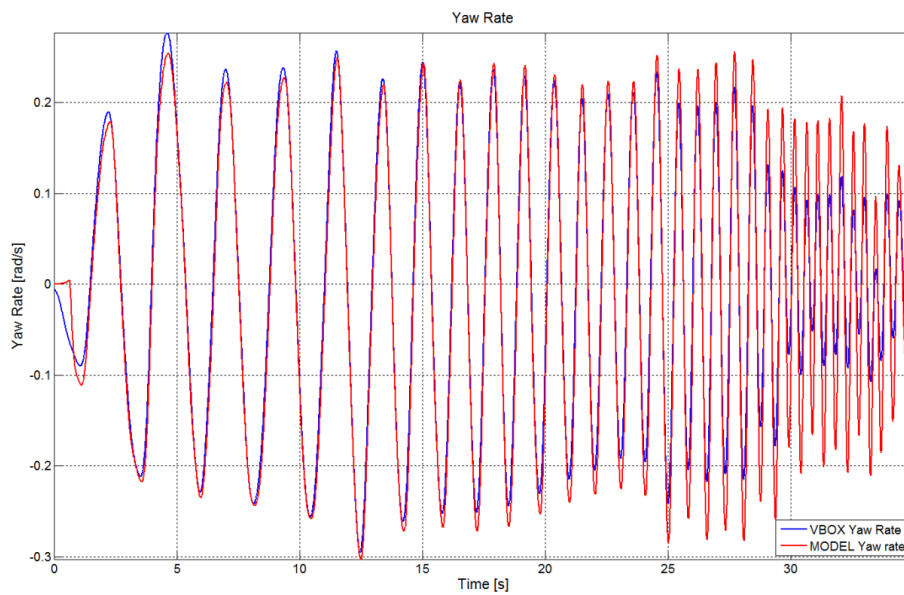


Figure 5.15: transient response of yaw rate, at 40 km/h.

The yaw rate of the model matches in a good way the red curve. A small discrepancy appears at a frequency of 2 Hz, as shown in *Figure 5.16*. The reasons of this difference have already been mentioned when discussing lateral acceleration. Yaw rate is related to lateral force (and thus acceleration) according to *Equations 2.9, 2.10 and 2.11*.

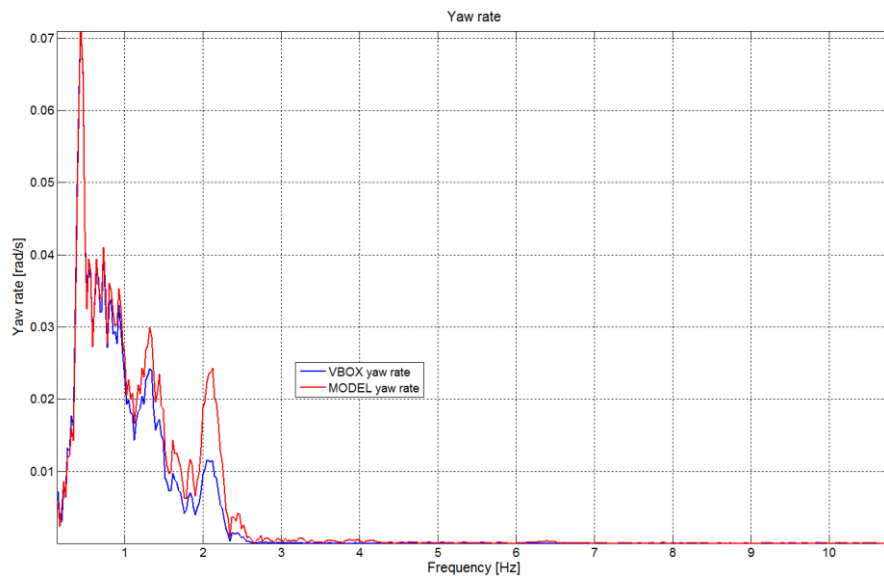


Figure 5.16: transient frequency response of lateral acceleration, at 40 km/h.

The pitch rate in function of time is shown in *Figure 5.17*.

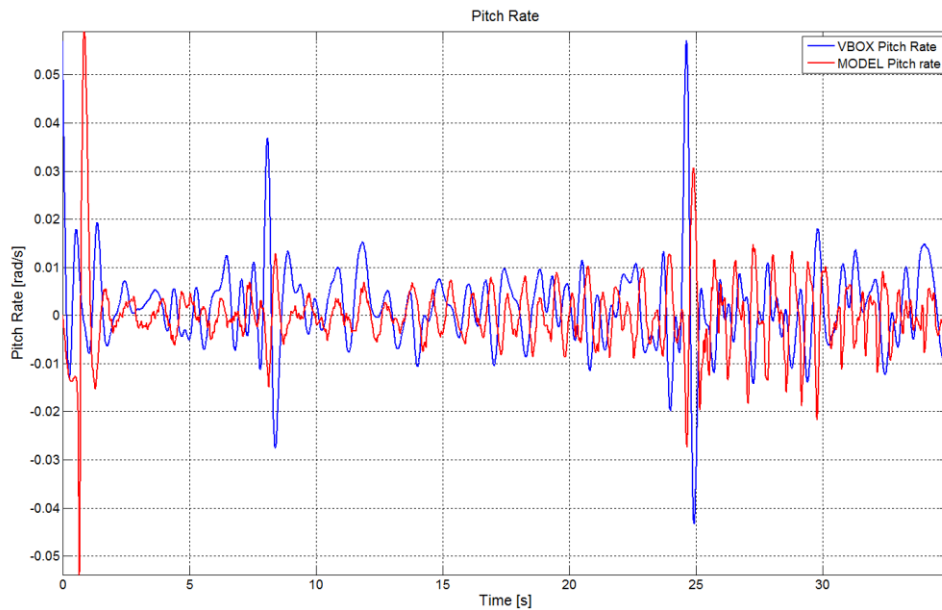


Figure 5.17: transient response of pitch rate, at 40 km/h.

The model represents well the behavior of the real vehicle, and the two peaks in the blue curve are probably due to road asperities on the test track. The good description of the phenomenon is emphasized by the pitch rate FRF of *Figure 5.18*. The correspondence among data holds for the whole frequency range.

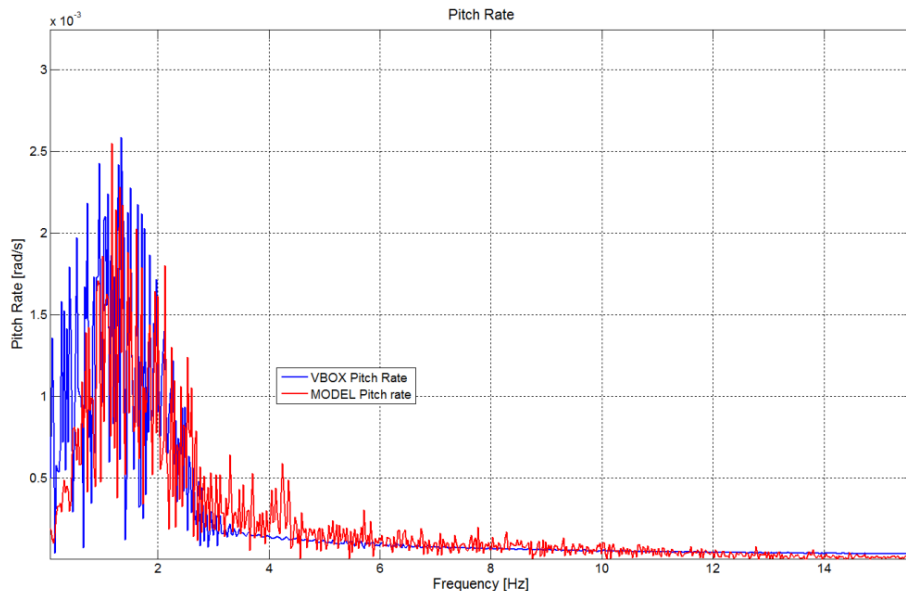


Figure 5.18: transient frequency response of pitch rate, at 40 km/h.

5.1.3 Straight driving

During straight driving the vehicle is driven on a straight road, performing accelerations and braking. To control the VDM speed, two PID controllers are used to generate the appropriate throttle and brake input signals in the model. These PID controllers will generate the inputs trying to minimize the difference between the

measured longitudinal velocity and the VDM longitudinal velocity. The gear shift also will be set equally to the test experiments.

The characteristics plotted are the longitudinal acceleration and pitch rate, in order to understand how the former affects the latter. The longitudinal acceleration is shown in *Figure 5.19*:

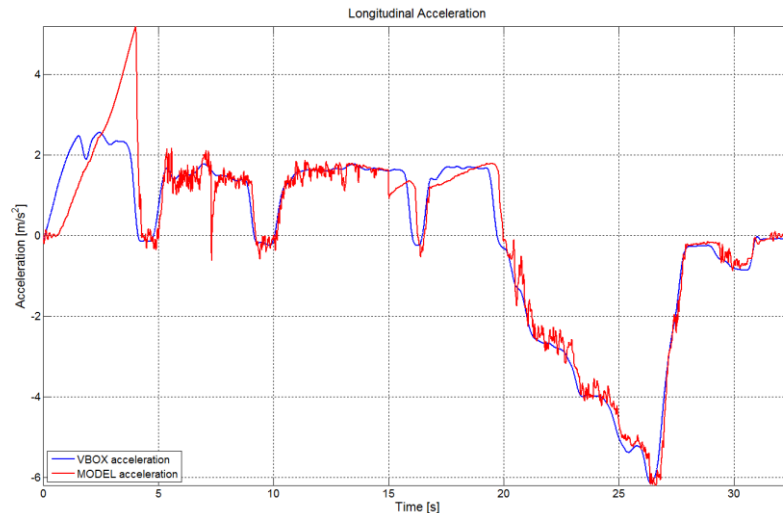


Figure 5.19: straight driving, longitudinal acceleration.

The VDM is able to generate the same range of longitudinal accelerations when accelerating and braking. The model of the transmission is very simple and not so accurate: this is the cause of the main peak between 0 and 5 sec. The longitudinal acceleration is generated by the PID controllers stating from the measured speed as a reference signal. The derivative of this signal is noisy and as a result the acceleration of the VDM is noisy too. It is fair to say that the VDM driveline and braking systems present a smooth behaviour when these inputs are smooth, like in normal driving conditions.

The pitch rate is shown in *Figure 5.20*:

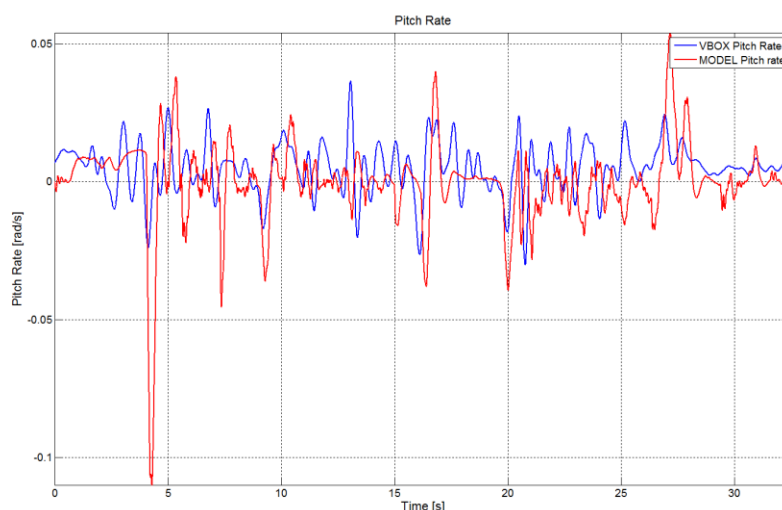


Figure 5.20: straight driving, pitch rate.

A part from the peak between 0 and 5 sec, due to the longitudinal acceleration, the trend with real data is matched in a satisfactory way.

5.2 Comparison between VDM-10 and VDM-14

As mentioned in *Section 1.2*, one of the objectives of this Master's thesis is to improve the response of the model in terms of roll, pitch and lateral acceleration in quick transient manoeuvres. In the following paragraphs a comparison of these variables will be made between the old VDM-10 and the new VDM-14. In particular the transient response at 40 km/h is compared.

5.2.1 Lateral acceleration

The VDM-10 response is shown in *Figure 5.21*, while the VDM-14 in *Figure 5.22*.

Both the trends match well the real data, but the VDM-14 appears to be more on phase after 15 sec. Furthermore the over-estimation of the magnitude of lateral acceleration at frequencies around 2 Hz is less marked in the VDM-14.

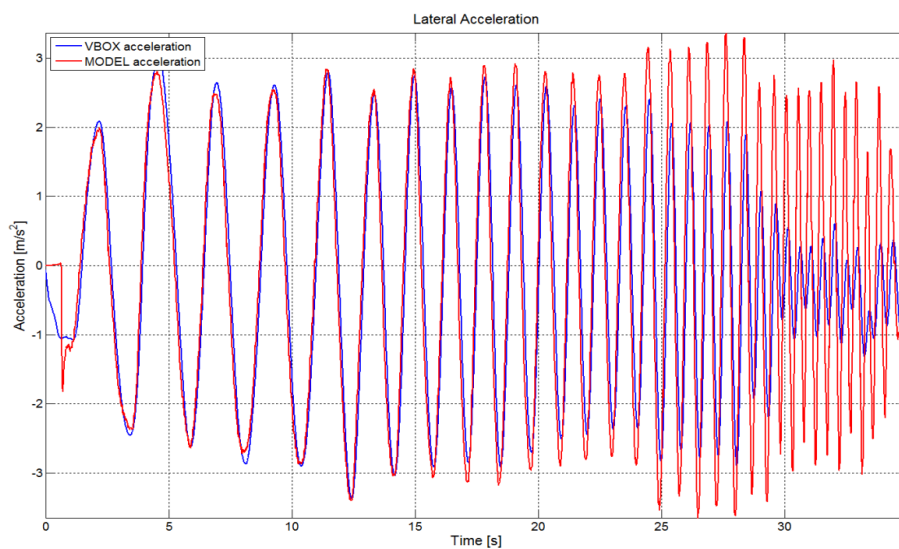


Figure 5.21: VDM-10 transient response of lateral acceleration, at 40 km/h.

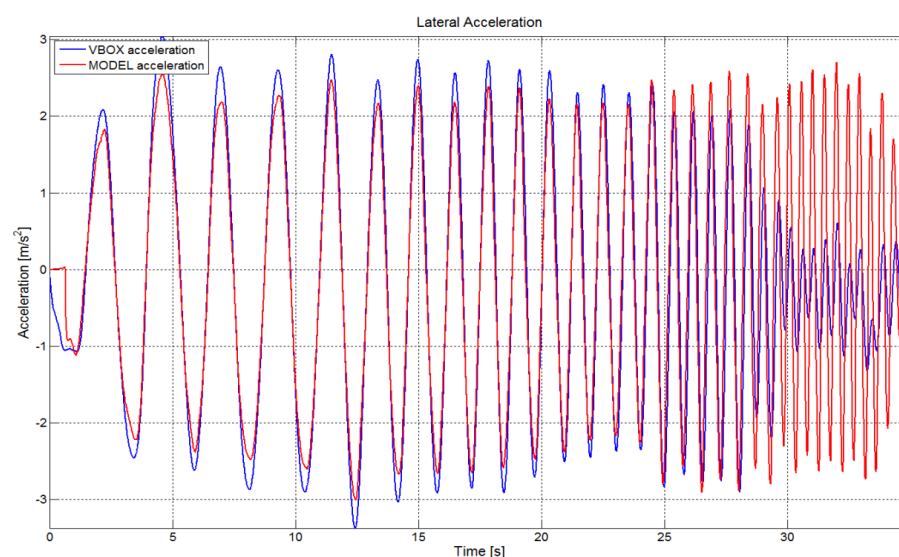


Figure 5.22: VDM-14 transient response of lateral acceleration, at 40 km/h.

5.2.2 Roll rate

The roll rate of VDM-10 is shown in *Figure 5.23*, while the one of VDM-14 in *Figure 5.24*.

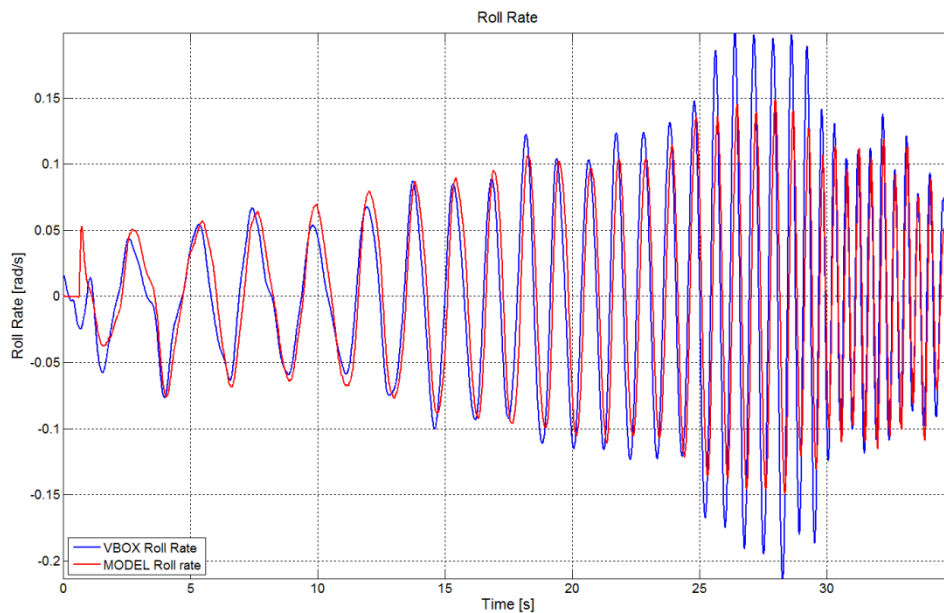


Figure 5.23: VDM-10 transient response of roll rate, at 40 km/h.

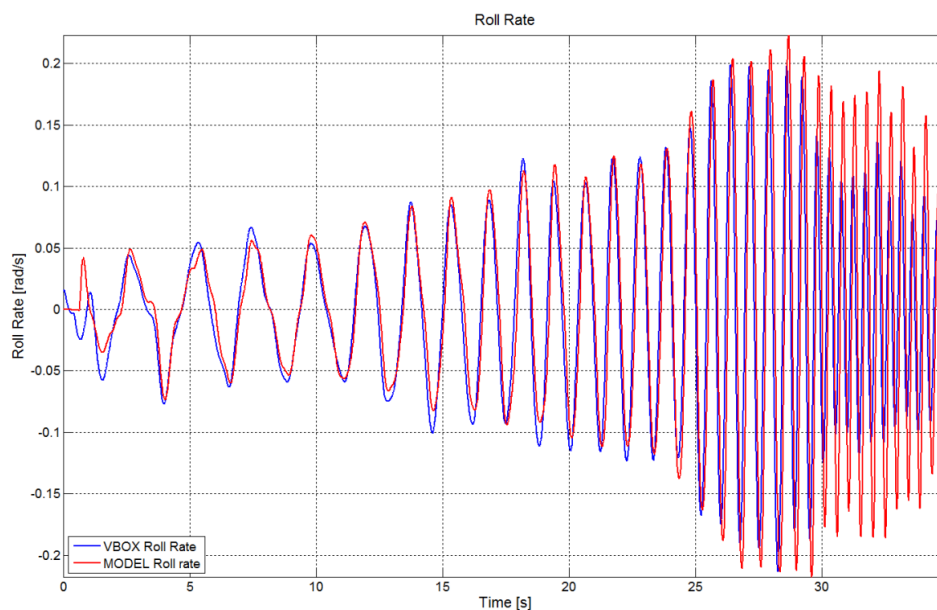


Figure 5.24: VDM-14 transient response of roll rate, at 40 km/h.

The roll rate of VDM-14 appears to be more on phase with the real data, from the beginning of the experiment. The VDM-10 does not seem to catch the trend of the real data, especially in terms of magnitude, neither it seems to be influenced by the lateral acceleration trend around 2 Hz.

5.2.3 Yaw rate

Figure 5.25 shows the yaw rate of VDM-10, while Figure 5.26 the yaw rate of VDM-14.

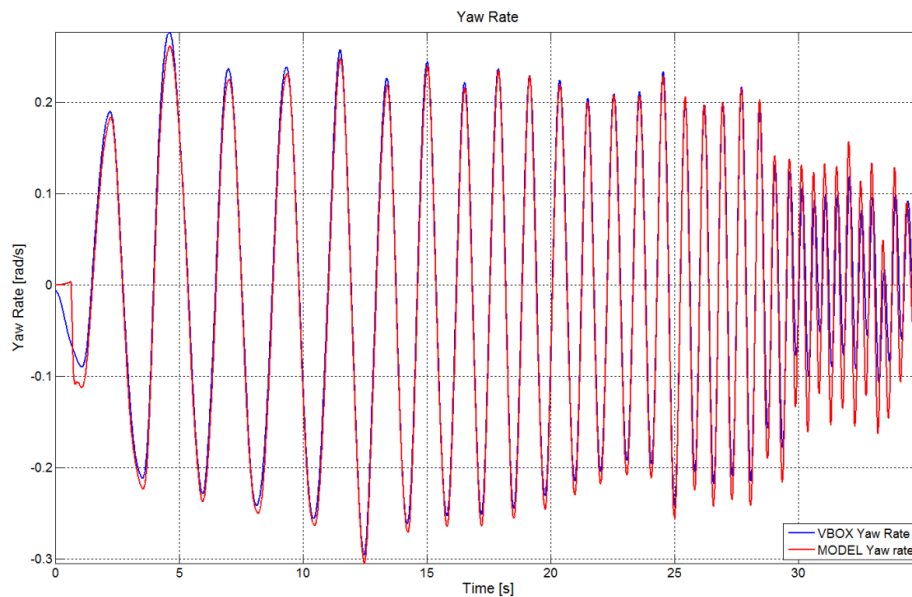


Figure 5.25: VDM-10 transient response of yaw rate, at 40 km/h.

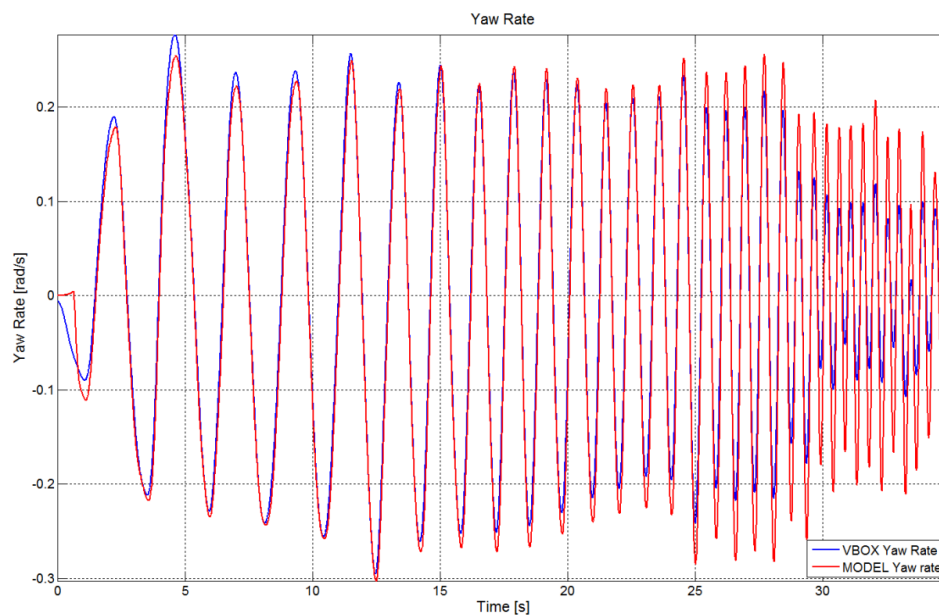


Figure 5.26: VDM-14 transient response of yaw rate, at 40 km/h.

Both the curves match the real data well, but the VDM-14 seems to be worse between 25 and 35 sec. In this time window, and for these frequencies, the discrepancies with the real data are a bit higher with respect to the VDM-10. This can be explained by considering one fact: the yaw rate is connected to the road wheel angles. The road wheel angles have been computed starting from the pinion angle. But in the case of VDM-10 according to Equations 2.34 and 2.35 there is no relation between pinion angle and tire forces. It is true that with this angle there is a better matching with real data, but the way in which it is computed does not represent reality very well. On the

contrary the pinion angle used by VDM-14, is related to these forces according to *Equations 4.13* and *4.15*. As a result road wheel angles are more influenced by lateral force and by lateral acceleration trend, which has a discrepancy around 2 Hz which, according to *Equation 2.9*, is clearly reflected also in the yaw rate.

5.2.4 Pitch rate

The pitch rate of VDM-10 is represented in *Figure 5.27* while the one of VDM-14 in *Figure 5.28*.

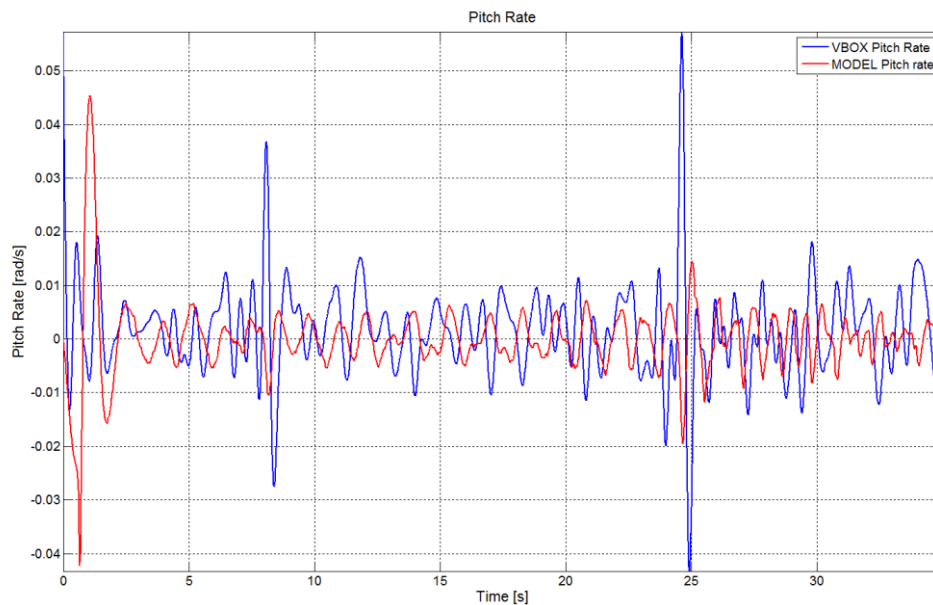


Figure 5.27: VDM-10 transient response of pitch rate, at 40 km/h.

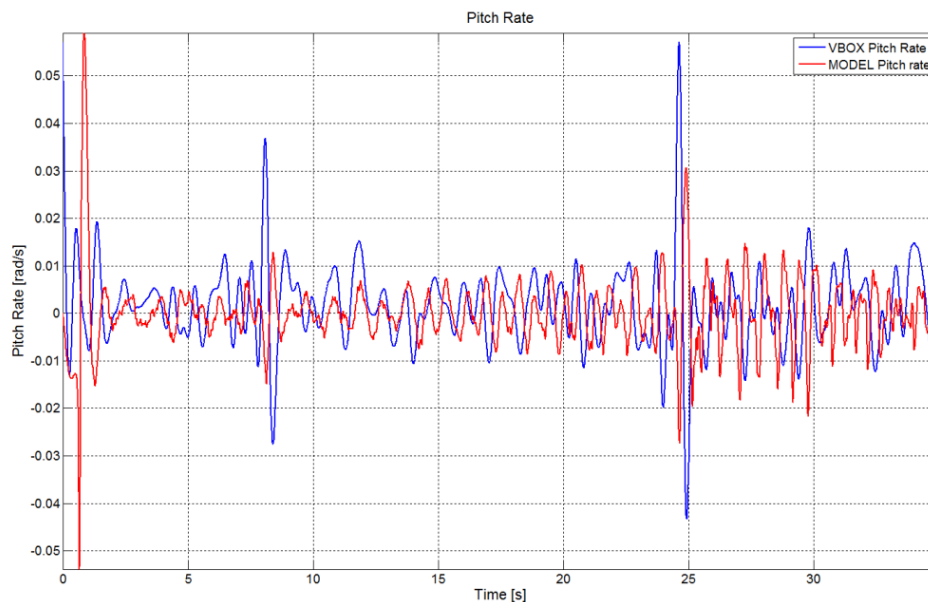


Figure 5.28: VDM-14 transient response of pitch rate, at 40 km/h.

Both the curves match well the real data, a part from the peak in the beginning due to the transmission model. At a first glance it seems that the VDM-14 captures better the real data trend both in terms of phase and magnitude. This is actually confirmed by

the pitch rate FRF. The one of VDM-10 is shown in *Figure 5.29*, while *Figure 5.30* shows the one of VDM-14.

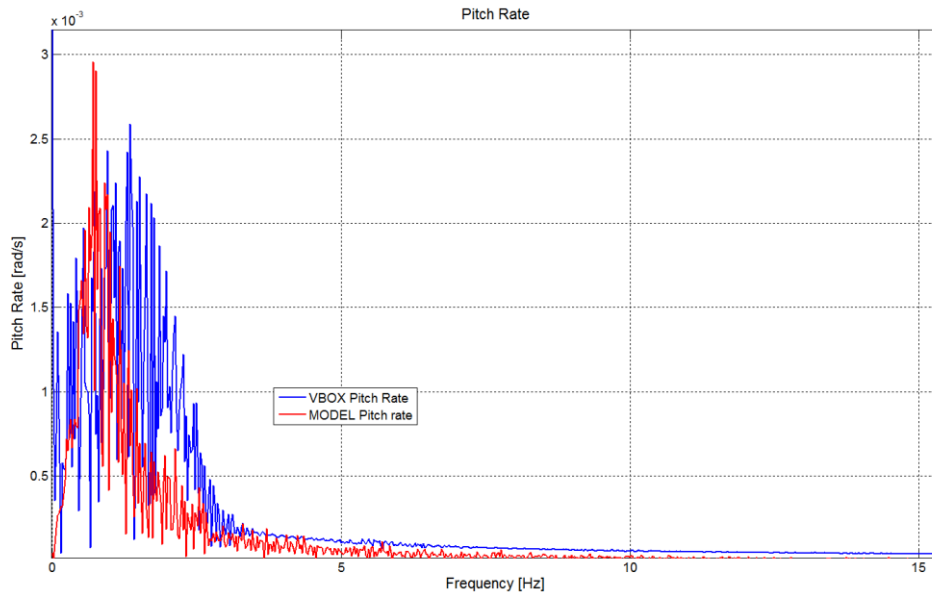


Figure 5.29: *VDM-10 transient frequency response of pitch rate, at 40 km/h.*

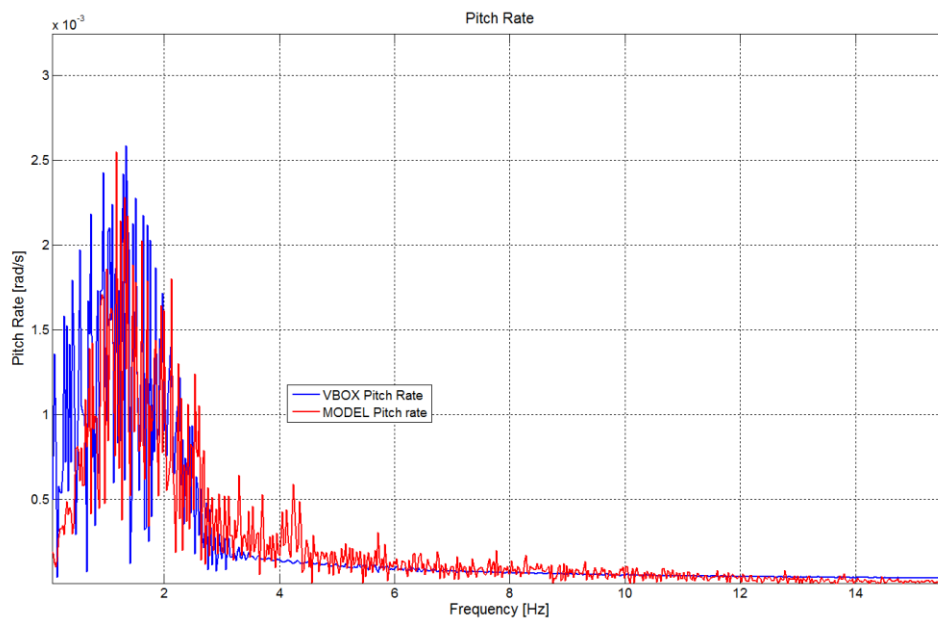


Figure 5.30: *VDM-14 transient frequency response of pitch rate, at 40 km/h.*

5.2.5 Conclusion

Through the comparison with real data the VDM-14 can be validated, providing good matching with the behaviour of a car. Furthermore, the expected improvements with respect to the VDM-10 have been reached. This has an important meaning not only because the VDM-14 works and describes reality in an acceptable way, but also because it has the potential to improve the driving experience in the *Sim IV*.

5.3 Validation in *Sim IV*

After having validated the model versus real data, VDM-14 has to be validated in the simulator, to prove to work properly. The testing activity performed in the *Sim IV* can be divided into two parts:

- Tests for evaluating the overall functionality
- Tests for evaluating the steering response

5.3.1 Tests for evaluating the overall functionality

The main aim of these tests is to check the functionality of VDM-14 on the simulator. During the first part of the validation, the model is simulated and tuned up in a standalone computer, but when it is downloaded to the simulator and used in real time, problems and numerical instabilities tend to appear. Some of these problems are usually related with combinations of inputs that never appear in the computer simulations. A long debugging process has been done in order to eliminate all these defects and get the model running in the simulator in the best possible way. After that, the VDM-14 has been tested successfully with motion on the *Sim IV*. All these simulations were performed internally at VTI, without involving volunteers to drive. The model proved to work well both on flat and uneven roads, but it still needs some improvements especially for what concerns the transmission model.

Another important aspect related to the “reality of the performance” is the motion cueing, which is the part of the software that controls the motion of the platform. The tuning of the motion cueing is essential to reproduce faithfully on the cabin the accelerations that are present in reality. In the case of *Sim IV*, the motion cueing is optimized specifically for the Fortran VDM model. So, if the Modelica VDM is run with the actual motion cueing settings, the overall realism of the performance can be affected, even if the model works well and matches well the real data. Some attempts were made to try to tune the motion cueing with respect to the Modelica model, but the process appeared to be very long, time-consuming and difficult. A lot of simulations are needed to find the correct tuning of the platform in order to get the “right feeling” in terms of accelerations, especially because the “feeling” is subjective and changes from person to person. For time reasons it has been decided not to tune the motion cueing algorithm with respect to the Modelica VDM, but this can be the starting point for a future work.

5.3.2 Tests for evaluating the steering response

After having verified the proper functioning of the VDM-14 in the *Sim IV*, some tests with volunteers were used to evaluate the steering feel. The aim of this activity is double: on one side there is the necessity to understand how far from reality is the new steering model developed in *Chapter 4* in terms of steering response. On the other side it is important to know how far is, always in term of response and steering feel, from the FORTRAN one, which is currently used in the simulator and is considered as a reference point. Furthermore it must be verified if the new steering model has brought some improvements with respect to the model used in VDM-10, which was judged to be “inferior” with respect to the FORTRAN.

These tests were performed without motion of the cabin. In fact if the motion system is on, it is much more difficult for the volunteers to focus on the steering response because their “attention” will be mainly affected by the accelerations, especially if they have never driven in a car simulator before. Furthermore, since the motion cueing is not optimized for Modelica model, the overall performance of VDM-14 could be negatively affected, even if the model itself works well, because the driver perceives accelerations which can be considered excessive, rough or too harsh. Since no motion is applied to the cabin, some tuning was made on the graphics to improve the effect of realism of pitch and roll motions. The volunteers had to drive both FORTRAN and Modelica VDM-14 on an uneven road and to express their judgement on different aspects. For what concerns the steering they had to judge both models in terms of:

- Steering feel at low speed
- Steering feel at medium speed
- Steering feel at high speed
- Feeling of road irregularities on the steering wheel

Then they were asked to express their judgement on:

- Evaluate the vertical motion of the vehicle when negotiating road irregularities
- Evaluate the overall model behaviour in terms of handling

Since the motion system was off, there was no physical vertical acceleration acting on the drivers when passing over a road irregularity even if the vehicle was moving vertically. Basically they were asked to evaluate the “entity” of these motions, to understand if they were too low, excessive or, in general, how far from reality were them. A similar reasoning was done for overall handling.

5.3.2.1 Description of the experiment

Seventeen volunteers participated to the experiment. Every person drove both models, each one for ten minutes. The drivers were not told which model they were testing. Furthermore, to make the comparisons more objective, the order in which the models were tested was changed every time, to try to reduce the influence of the “learning effect”. In fact, after a volunteer drives the first model, he learns “something” (how driving in a simulator is, how the car behaves in terms of handling, etc.): as a consequence he drives the second model in a “different” way and obviously this will affect the final judgment of the VDM.

To evaluate the steering response at low speed, they were asked to drive in between 40 and 60 km/h. Then they were also asked to perform some line changes with sinusoidal steering input, going from one line to the other using big steering angles:

To evaluate the steering feel at medium speed the volunteers had to drive between 70 and 90 km/h. Then they were also asked to perform some line changes (around 80 km/h).

To evaluate the steering response at high speed they were asked to drive between 120 and 140 km/h. Then they were asked to perform some smooth line changes, as if they were driving on a highway, at 120 km/h.

After the test, people were asked to fill in a questionnaire (see Appendix A), where they had to rate the model with respect to reality. The rate goes from 1 (very poor) to 7 (very good): this is the same system used in the previous Master Thesis to evaluate VDM-10 performance.

In the following sections the results of these experiments are reported. They are described both in terms of the mean value obtained by the models in the different areas and in terms of standard deviations.

The average is the average of the sample, and not of the population:

$$\bar{x} = \frac{\sum_{i=1}^N x_i}{N} \quad (5.1)$$

Since the average of the population is unknown, the standard deviation has been computed with respect to the sample average:

$$s = \sqrt{\frac{(x_i - \bar{x})^2}{N - 1}} \quad (5.2)$$

5.3.2.2 Result analysis

The results of the experiments show not only that the new steering model is close to the FORTRAN one, but also that is slightly better.

In *Figure 5.35* the overall steering feel is shown:

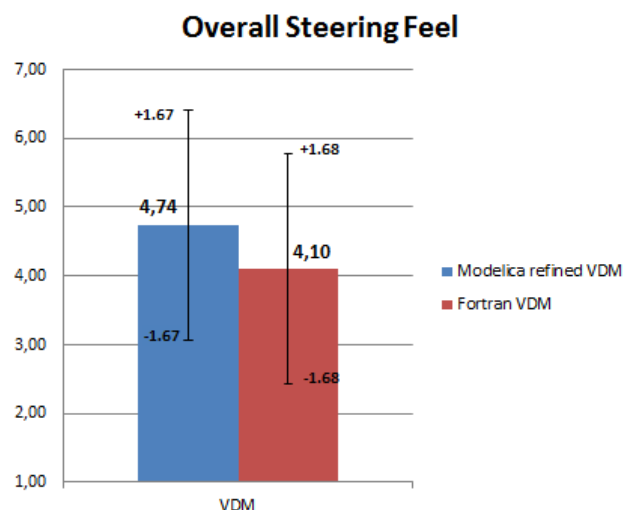


Figure 5.35: overall steering feel score of VDM-14 (blue) vs FORTRAN VDM (red).

The VDM-14 has been judged better in terms of steering feel. Anyway this difference is not big and actually the two models are quite similar. Also the standard deviations are close, and so the variability of the data is more or less the same for the two models. The overall steering feel score, is the average mark of the steering feel in four different conditions:

- Low speed
- Medium speed
- High speed
- Feel of road irregularities on the steering

The steering feel result at low and medium speed is reported in *Figure 5.36*:

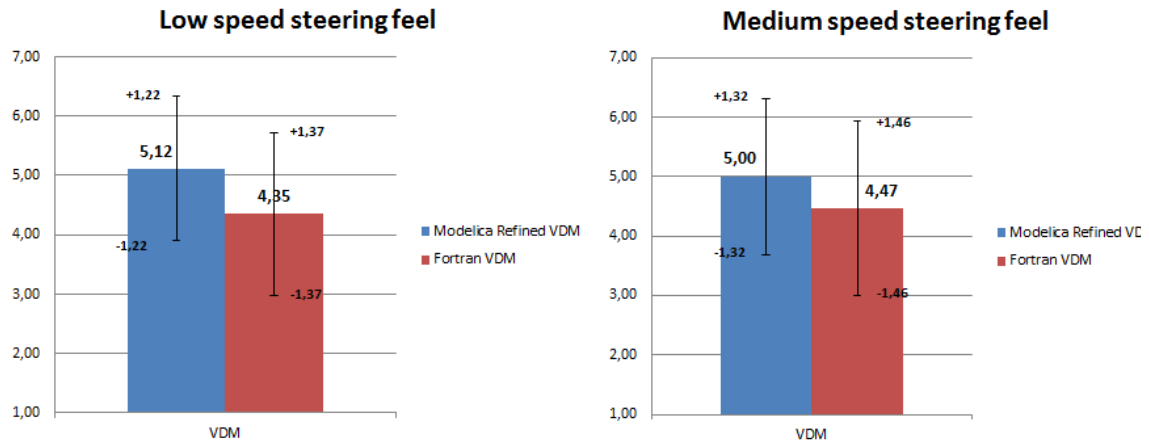


Figure 5.36: low and medium speed steering feel score of VDM-14 (blue) vs FORTRAN VDM (red).

The difference at low speed is not high, but remarkable. The FORTRAN model has an aligning torque which is more “elastic”, with a high self-aligning-torque:

“It seems to be rough at low speeds and hence not very realistic. I feel, for instance, too much torque response when doing the low speed turning.” [Volunteer on FORTRAN steering]

The Modelica one appears to be more natural, with the steering wheel returning in centre position gradually. Many efforts have been put in this area during the pre-test tuning process of the steering, regulating friction and servo assistance to have a homogeneous aligning-torque. The standard deviation of the VDM-14 model is lower than the FORTRAN one, thus indicating that in the new steering model there are more data closer to the mean value with respect to the FORTRAN model. The responses of the two models at medium speed are quite close, but if the line-change manoeuvre is sufficiently harsh some differences emerge. The self-aligning torque in the FORTRAN model has a drop-off in the first phase of counter-steering (even if the car is not sliding). There seems to be a delay in the response of the steering for fast manoeuvres. But this is difficult to perceive, and in fact only a few volunteers noticed a difference. For the others the models were quite close. Again the standard deviation indicates a minor dispersion of the data for the VDM-14 than for the FORTRAN VDM.

The steering feel at high speed and the perception of road irregularities on the steering wheel are shown in *Figure 5.37*:

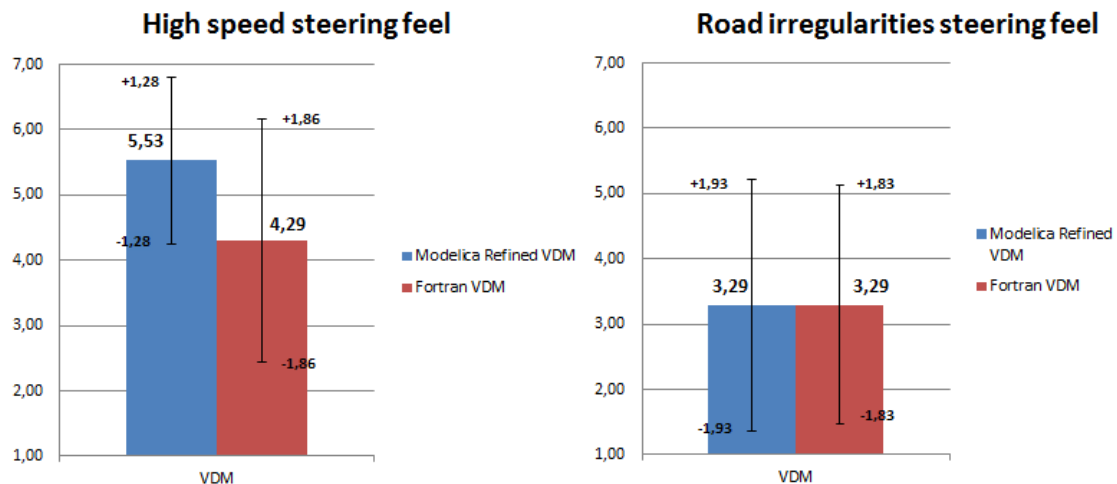


Figure 5.37: high speed steering feel score and perception of road irregularities of VDM-14 (blue) vs FORTRAN VDM (red).

At high speed the new steering model brings significant improvements. The difference in the two models is remarkable: the Modelica steering model is far better than the FORTRAN one at high speeds and this has a strong affection on the overall steering feel score. Basically the FORTRAN model becomes unstable at high speeds, with some excessive oscillations in the self-aligning torque that appears also with slow steering angles.

“Steering oscillations at high speed are too much.” [Volunteer on FORTRAN steering]

The big difference in the standard deviation is explained by the fact that a few drivers liked these “oscillations” because, according to their opinion, they helped them to control better the car.

The two models reached the same average score in the perception of road irregularities on the steering wheel. The two standard deviations are also quite close, even if they are very big. The magnitude of the standard deviation is explained by the fact that some drivers really liked the way in which the models were describing this feeling while other volunteers totally disliked it. Anyway, the overall score is low and can be object of investigation in future works. Actually the road had some slope, banking and smooth holes. So the effective forces transmitted to the driver were not so high. It can be possible that the drivers were expecting to feel more bumps on the road and so they gave a negative judgement of the models. The author suggest to verify the two models on a more uneven and bumpy road. It is clear that this area is the weakest of the new steering system model and affects considerably the final score. So a further improvement in the steering response when negotiating road asperities could be object of future studies, in order to understand how to improve the model. In fact this could lead to even higher scores, making the driving experience with the VDM-14 closer to reality.

The perception of road irregularities on the motion of the vehicle and the overall handling behaviour is reported in *Figure 5.38*.

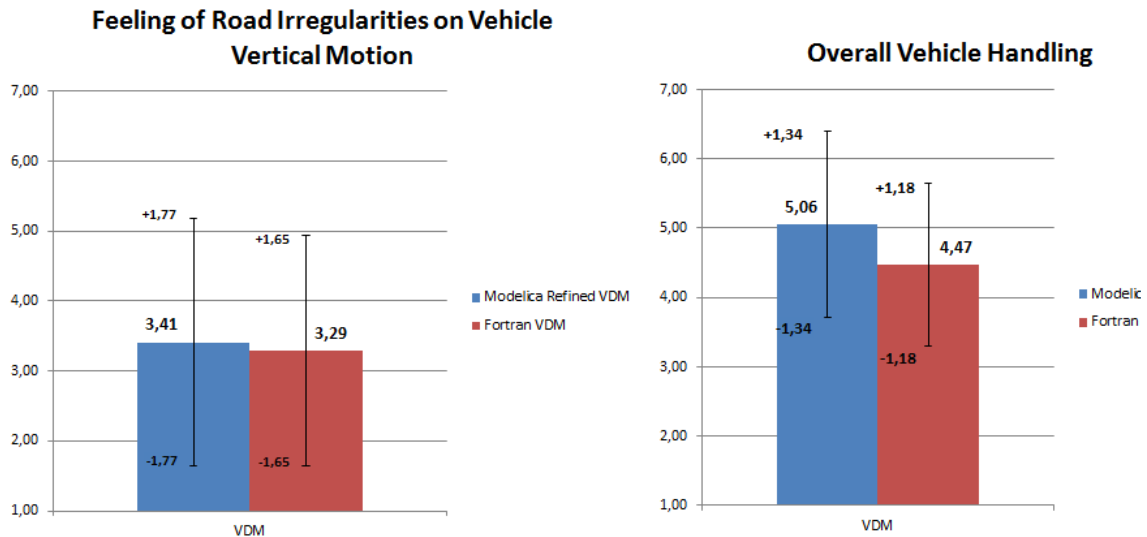


Figure 5.38: road irregularities steering feel and overall vehicle handling score of VDM-14 (blue) vs FORTRAN VDM (red).

The scores of the feeling of road irregularities on vehicle motion are quite close and there are aspects that can be improved. For time reasons, the suspensions of VDM-14 were not tuned specifically for this test, so maybe with different regulations of springs and dampers it is possible to obtain a better response. A big factor influencing the perception of road irregularity in terms of vehicle motion is made by the graphic system. As mentioned before, some tuning of the graphic was made for both models (taking into account that no motion of the cabin was applied) but, always for time reasons, not many efforts were put in this area. The target was to achieve an “acceptable” performance. Some tuning of the graphic could be made in future also to try to make the simulation without motion closer to reality. The result in terms of score is not so high, and according to many volunteers it was difficult to perceive road irregularities without cabin motion.

In terms of overall handling a small superiority of the VDM-14 emerges, but the two models are very close. The dispersion of the data for the Modelica model is higher.

5.3.2.3 Conclusions

A slight superiority of the new steering model emerged in these tests. The two models are very similar at low and medium speeds. There are actually some differences, but not all the drivers have been able to detect them because they are not easy to find in normal driving. The new model brought some concrete and improvements at high speed that were “felt” by the majority of the volunteers.

All the data are characterized by high standard deviation. The steering feel in fact is a very subjective theme and the scores obtained strongly depend on drivers opinion. As an example, the following statements report some quotes of the drivers (written in the final questionnaire) about the VDM-14 steering at low speed:

“The steering wheel return is too soft at low speed”

“At low speed the steering was stiff enough, which was personally ok and better, because you receive better feedback from the road.”

Furthermore the different manoeuvres the drivers were asked to perform were not performed exactly in the same conditions (velocity, steering wheel angle, steering wheel velocity etc.) because they were very difficult to control. The subjectivity of the steering feel make 17 people to be insufficient to give an objective judgement. No statistical study of the data has been made, but at first glance it doesn't seem that the difference between the two models are statistically significant. What emerges from these tests is that the VDM-14 steering model and the FORTRAN one are very close each other, and for many drivers they are difficult to compare:

"Steering wheel torque is similar in both"

"Difficult to make a difference and compare"

"Very difficult to feel a difference between the two models"

Even if it is difficult to say if the VDM-14 steering model is really superior to the FORTRAN one, surely they are very close and this is a big improvement with respect to the Modelica steering model adopted by the VDM-10, which was judged to be "inferior" to the FORTRAN steering model.

Finally, people feedbacks were important to gather some inputs for future works to improve both the VDM-14 steering and the reality of the simulations experience. For what concerns VDM-14 steering some suggestions are:

"On centre driving feels too stiff"

"Torque could be more speed dependant"

"The steer is not as soft as in a real model"

Some suggestions about the overall driving experience in the *Sim IV* are:

"Develop better graphics for a more real feel drive."

"Speedometer does not work sometimes. Audio feedback is not enough to control the speed."

"It didn't feel as if I was driving as fast as indicated."

"It would be better a simulation with motion to give a feedback of road irregularities."

6 Conclusions

The objective of this Master's thesis was to refine an existing VDM used in *Sim IV* at VTI, Göteborg. The refinement activity interested two areas: suspensions and steering system. For what concerns the suspensions the main improvements that are present in the new VDM-14 are:

- Vertical degrees of freedom of the wheels as a response to road irregularities
- Non-linear springs and shock absorbers

The improvements in the steering area are:

- Development of a completely new steering system model
- Improvement of the steering feel

The VDM-14 has been developed using Modelica as programming language and it has been validated both with a comparison versus real data (coming from test track experiment) and with simulations performed in the *Sim IV*.

The model has been developed for being representative of normal (linear) driving conditions and it presents good accuracy, but it works in the simulator also for limit driving conditions, without verified accuracy.

VDM-14 can be seen as an evolution of VDM-10: as a result it maintains the flexibility of VDM-10 (coming from the adoption of the Modelica programming language) and at the same time it improves the realism, getting very close to the FORTRAN model, which is currently used in the *Sim IV*, and is the reference model of a complete vehicle.

The refined VDM-14 represents a solid base for future developments which will further improve it, in order to have a complete vehicle model developed in Modelica ® ready to replace the FORTRAN one.

VDM-14 has been developed to work for *Sim IV* at VTI, but it is possible to run it (with some minor adjustments) also in Chalmers driving simulators.

Even if VDM-14 has been developed in order to be used in simulators, its flexibility and accuracy also make possible to use it for standalone simulations, for different vehicle dynamic studies. For example, VDM-14 is being used in a project carried on at Chalmers for studying post-impact stability, where it has been parameterized both as a Saab 9.3 and as a Volvo V40.

7 Future work

This section is devoted to some suggestions for future work and developments of VDM-14. In particular, it would be interesting:

- Parameterize the suspensions according to a NVH (Noise, vibrations and harshness) analysis. This will also be useful when the model is run in the *Sim IV* with motion, so that the driver perceives a vertical behaviour of the vehicle (in terms of accelerations and vibrations), which is closer to the one of a real car.
- Improve the suspension model, to take into account wheel-lift phenomenon.
- Implement some active safety systems, such as ABS (which now is compulsory on every vehicle) and ESP.
- Improve the steering model to take into account the dynamics in parking conditions.
- Model the damping of the rack as non-linear and the friction as variable in function of the rack displacement.
- Model the servo assistance dependency in function of the speed.
- Adopt a more realistic transmission model, by introducing flexibility and damping in the shafts.

Finally, the experiments performed with volunteers were also useful to gather some pieces of information to improve the overall quality of the simulation inside the *Sim IV*, and in particular:

- Improve the quality graphic of the sceneries in which the car is driven.
- Improve the graphic to provide a better feel of velocity.
- Improve the audio.

8 References

- [1] Jacobson B., (2013): *Vehicle Dynamics, Compendium of the Course MMF062*. Division of Vehicle Dynamics and Autonomous Systems, Chalmers University of Technology, Göteborg, Sweden.
- [2] Olsson G., Jacobson B., (2013): *Suspensions & Steering System Modelling*. FTME030, Tire and Vehicle Dynamics, Division of Vehicle Dynamics and Autonomous Systems, Chalmers University of Technology, Göteborg, Sweden.
- [3] Velardocchia M., (2011): *Dinamica del Veicolo*.
- [4] Velardocchia M., Galvagno E., (2010): *Meccanica del Veicolo, Esercitazioni*. C.L.U.T.
- [5] Velardocchia M., Galvagno E., (2010): *Complementi di Meccanica del Veicolo*. C.L.U.T.
- [6] Genta G., Morello L., (2009): *The Automotive Chassis, Volume 1*. Springer.
- [7] Genta G., Morello L., (2009): *The Automotive Chassis, Volume 2*. Springer.
- [8] Miliken W.F., Milliken D.L., (1994): *Race Car Vehicle Dynamics*. SAE International, Englewood Cliffs, New Jersey.
- [9] Jorns R., Helmut S., Jurgen W. B., (2002): *The Automotive Chassis: Engineering Principles, Second Edition*. SAE International, 400 Commonwealth Drive, Warrendale, PA 15096-0001USA.
- [10] Nordmark S., (1984): *Mathematical Model of a Four-Wheeled Vehicle for Simulation in Real Time*. VTI Report, publication n° 267 A 1984, Linköping, Sweden.
- [11] Gómez Fernández J., (2012): *A Vehicle Dynamic Model for Driving Simulators*. Master's thesis, department of Applied Mechanics, division of Vehicle Engineering and Autonomous Systems, Chalmers University of Technology, Göteborg, Sweden.
- [12] Mula Viviero I., (2009): *Estudio del Comportamiento Dinámico de un Vehículo Utilizando la Herramienta Simmechanics de Matlab*. Proyecto fin de Carrera, Departamento de Ingeniería Mecánica, Universidad Carlos III de Madrid.
- [13] Blundell M., Harty D., (2004): *The Multibody Systems Approach to Vehicle Dynamics*. Elsevier Butterworth-Heinemann.
- [14] Katzourakis D., (2012): *Driving Steering Support Interfaces Near the Vehicle Handling Limits*. Ph.D. Thesis, Printed in The Netherlands: CPI Koninklijke Wöhrmann.
- [15] Lúcio Patrício F.S., Becker M., Jánes Landre Jr., Clovis Barcellos S., (2006): *A New Vehicle 3D Model with 7 Degrees of Freedom for Vehicle Dynamic Response Study*. Pontifical Catholic University of Minas Gerais, Belo Horizonte, MG 30-535610 Brasil.
- [16] Adams F.J., (1981): *Proceedings of the Institution of Mechanical Engineers, Automotive Power Steering "Feel"*. SAGE.

- [17] Erdelyi H., Talaba D., Girbacia F: *Virtual Prototyping of an Automobile Steering System using Haptic Feedback*. Transilvania University of Brasov, Product Design and Robotics Department, Brasov, Romania.
- [18] Marouf A., Sentouh C., Djemai M., Pudlo P., (2011): *Control of an Electric Power Assisted Steering Using Reference Model*. 50th IEEE Conference on Decision and Control and European Control Conference (CDC-ECC), Orlando, FL, USA.
- [19] Olsson H., Åström K.J., Canudas de Wit C., Gäfvert M., Lischinsky P. (1997): *Friction Models and Friction Compensation*.
- [20] Linden P., Geluk T., Nijmeijer H., (2007): *Friction and Compliance Identification in a Vehicle's Steering System*. DCT 2007.095, Eindhoven.
- [21] Rosth M., (2007): *Hydraulic Power Steering System Design in Road Vehicles*. Dissertation n°1068, Division of Fluid and Mechanical Engineering Systems, Department of Mechanical Engineering, Linköping, Sweden.
- [22] Åström K.J., Canudas-de-Wit (2008): *Revisiting LuGre Model*. IEEE Control System Magazine 28, 6 (2008) 101-114.
- [23] Robinson R. W., (2007): *Optimal Passive Non Linear Damper Design Methodology For Road Race Application*. Master's thesis in Mechanical Engineering, University of New Mexico, Albuquerque, New Mexico.
- [24] Schmeitz A.J.C., Besselink I.J.M., Nijmeijer H., (2006): *Run Flat Tires vs Conventional Tires, an Experimental Comparison*. DCT 2006.042, Department of Mechanical Engineering, Dynamics and Control Technology Group, Eindhoven University of Technology.

9 APPENDICES

APPENDIX A: Questionnaire

DRIVER INFORMATIONS

Name (optional): _____

| | | | | |
|--|-----------------------------------|---|---|------------------------------------|
| Gender | <input type="checkbox"/> Male | <input type="checkbox"/> Female | | |
| How many times have you used a simulator before? | <input type="checkbox"/> Never | <input type="checkbox"/> 1-3 | <input type="checkbox"/> More than 3 | |
| How many different cars do you usually drive? | <input type="checkbox"/> 0 | <input type="checkbox"/> 1 | <input type="checkbox"/> 2 | <input type="checkbox"/> 3 or more |
| How many km do you drive per year? | <input type="checkbox"/> 0-10.000 | <input type="checkbox"/> 10.000-20.000 | <input type="checkbox"/> More than 20.000 | |
| Do you play car related video games? | Never | <input type="checkbox"/> | Often | |

MODEL COMPARISON

| | | | |
|--|--------------------|---|-----------|
| How do you perceive the steering response when negotiating low speed turns? | Model 1: Very poor | <input type="checkbox"/> | Very good |
| | Model 2: Very poor | <input type="checkbox"/> | Very good |
| How do you perceive the steering response when negotiating medium speed turns? | Model 1: Very poor | <input type="checkbox"/> | Very good |
| | Model 2: Very poor | <input type="checkbox"/> | Very good |
| How do you perceive the steering response when negotiating high speed turns? | Model 1: Very poor | <input type="checkbox"/> | Very good |
| | Model 2: Very poor | <input type="checkbox"/> | Very good |
| Can you feel the road irregularities on the steering wheel? | Model 1: Very poor | <input type="checkbox"/> | Very good |
| | Model 2: Very poor | <input type="checkbox"/> | Very good |
| Can you feel road irregularities in the vertical movement of the vehicle? | Model 1: Very poor | <input type="checkbox"/> | Very good |
| | Model 2: Very poor | <input type="checkbox"/> | Very good |
| Evaluate the overall model behavior in terms of handling in normal driving. | Model 1: Very poor | <input type="checkbox"/> | Very good |
| | Model 2: Very poor | <input type="checkbox"/> | Very good |

What should be improved in the models, in your opinion?

Model 1:

Model 2:

Additional comments (thoughts, impressions, suggestions, etc.):

APPENDIX B: VDM-10

B.1 Coordinate system

The system of coordinates adopted is in accordance to ISO standards, as described in ISO 8855. It is shown in *Figure B.1*.

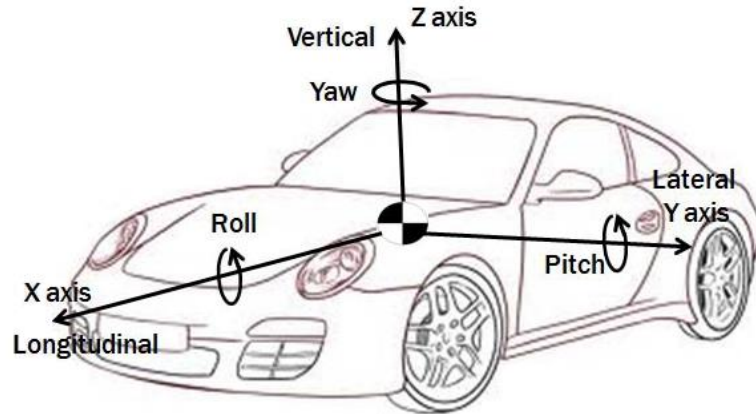


Figure B.1: Vehicle reference frame. Adapted from Jorge Gómez Fernández (2012).

In addition to this reference frame, a local coordinate system is used independently for each tire, also according ISO 8855. The wheel coordinate system is shown in *Figure B.2*.

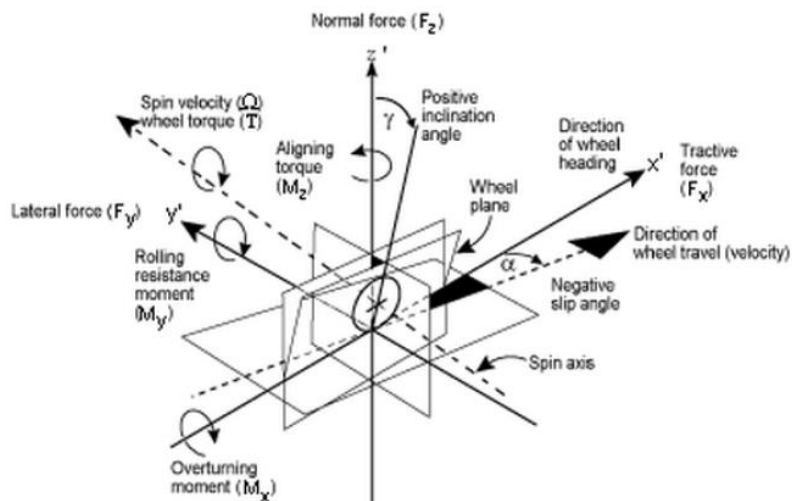


Figure B.2: wheel coordinate system, as defined by ISO 8855.

The vehicle model developed is a two track vehicle. *Figure B.3* shows the different forces acting on the vehicle:

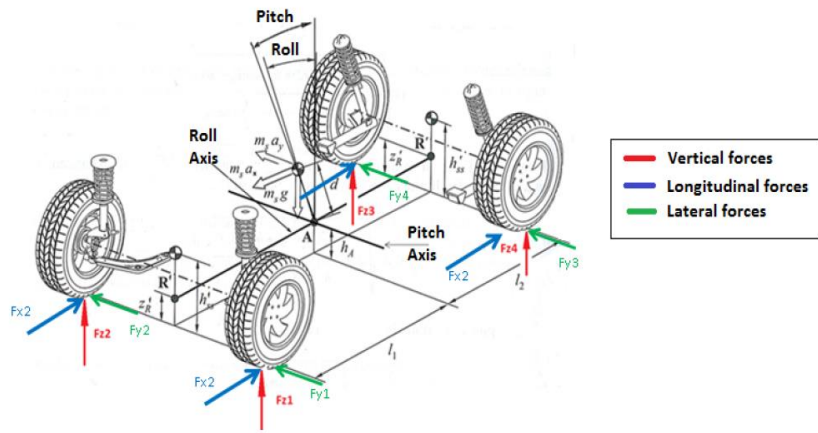


Figure B.3: Schematic view of a two track vehicle, adapted from Jorge Gómez Fernández (2012).

B.2 Wheels

The equation describing the wheel motion is:

$$T_{di} - T_{bi} - Fx_i \cdot R_{nom} = I_{wheel} \cdot \alpha_{wheel} \quad (B.1)$$

The wheel acceleration is related to the wheel velocity in the following way:

$$\alpha_{wheel} = \frac{d\omega_{wheel}}{dt} \quad (B.2)$$

Starting from Figure B.4, wheel velocities are computed:

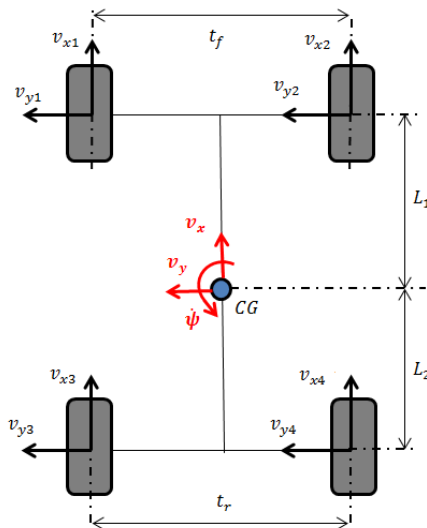


Figure B.4: relationship between vehicle velocity and wheel velocities. All velocities are shown as positive.

$$v_{xi} = v_x \pm \dot{\psi} \cdot \frac{t_{f,r}}{2} \quad \text{with } i = 1, \dots, 4 \quad (\text{B.3})$$

$$v_{yi} = v_y \pm \dot{\psi} \cdot L_{1,2} \quad \text{with } i = 1, \dots, 4 \quad (\text{B.4})$$

Tire slip velocities are expressed through the following equation:

$$v_{si} = \omega_{wheeli} \cdot R_{nom} \quad \text{with } i = 1, \dots, 4 \quad (\text{B.5})$$

Limitations

For sake of simplicity, all the calculations referred to wheels and tires use the tire nominal radius, which is considered constant. Actually the real tire radius is not constant, but it depends on different factors such as vertical load, inflation pressure, carcass stiffness, rotational speed, etc. Furthermore no tire damping is considered in *Equation B.1*.

B.3 Tires

A tire brush model has been adopted. It his based on six inputs and four parameters, shown in *Table B.1* and *Table B.2*.

Table B.1: tire model inputs and outputs.

| TIRE MODEL INPUTS | TIRE MODEL OUTPUTS |
|--|-----------------------------|
| Tire vertical load Fz_i | Longitudinal force Fx_i |
| Tire longitudinal velocity v_{xi} | Lateral force Fy_i |
| Tire lateral velocity v_{yi} | Self-aligning torque Mz_i |
| Tire slip velocity v_{si} | Longitudinal slip S_{xi} |
| Steering wheel angle δ | Lateral slip S_{yi} |
| Tire-road friction coefficient μ_i | |

Table B.2: tire model parameters.

| TIRE MODEL PARAMETERS | VALUES |
|--------------------------------------|---------------|
| Normalized thread stiffness C | 30 ÷ 80 [N/m] |
| Contact path length a | 0.1 [m] |
| Caster trail c_t | 0.03 [m] |
| Sliding friction constant μ_{vi} | 0.8 |

The longitudinal slip is computed as:

$$S_{xi} = \frac{v_{si} - v_{xi}}{\max(v_{si}, 1)} \quad \text{with } i = 1, \dots, 4 \quad (\text{B.6})$$

The form of the denominator of *Equation B.6* is due to avoid numerical instabilities. The lateral slip for front and rear wheels is expressed by *Equations B.7* and *B.8*.

$$S_{yi} = f(v_{xi}) \cdot \left(\delta_{wi} - \frac{v_{yi}}{\max(v_{si}, 1)} \right) \quad \text{with } i = 1, 2 \quad (\text{B.7})$$

$$S_{yi} = f(v_{xi}) \cdot \left(\frac{v_{yi}}{\max(v_{si}, 1)} - \delta_{wi} \right) \quad \text{with } i = 3, 4 \quad (\text{B.8})$$

Again the term $\max(v_{si}, 1)$ has been introduced to avoid numerical instabilities. The same for the function $f(v_{xi})$:

$$f(v_{xi}) = \left(\frac{\tanh(10 \cdot v_{xi} - 8) + 1}{2} \right) \quad \text{with } i = 1, \dots, 4 \quad (\text{B.9})$$

According to *Equations B.7* and *B.8*, if the car is stopped and the steering wheel is turned, $\delta_{wi} \neq 0$. Then a lateral slip would appear and this is unrealistic. This is the reason that led to the introduction of $f(v_{xi})$. So, for low speeds the lateral slip is multiplied by the hyperbolic tangent function of *Equation B.9*, represented in *Figure B.5*.

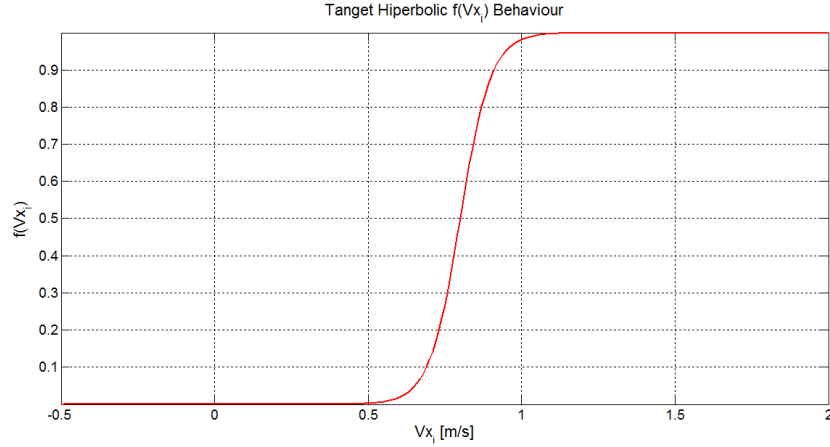


Figure B.5: brush model hyperbolic tangent function, adapted from Jorge Gómez Fernández (2012).

The combined slip for each wheel is given by:

$$S_i = \sqrt{(S_{xi}^2 + S_{yi}^2)} \quad \text{with } i = 1, \dots, 4 \quad (\text{B.10})$$

The variable ξ_i is used to evaluate if the tire is working in linear ($\xi_i < 1$) or sliding ($\xi_i > 1$) conditions.

$$\xi_i = \frac{C}{3 \cdot \mu_i} \cdot S_i \quad \text{with } i = 1, \dots, 4 \quad (\text{B.11})$$

Once the working condition is known, the tire forces will be calculated with Equations B.12 to B.15.

$$F_i = \begin{cases} -C \cdot \left(-1 + \xi_i - \xi_i^{\frac{2}{3}} \right) \cdot Fz_i & \xi_i < 1 \\ \left[\mu_{vi} + (1 - \mu_{vi}) \cdot e^{-0.01 \cdot (\xi_i - 1)^2} \right] \cdot \frac{\mu_i \cdot Fz_i}{S_i} & \xi_i > 1 \end{cases} \quad (\text{B.12})$$

$$Fx_{i_wo_rlx} = F_i \cdot S_{xi} \quad \text{with } i = 1, \dots, 4 \quad (\text{B.13})$$

$$Fy_{i_wo_rlx} = F_i \cdot S_{yi} \quad \text{with } i = 1, \dots, 4 \quad (\text{B.14})$$

$$Mz_{i_wo_rlx} = -\frac{a \cdot C \cdot S_{yi}}{3} \cdot [\min(0, \xi_i - 1)]^3 \cdot Fz_i - r_c \cdot F_i \cdot S_{yi} \quad (\text{B.15})$$

with $i = 1, \dots, 4$

Figure B.6 shows, as an example, the longitudinal force generated by the tire in function of the longitudinal slip.

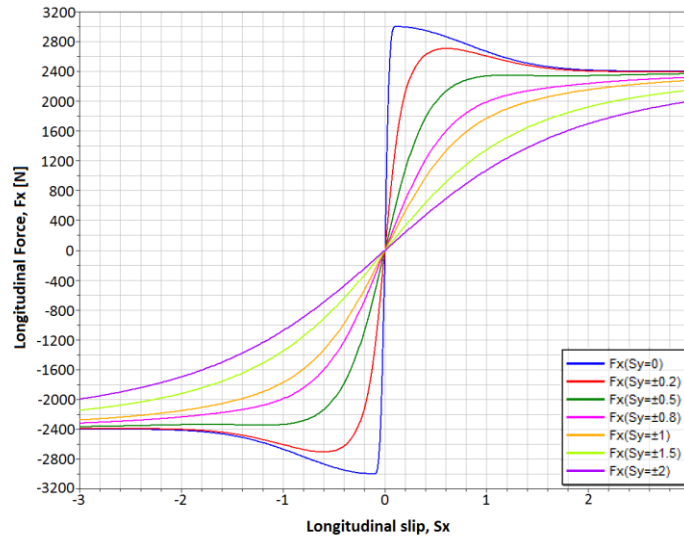


Figure B.6: longitudinal force versus longitudinal slip, for different lateral slip combinations. Adapted from Jorge Gómez Fernández (2012).

To take into account of the effect of the relaxation length *Equations B.16 to B.18* are used.

$$\dot{F}x_i = -\max\left(\frac{v_{si}}{l_{rx}}, 0.1\right) \cdot (Fx_i - Fx_{i_wo_rlx}) \quad \text{with } i = 1, \dots, 4 \quad (\text{B.16})$$

$$\dot{F}y_i = -\max\left(\frac{v_{si}}{l_{rx}}, 0.1\right) \cdot (Fy_i - Fy_{i_wo_rlx}) \quad \text{with } i = 1, \dots, 4 \quad (\text{B.17})$$

$$\dot{M}z_i = -\max\left(\frac{v_{si}}{l_{rx}}, 0.1\right) \cdot (Mz_i - Mz_{i_wo_rlx}) \quad \text{with } i = 1, \dots, 4 \quad (\text{B.18})$$

Limitations

The tire model works well, but has some limitations. First off all the relaxation length is assumed to be constant, and its effect is described only through a first order filter (*Equations B.16 to B.18*) that models the delay by which the tire forces reach the steady state, after a slip has been applied. Actually the relaxation length is a more complex phenomenon and the delay depends on the behaviour of the carcass in terms of stiffness and deflection. Another limitation is that the tire threads are considered as isotropic. This tire model does not hold for very low speed. In this condition, the tire behaves like a spring, and the forces exchanged with the road must be evaluated considering different methods, for instance the friction force between tire and road.

B.4 Driveline

A provisional driveline has been adopted for this VDM. The engine torque characteristic is the one coming of a Saab 9.3 equipped with a 2.0 petrol engine performing 175 brake horse power. The torque characteristic is shown in *Figure B.7*.

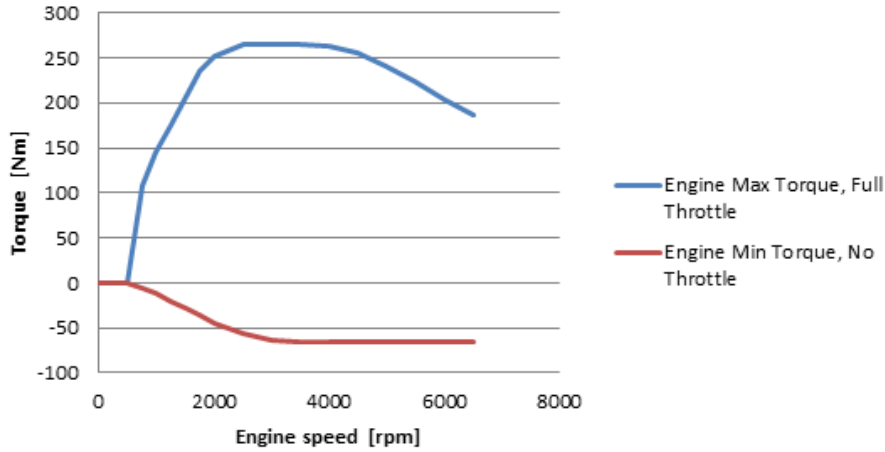


Figure B.7: Saab 9.3 2.0 torque characteristic, adapted from Jorge Gómez Fernández (2012).

The maximum and the minimum engine torques have been obtained by parameterizing the curves of Figure B.7. The resulting expressions for the engine torques are:

$$T_{eng,max} = 2.1486 \cdot 10^{-6} \cdot \omega_{eng}^3 - 3.7390514 \cdot 10^{-6} \cdot \omega_{eng}^2 + 1.8250297732 \cdot \omega_{eng} \quad (B.19)$$

$$T_{eng,min} = 2.152813 \cdot 10^{-4} \cdot \omega_{eng}^2 - 0.2413794863 \cdot \omega_{eng} \quad (B.20)$$

The total transmission ratio is the product of the ratio of the engaged gear and the final gear.

$$i_T = \begin{cases} i_{gear,i} \cdot i_{final} , & \text{with } i = 1, \dots, 5 \\ 0, & i_{gear,0} = 0 \text{ (neutral)} \end{cases} \quad (B.21)$$

When the gas pedal is pressed, $C_{input} > 0$, or the vehicle is in neutral $i_T = 0$, engine speed will depend on the throttle input and on the internal inertia of the engine, but it has been calculated in a simplified way, just as a function of the throttle position. The intermediate variable $\omega_{eng,int}$ it is used to compute the engine velocity when it is engaged with the wheels:

$$\omega_{eng,int} = \max\left(\frac{\omega_{wheel1} + \omega_{wheel2}}{2} \cdot i_T, 73\right) \quad (B.22)$$

This intermediate variable is then used to compute the engine speed, taking also into account the clutch and neutral influence:

$$\omega_{eng} = \begin{cases} 680 - (1 - T_{input}) \cdot (680 - 73) & \text{if } i_T = 0 \text{ or } C_{input} > 0.5 \\ \min(\omega_{eng,int}, 680), & \text{if } i_T \neq 0 \text{ or } C_{input} \leq 0.5 \end{cases} \quad (B.23)$$

The clutch input can assume values from 0 [pedal released] to 1 [pedal pressed]. The engine is considered disengaged from the gearbox for $C_{input} > 0.5$. The input engine

torque to the gearbox T_{eng} , is computed through an internal variable $T_{eng,int}$ as follows:

$$T_{eng,int} = \begin{cases} 0 & \text{if } C_{input} > 0.5 \\ (1 - C_{input}) \cdot T_{input} \cdot (T_{eng,max} - T_{eng,min}) \\ \quad + T_{eng,max} & \text{if } C_{input} \leq 0.5 \end{cases} \quad (\text{B.24})$$

According to *Figure 2.12*, when the throttle pedal is released, the engine is generating a negative torque. If $v_x < 0$, for example on reverse gear or during spin, that negative torque increases the vehicle negative v_x and this is unrealistic. To prevent this kind of situation the torque will be kept positive also if $v_x < 0$.

$$T_{eng} = \begin{cases} \max(0, T_{eng,int}) & \text{if } v_x < 0 \\ T_{eng,int} & \text{if } v_x \geq 0 \end{cases} \quad (\text{B.25})$$

The driving torque transmitted to the wheels is computed considering an ideal differential.

$$T_{d1,2} = \frac{T_{eng} \cdot \eta_{trans} \cdot i_T}{2} \cdot \left[-\frac{\tanh(\omega_{eng} - 677) + 1}{2} \right] \quad (\text{B.26})$$

$$T_{d3,4} = 0 \quad (\text{B.27})$$

Limitations

The transmission model adopted does not take into account any dynamics of the system, for example damping and inertia of the various components (engine, differential, clutch, gearbox, etc.) are neglected. For these reasons, a new transmission model is being developed at VTI in Linköping. *Figure B.8* shows a schematic model of the transmission.

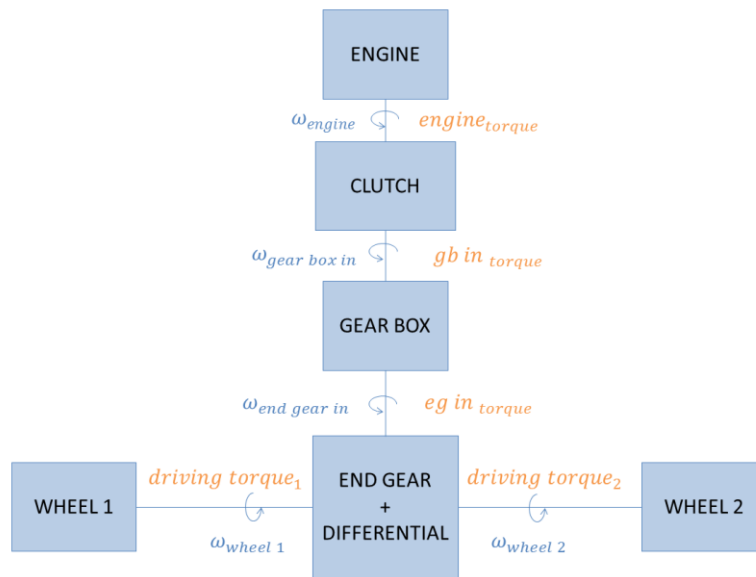


Figure B.8: schematic view of the driveline model, adapted from Jorge Gómez Fernández (2012).

B.5 Braking system

The braking model represents a typical braking system equipped with four disk brakes. To prevent that rear wheels lock before the front ones during braking, the hydraulics of the braking system are fitted with control valves that regulates the pressure on the rear brakes, according to Figure B.9. These valves act by keeping the rear axle brake pressure constant when the pressure at the master cylinder exceeds the set limiting value. The pressure applied to the front callipers $P_{b,f}$, is an input for the model.

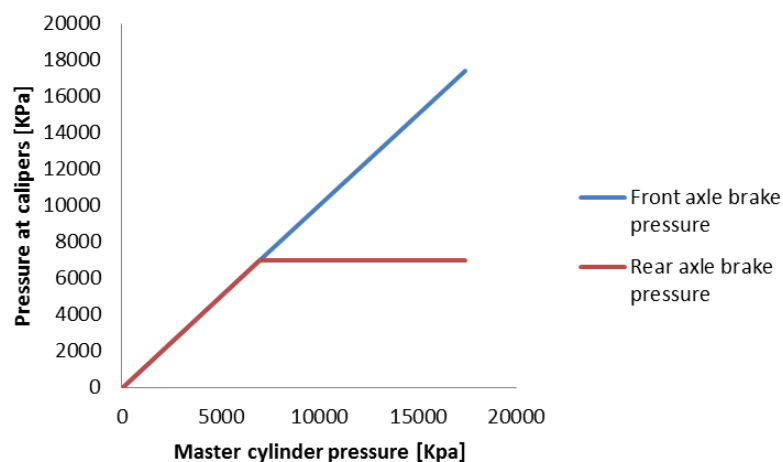


Figure B.9: Relationship between master cylinder pressure and brake pressure at rear callipers, using a rear limiting pressure valve. Adapted from Jorge Gómez Fernández (2012).

The pressure applied to the rear callipers is computed as:

$$P_{b,r} = \begin{cases} P_{b,f} & \text{if } P_{b,f} < P_{b,r} \text{ limit} \\ P_{b,r} \text{ limit} & \text{if } P_{b,f} \geq P_{b,r} \text{ limit} \end{cases} \quad (\text{B.28})$$

In the simulator, the brake pedal, the booster and the master cylinder from the original Volvo XC-60 are still in the cabin, and they are used to generate the input brake pressure, that can be measured.

The braking torque on the front wheels is expressed by *Equation B.29*:

$$T_{b1,2} = 2 \cdot 0.58 \cdot d_{df} \cdot P_{b,f} \cdot 10 \cdot \frac{\frac{\pi}{4} \cdot d_{piston}^2}{A_{pad}} \cdot \pi \cdot C_{f\ pad} \cdot [d_{df}^2 - (0.58 \cdot d_{df})^2] \cdot \tanh(\omega_{wheel\ i}) \quad \text{with } i = 1,2 \quad (\text{B.29})$$

In the same way the braking torque on the rear wheels is computed:

$$T_{b3,4} = 2 \cdot 0.58 \cdot d_{dr} \cdot P_{b,r} \cdot 10 \cdot \frac{\frac{\pi}{4} \cdot d_{piston}^2}{A_{pad}} \cdot \pi \cdot C_{f\ pad} \cdot [d_{dr}^2 - (0.58 \cdot d_{dr})^2] \cdot \tanh(\omega_{wheel\ i}) \quad \text{with } i = 3,4 \quad (\text{B.30})$$

Limitations

This model describes a basic brake system. No ABS nor ESP or any other active safety devices are taken into account.